Summer 2014

Laboratory Apparatus For Gas Turbine Combustion Development

Dustin Lee Cruise
Purdue University

Graduate School ETD Form 9
(Revised 01/14)

PURDUE UNIVERSITY
GRADUATE SCHOOL
Thesis/Dissertation Acceptance

This is to certify that the thesis/dissertation prepared

By Dustin Lee Cruise

Entitled
Laboratory Apparatus for Gas Turbine Combustion Development

For the degree of Master of Science in Mechanical Engineering

Is approved by the final examining committee:

Galen King

Hukam Mongia

Peter Meckl

William Anderson

To the best of my knowledge and as understood by the student in the *Thesis/Dissertation Agreement. Publication Delay, and Certification/Disclaimer (Graduate School Form 32)*, this thesis/dissertation adheres to the provisions of Purdue University's "Policy on Integrity in Research" and the use of copyrighted material.

Galen King, Hukam Mongia

Approved by Major Professor(s): _____

_____

Approved by: Dave Anderson 07/28/2014

Head of the Department Graduate Program Date

LABORATORY APPARATUS FOR GAS TURBINE COMBUSTION DEVELOPMENT

A Thesis

Submitted to the Faculty

of

Purdue University

by

Dustin Lee Cruise

In Partial Fulfillment of the

Requirements for the Degree

of

Master of Science in Mechanical Engineering

August 2014

Purdue University

West Lafayette, Indiana

To my wife, Denise.

ACKNOWLEDGEMENTS

My most sincere gratitude is extended to Professor Galen King and Professor Hukam Mongia for letting me share in this experience with them. Although most students only have one academic advisor, I have had the privilege of two of the most experienced and knowledgeable professors on this campus. I owe my academic success, and a large portion of my personal growth, to their varied backgrounds and experience, and most importantly their patience with me during this process.

To my colleague, Nathan Toner, I thank for his many selfless contributions to my work, from the translation table to the LabVIEW codes used for automation.

I also wish to thank the undergraduate assistants that have passed through our lab. I would not have been able to complete the translation table without the many hours Julian Merkison and Sean Stevens spent helping me to design and manufacture it. Matthew Clark was an instrumental part of the experimental team, doing whatever was necessary to keep the fire lit. I'm sure all of these students will find great success in their future endeavors.

To my wife, Denise, I thank her for her endless encouragement, focus, and balance, during this journey we've had together. I can't wait for the next part with her, and the many other adventures after.

TABLE OF CONTENTS

Page

LIST OF TABLE

LIST OF FIGURES

Figure Page

Figure Page

Figure Page

Figure Page

ABSTRACT

Cruise, Dustin L. M.S.M.E., Purdue University, August 2014. Laboratory Apparatus for Gas Turbine Combustion Development. Major Professors: Galen King, Hukam Mongia, School of Mechanical Engineering.

The next generation of combustor technology will be required to meet the demands of a world more focused on greenhouse gases and global warming. Due to this new focus on emission control, combustors must produce less NO_x, while operating in a higher pressure environment that is more prone to combustion instabilities.

This work focuses on the development of a lab and combustor that will be used for the next generation combustor development. The lab development includes layout and organization, facilities, measurement and instrumentation, automation of the testing process, and an imaging tool for diagnostics.

A Lean Direction Injection (LDI) single element combustor has been designed, built, and tested. Results included chemiluminescence imaging and measurements of combustion instabilities. Initial results are promising for future controls and combustion development.

A three axis translation table has been developed to support diagnostic efforts. Initial performance measurements indicate the table will be capable of fast scanning of flames compared to other translation options. In addition to

achieving the desired performance, the size of the table was kept compact without sacrificing travel, allowing more access to the burners, and more burners to be mounted onto the table.

One of the first projects will be the application of the Laser-induced Fluorescence Triple-integration Method (LIFTIME) method to the LDI to assist combustion controls development. After the experience gained with the charge coupled device (CCD) camera, we see potential to use this in parallel with the LIFTIME system to better map the flame. The image processing capabilities of the LabVIEW software have been briefly explored, and look promising as a method for automated flame geometry analysis to improve the flame mapping.

In addition to the application of LIFTIME to the LDI, the exploration of the combustion control using the variable injector position, and the variable impedance exit area will begin.

Due to the work presented in this thesis, a fully-functional combustion lab is available for current and future students, and more in-depth combustion research can now begin. In addition to providing resources for the students of our research group, this lab will continue to support Senior Design students as well as those in graduate level combustion courses.

CHAPTER 1. INTRODUCTION

1.1 Motivation

Each day, approximately 30,000 commercial aircraft take off around the world, transporting people and products. With this current volume and future projected growth, emissions become an increasing concern for climate change. Aircraft contribute 7-9% of annual CO_2 production [1], and the NO_x output is particularly significant because its high altitude introduction forms more ozone than ground based sources. To combat the harmful effects of these emissions, in 1983 the United Nations, through the International Civil Aviation Organization, (ICAO), formed the Committee on Aviation Environmental Protection (CAEP). CAEP has the task of creating regulations to limit the impact commercial aviation has on the environment. Since its founding, CAEP has released four sets of emissions regulations with the newest standard, CAEP/6, being adopted in 2008 [2]. Figure 1-1 shows the reductions CAEP has made on NO_x since its beginning, with an overall decrease of 53% since CAEP/1.

To achieve the CAEP goals, the FAA and NASA each have created projects, CLEEN and ERA, respectively, to provide guidelines to aircraft and engine manufacturers in developing future technology. These projects are focused on the technology for the N+2 generation, entering service sometime

after 2020 [2]. The emissions goals of these projects are to reduce CO_2 output through a 50% reduction of fuel burn, and reduce NO_x by 75% [3]. To meet these goals, NASA's ERA project is critically examining all parts of the aircraft, from lightweight composites for the airframe, to unducted propulsors for the engine [4]. Of all the components being investigated, the combustor will play one of the most critical roles for reducing CO_2 and NO_x.

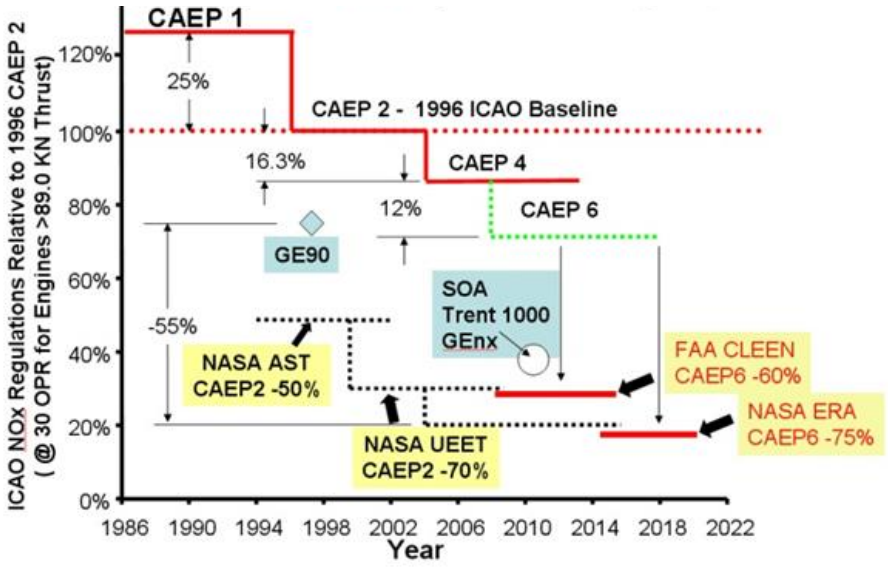

Figure 1-1: History of ICAO NO_x regulations for engines. The NASA ERA N+2 generation goal is a 75% reduction of the CAEP/6 NO_X standard by 2020.

One technology researched in the past for meeting goals like these was variable geometry. It has been researched for applications such as zone equivalence ratio control and instability suppression, and has shown promising results. However, it has not been applied to flight hardware because the other technologies needed to use it, sensors, actuators, and electronics, are not, as yet, sufficiently robust enough for flight. Each of these areas are rapidly progressing,

so variable geometry may eventually become feasible for production implementation [5]. Considering the potential impact that improved mixing and instability suppression could have towards N+2 and future goals, the research community should now be exploring the combination of the two. The work of this thesis begins the study of variable geometry with the development of a laboratory scale test rig, and equipment to support it.

1.2 Background

The initial stage of this research project was to determine the current state of combustion design and associated turbine hardware. In this section, reviewed are the next generation gas turbine technologies that will impact the combustor. The NASA ERA project provides an excellent glimpse into this future, as reported by Lee and Suder [2], [4].

1.2.1 NASA ERA Technology

One of the most significant changes for the next generation combustor is increasing the overall pressure ratio (OPR) from 45 to 55. This will increase the engine's efficiency, giving an expected fuel burn reduction of 2.5%. The impact on the combustor will be a higher inlet temperature and pressure. This increase in temperature will negatively impact NO_x formation as it's exponentially related to flame temperature. Keeping NO_x down with the increased OPR is seen as one of the biggest challenges for the next generation combustor.

Critical to reducing flame temperature and NO_x is lean burning [6]. Lean burning will be accomplished by putting more air, from reduced liner cooling,

through the fuel nozzle to produce a leaner mixture. Advanced ceramic matrix composite (CMC) liners and environmental barrier coatings (EBC), capable of 2700°F, are being developed for this need, and will allow a 60% reduction in cooling. This reduction is predicted to decrease NO_x levels by 40%; however this reduction in linear cooling will not have a positive impact on combustion instabilities. Combustion instabilities are due to the interaction of combustion heat release and the natural acoustic modes of the combustor. Liner cooling helps dampen instabilities, so with its reduction, the instability amplitude will increase.

One solution being worked on through ERA is high frequency modulation of the fuel supply, which is a form of feedback control. This method has shown very promising results in the lab, but hasn't been turned into flight-ready hardware due to the cost and complexity of the actuators [2].

The addition of feedback control to the engine has the potential to address instabilities along with many of the combustor challenges such as pattern factor and emissions minimization. To make feedback control possible, high temperature sensors and electronics are needed that can function properly around the combustor environment [7]. Under the ERA project, 600°C pressure sensors and 500°C signal conditioning electronics are being developed, allowing combustor pressures to be measured [8].

As stated earlier, mixture preparation is the key to lean burning and NOx reductions. Many advanced mixing concepts that have been developed use premixing of the fuel and air. This has been deemed impractical with the higher

OPR due to auto-ignition and flashback concerns. Lean Direct Injection (LDI) is seen as the best mixer configuration for high OPRs because fuel is added at the flame front, reducing the chance of auto-ignition and flashback [9]. The next generation LDI fuel nozzles, besides having increased air flow, will most likely be multi-element arrays composed of smaller diameter fuel nozzles (Figure 1-2). There are several advantages to this array configuration. The first is an array of nozzles reduces the radial distance from each nozzle to the flame front, decreasing the distance fuel must be injected. Second, the turbulence and shear created between the individual nozzles of the array enhance mixing [10]. Lastly, the array configuration allows fuel staging amongst the nozzles, which has been shown to increase the range of operability [3].

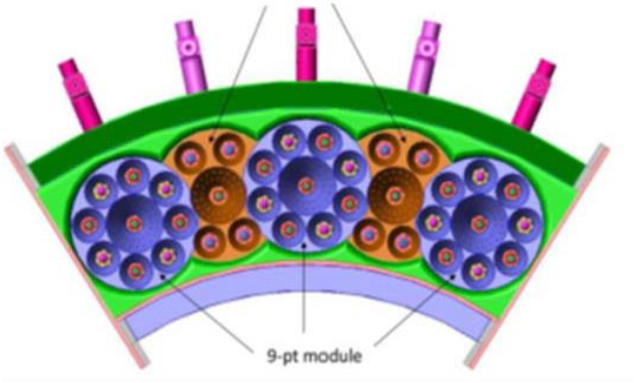

Figure 1-2: Woodward's ERA concept for using arrays of Swirler-Venturi Lean Direct Injectors (SV-LDI). The center injector in each 9 point module is used as a pilot [4].

1.2.2 Variable Geometry

An idea not being addressed by the ERA project is variable geometry. Variable geometry is the physical modification of the geometry by an actuator in real time. A common example is the variable area exhaust nozzle for an

afterburner. Its function is to increase the nozzle exit area to account for the increase in mass flow from the afterburner process [11]. Variable geometry research for gas turbine combustors has covered two areas – zone equivalence ratio control [12], and combustion instabilities suppression [3].

Zone equivalence ratio control is accomplished by controlling the amount of air flow into a zone, given a measured rate of fuel. There have been several configurations researched [13], [14], [15], but they all function in a similar manner, by adjusting the mixer inlet area. Typically, when an adjustment is made to one zone's mixer area, a counter adjustment is made at another part of the combustor to keep the total pressure drop across the combustor constant. In the past, this adjustment mechanism had been in the form of devices like registers, or variable vane angle swirlers [16], [17]. One of the more recent examples by Giuliani et al. [4] uses a pintle style injector, a concept borrowed from the rocket community, to vary the mixer effective area.

The work of Giuliani et al. focused on increasing the operability of the combustor by controlling the flame transition (attached/detached). They showed the air flow through a fixed geometry combustor could only be decreased by 30% before a flame transition occurred, attaching the flame to the hardware. Under the same air flow reduction, they used the injector to reduce the mixer effective area, keeping the fluid velocity high enough to keep a detached, stable flame. This method allowed them to decrease air flow by up to 50% while still keeping a detached flame.

1.3 Overview of Thesis

This work begins the study of variable geometry and combustion design, with the development of an experimental setup. This task is divided into three main parts:

1. Development of lab infrastructure to support combustion experiments, including facilities, measurement and instrumentation, and laboratory automation.
2. Development of an atmospheric LDI combustor with variable geometry features, including design, and initial testing using chemiluminescence imaging.
3. Development of a multiaxis translation table for use with optical diagnostics, to spatially locate multiple burners, providing rapid testing and transition between them.

CHAPTER 2. LAB INFRASTRUCTURE

2.1 Introduction

This experiment is located in the Applied Laser Spectroscopy Laboratory in the Mechanical Engineering building. This lab, formerly known as the Flame Diagnostics Laboratory, has a long and successful history of optical diagnostic development, and application to flames. The focus of this new section of the lab is advanced combustor design, combustion control, and diagnostic techniques. This section will detail the lab layout, facilities development, measurement and instrumentation, a charge-coupled device (CCD) camera for flame imaging, and the automation of the equipment in the lab.

2.2 Facilities

Figure 2-1is an overhead layout of this section of the lab. The combustors are placed on the translation table underneath a fume head. Optics tables are on each side of the translation table. The larger table is for beam generation and tuning, while the smaller table is for collection. Most of the equipment is remotely controlled by a National Instruments PXI-1033 chassis interfaced through a computer. Details of the equipment will be covered in the following sections.

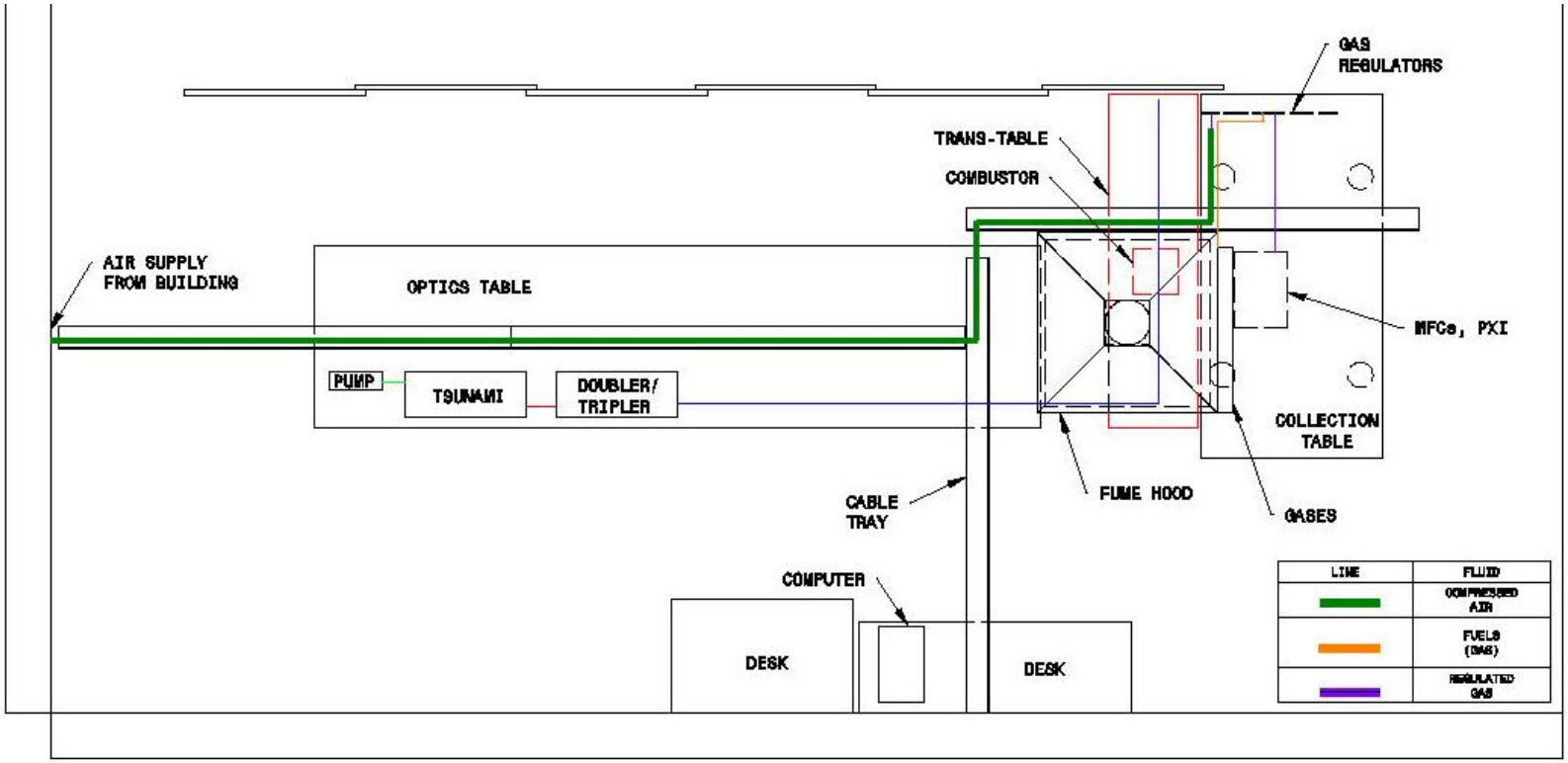

Figure 2-1: Overhead view of lab layout showing optics tables, combustor location on translation table (red), main air line (green), gas regulator panel, and mass flow controllers.

The main air supply for combustion comes from a building air compressor. Since the distance from the wall source to the test area was rather far, time was taken to run ¾" pipe for this section to minimize pressure losses. This system has been measured to 40 cfm output with a 10 psi drop in line pressure. The limitation in output was the measurement device, and it's believed more flow is available based on the small pressure drop in the line. At the wall outlet, a cartridge filter was installed to catch any debris before entering the regulators.

Any gas bottles are kept outside the lab, either in the oxidizer room across from the B102 lab, or the fuel storage area outside of the building. They enter the B102 lab in 3/8" stainless tubing from the ceiling, and distribute next to each fume hood. The lines at the fume hood are quick connect fittings marked by color for fuel, oxidizer, or inert. For safety, there is a normally closed solenoid valve in each line that can be actuated by an emergency shut off button near the entrance to the lab. If gas flow needs to be shut off, it is done so outside at the bottle. Normally the bottles are opened during the day and closed at night if an experiment will be run that day. In cases of extreme cold (<20° F), the regulators outside were found to leak significantly, so the bottle is only opened during the experiment.

A liquid fuel line was installed to be used with Jet-A, or other similar aviation fuels. Figure 2-2 shows a diagram of this system. The fuel is kept in a stainless tank rated for 300 psi. Nitrogen gas from a bottle next to the fuel tank is used to pressurize the fuel tank from the top. The liquid pickup is located at the bottom of the fuel tank. Both the nitrogen gas bottle and fuel tank are kept in a

gas cabinet that is vented out of the lab for safety. An instrument rack panel was fabricated to meter the fuel flow rate by a needle valve and pressure reading. Plumbing and valves were included on this panel to purge the fuel line going to the burner with nitrogen if needed. Before this system was tested, the experiment was switched to gaseous fuel. To finish the liquid fuel system if needed, it should be pressure tested for leaks, and a more accurate metering method installed.

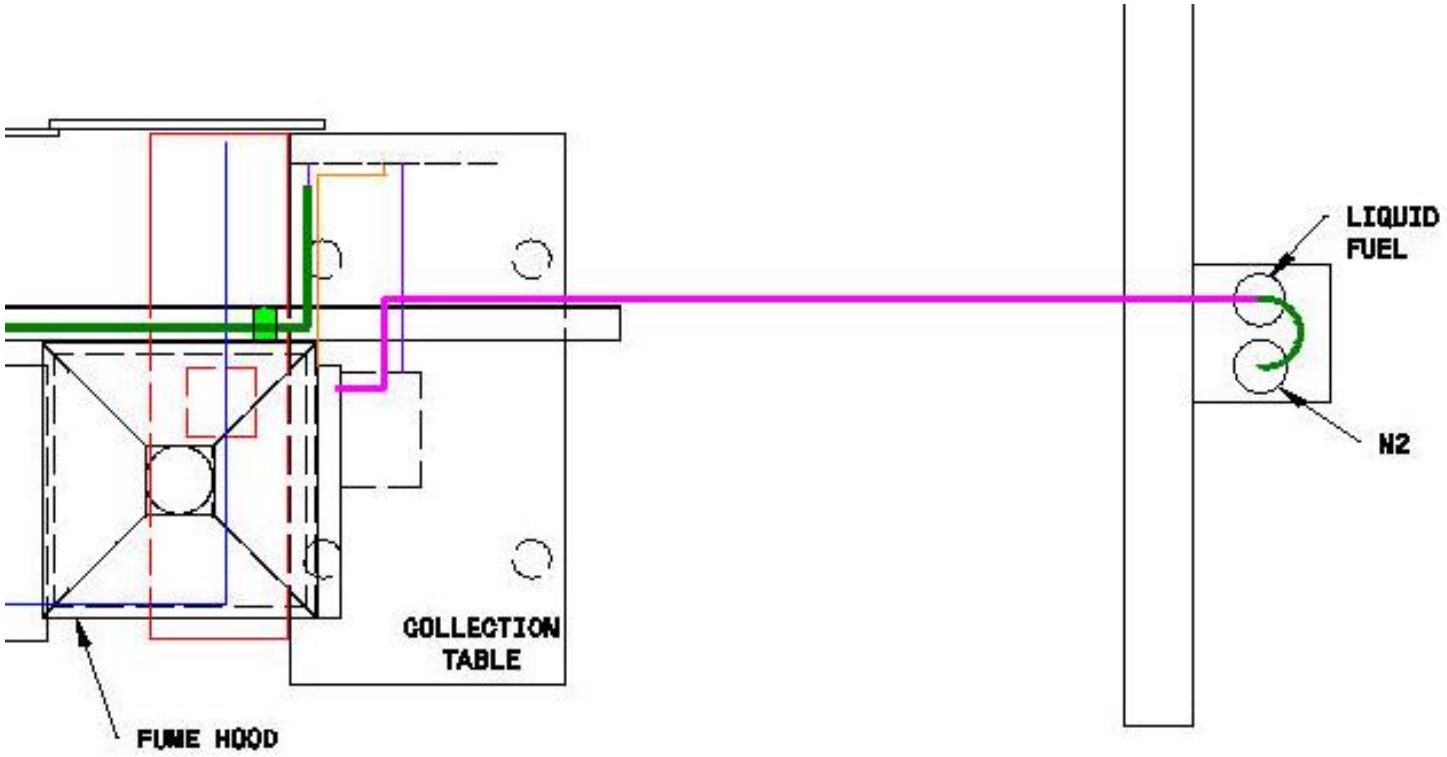

Figure 2-2: Overhead layout of liquid fuel line (pink) running from gas cabinet, where fuel tank and N_2 bottle are stored, to experiment. Fuel tank is pressurized by N_2 bottle and metered by panel near experiment.

2.3 Measurement and Instrumentation

The compressed air and gasses flow from their sources to a regulator panel located underneath the collection optics table. Each line on the regulator panel consists of a shut off valve, gas regulator (Matheson 3476-A), and a pressure gauge. These regulators allow each line's downstream pressure to be adjustable, an important feature with the mass flow controllers.

Mass flow controllers (MFCs) (Porter 203A) are used to meter the gas supplies to the combustor. These mass flow controllers have a built-in thermal mass flow meter, measuring true mass flow based on the cooling effect the process gas has on an internal heating element. They have an internal PI controller that adjusts the proportional control valve to meter the flow. The gains of the controller can be adjusted for each valve. This proved to be a useful feature in the case of controlling a flame, where one valve needs to track another valve to keep a constant equivalence ratio. The valve gains were adjusted to give a quick settling time, and each respond with a similar rate to give equivalence ratio stability. Having too high of an upstream pressure to the valves causes them to oscillate regardless of gain setting. A stable upstream pressure was found to be 50 psi.

The MFCs come calibrated from the factory with an accuracy of +/- 1% full scale (FS). The calibration is based on a specific gas, but a correction factor can be applied if a different gas is used. Up to four MFCs are controlled by the PCIM4 controller box. This desired flow rate can either be set at the front panel of

the controller box, or can be remotely controlled by a computer through an interface on the back.

An orifice plate flow meter (Lambda Square Oripac 5300) was installed in the air line just upstream of the pressure regulators. This orifice plate will be used in parallel with the MFCs to measure air flow supply rate, and has an accuracy of +/- .6% FS. The range of this flow meter, specified upon purchase, is 4-20 cfm with a pressure drop at 20 cfm of 80 inches of water. A differential pressure transducer (OMEGA PX2300-5DI) with a range of 0-5 psid, and accuracy of +/- .25% FS, is used to measure the pressure drop across the plate. The measured pressure drop across the plate is referenced to a calibration given by the manufacturer to find volumetric flow rate. To account for density variations, an absolute pressure transducer (AST 4100) and thermocouple (TBD) are installed just upstream of the plate.

2.4 CCD Camera

A common tool in any combustion lab is a CCD camera used for flame imaging. The system assembled for this lab consists of a UV lens, a CCD monochrome image sensor, a frame grabber, and software. To image hydroxyl at 310 nm, the equipment has to be UV capable. Only a few UV lens manufacturers exist and the one selected was a Coastal Optics 105mm f/4.5 lens designed for 250 nm to 650 nm (Figure 2-3 and Figure 2-4). It has a focal range of .5 m to infinity, and an aperture range of f/4.5 to f/32. It comes with a SLR F mount, so an F to C-mount adapter is used to attach it to the CCD body (Figure 2-5).

Figure 2-3: JENOPTIK's CoastalOpt 105 mm UV-Vis SLR lens with aperture range f/4.5 –f/32, and focus adjustment of .5 m – infinity [19].

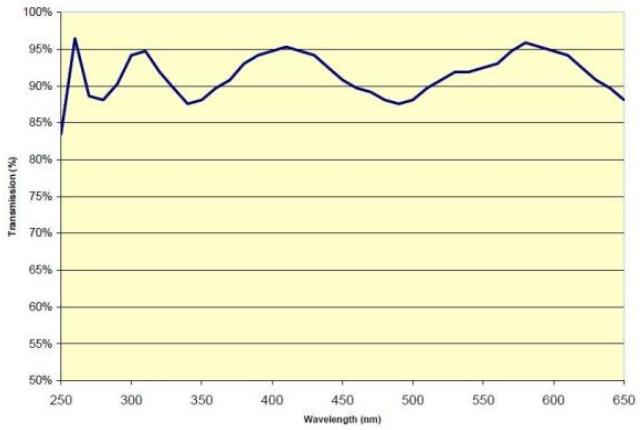

Figure 2-4: CoastalOpt 105 mm transmission curve showing excellent transmission from 250 nm to 650 nm [19].

Figure 2-5: JAI 4200CL-UV image sensor body, with C-mount lens interface, and Camerlink serial communication to frame grabber [20].

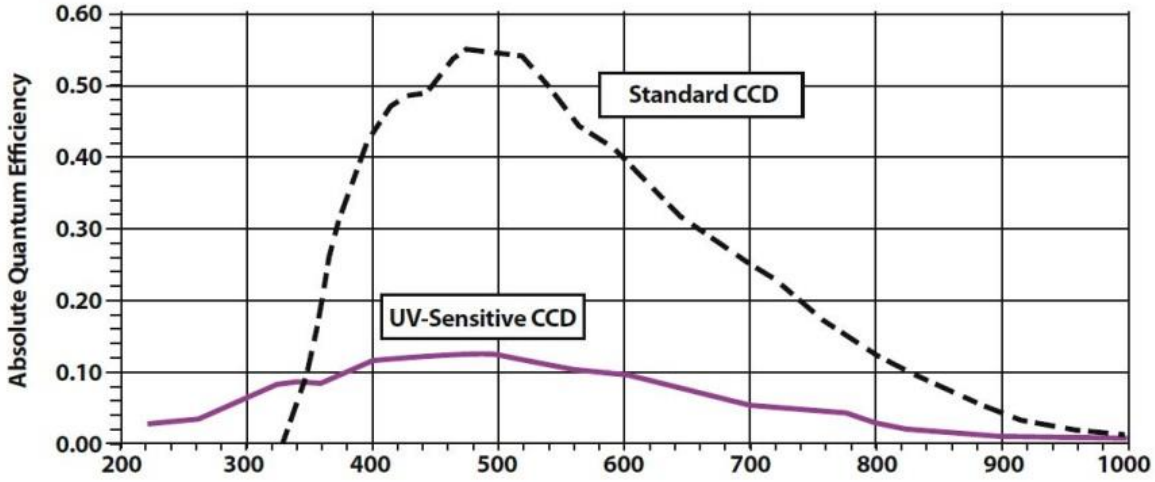

Figure 2-6: Transmission curve of Kodak KAI-4021 image sensor used in JAI 4200 UV CCD camera. UV sensitive option allows transmission at 310 nm with quantum efficiency of 8% [21].

The CCD imager (JAI RM-4200CL-UV) is a 2048 x 2048, monochrome sensor, with the front glass of the sensor removed to improve UV transmission (Figure 2-5 and Figure 2-6). This sensor has an electronic programmable shutter with a maximum frame rate of 30 frames per second. The camera interfaces to an external frame grabber (NI PCIe-1430), mounted in a PCIe slot of the main

computer. The camera functions such as shutter speed, gains, output type, etc., are controlled through JAI's Dualtap software (Figure 2-7). National Instruments© LabVIEW software is used to actually acquire an image. To acquire multiple images, as when doing time-average imaging, the main VI that runs the MFCs and pressure sensors was modified to also control the camera (Figure 2-8). This VI will capture a specified number of photos and save to the main drive for later processing.

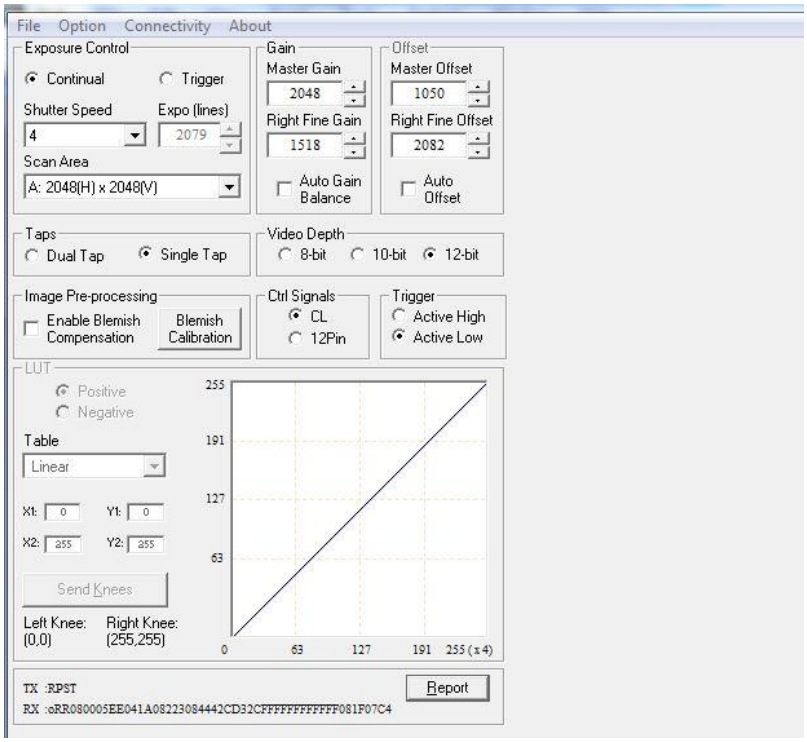

Figure 2-7: JAI's Dualtap software used to adjust sensor settings and debug camera through serial command line.

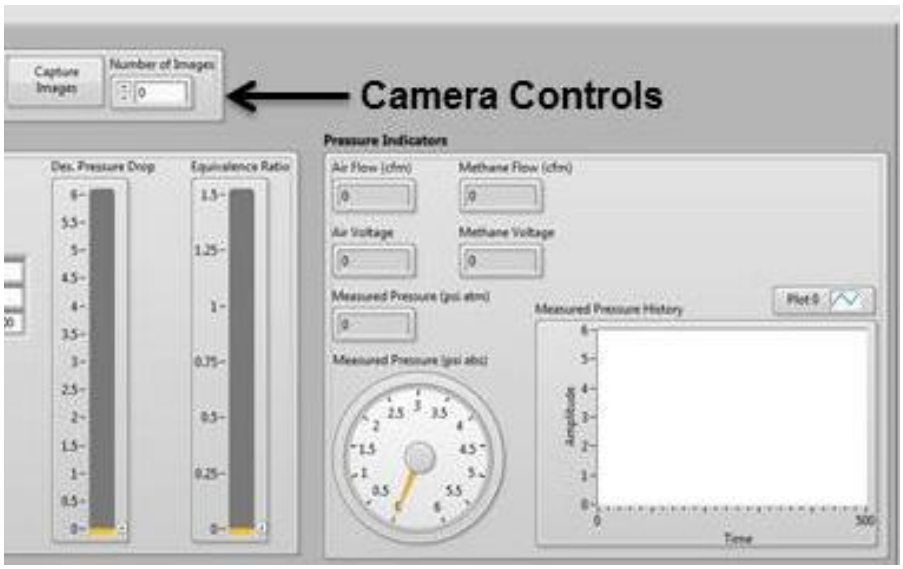

Figure 2-8: Main VI showing camera controls to set number of images to capture, and capture button that begins automated capture process. Images are automatically saved to a file specified.

Filters were purchased for CH*/OH* flame chemiluminescence imaging. These filters thread into the front of the main lens. The CH* filter (Edmund's 65-199) is a 50 mm diameter hard coated filter centered at 436 nm with a full width at half maximum (FWHM) of 10 nm (Figure 2-9). A narrow band filter was desired for imaging OH*, but the cost was prohibitively high, due to the materials needed for imaging in the ultraviolet. Instead, a less expensive alternative was found in the form of Schott UV glass (Hoya U340). This filter's transmission is much wider than a typical band-pass filter (Figure 2-10), but at less than $100 each, was worth trying.

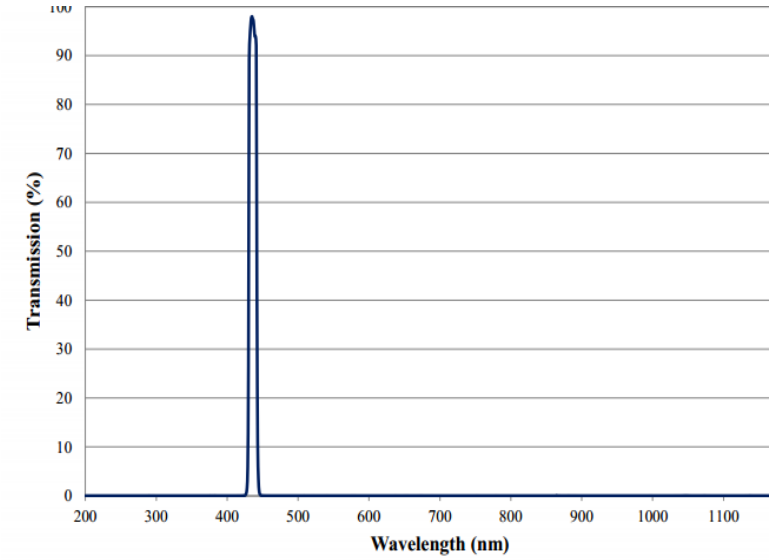

Figure 2-9: Edmund's Optics 436nm band-pass CH* filter, with 10 nm FWHM and 95% efficiency at 436 nm.

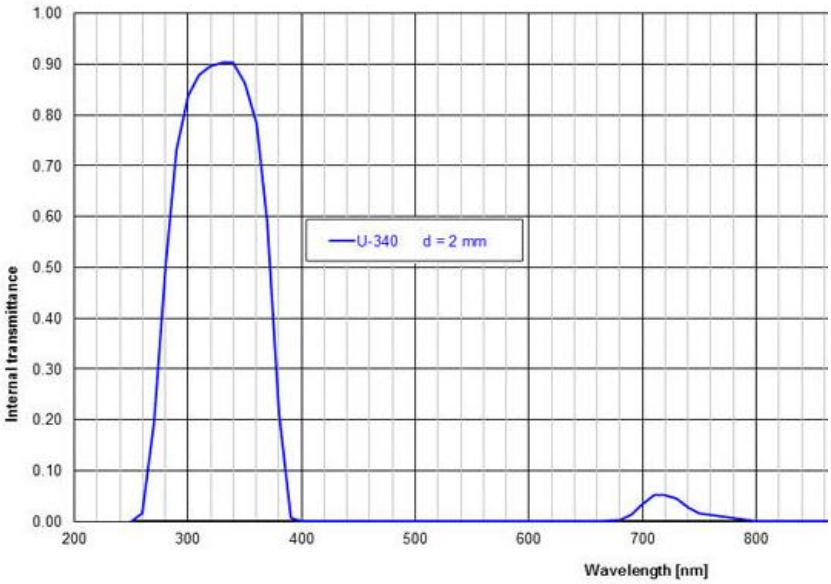

Figure 2-10: Hoya Optics U340 Schott UV glass filter. Filter has above 80% efficiency at 310 nm, but is wider than most band-pass filters used for chemiluminescence and is still being evaluated.

2.5 Laboratory Automation

A National Instruments (NI) PXI-1033 is used to automate the majority of the equipment in the lab. The equipment interfaced with this module includes the mass flow controllers, the P3 pressure sensor, orifice plate pressure sensors, translation table, and CCD camera. Figure 2-11 is the front panel of the Virtual Instrument (VI) used to run this equipment. This automation reduces the workload on the test operator, reduces the testing time, and provides some unique features over manual control. One of the most useful functions is the pressure and equivalence ratio control of the burner. In the combustion community, the air flow through the combustor is typically given as a pressure drop across the mixer, rather than the mass flow rate of air. This pressure drop across the mixer is measured with the P3 pressure sensor (OMEGA PX140), and sampled by the PXI-1033 chassis. A PID controller running on the host computer compares this pressure with the desired pressure drop, and adjusts the air flow from the MFC accordingly. Also, it is more convenient to adjust fuel flow rate by Fuel to Air Ratio (FAR), or equivalence ratio, rather than direct fuel flow rate. The VI uses the current air flow setting to calculate the required fuel flow rate for a specified equivalence ratio, and adjusts the fuel flow rate from the MFC. The operation of the translation table through the VI will be covered in chapter 4.

2.6 Conclusion and Future Work

The lab facilities and infrastructure have been developed to support future combustor development and diagnostic efforts. The development includes lab

layout and organization, facilities, measurement and instrumentation, automation of most processes associated with testing, and an imaging tool for diagnostics.

One of the more important tasks for the immediate future will be ending the construction phase that existed to build up the lab, so that work can begin with the laser diagnostics. There is a need for more instrumentation with the combustor, adding pressure sensors to the confinement for acoustical measurement, and thermocouples to capture the thermal boundary conditions.

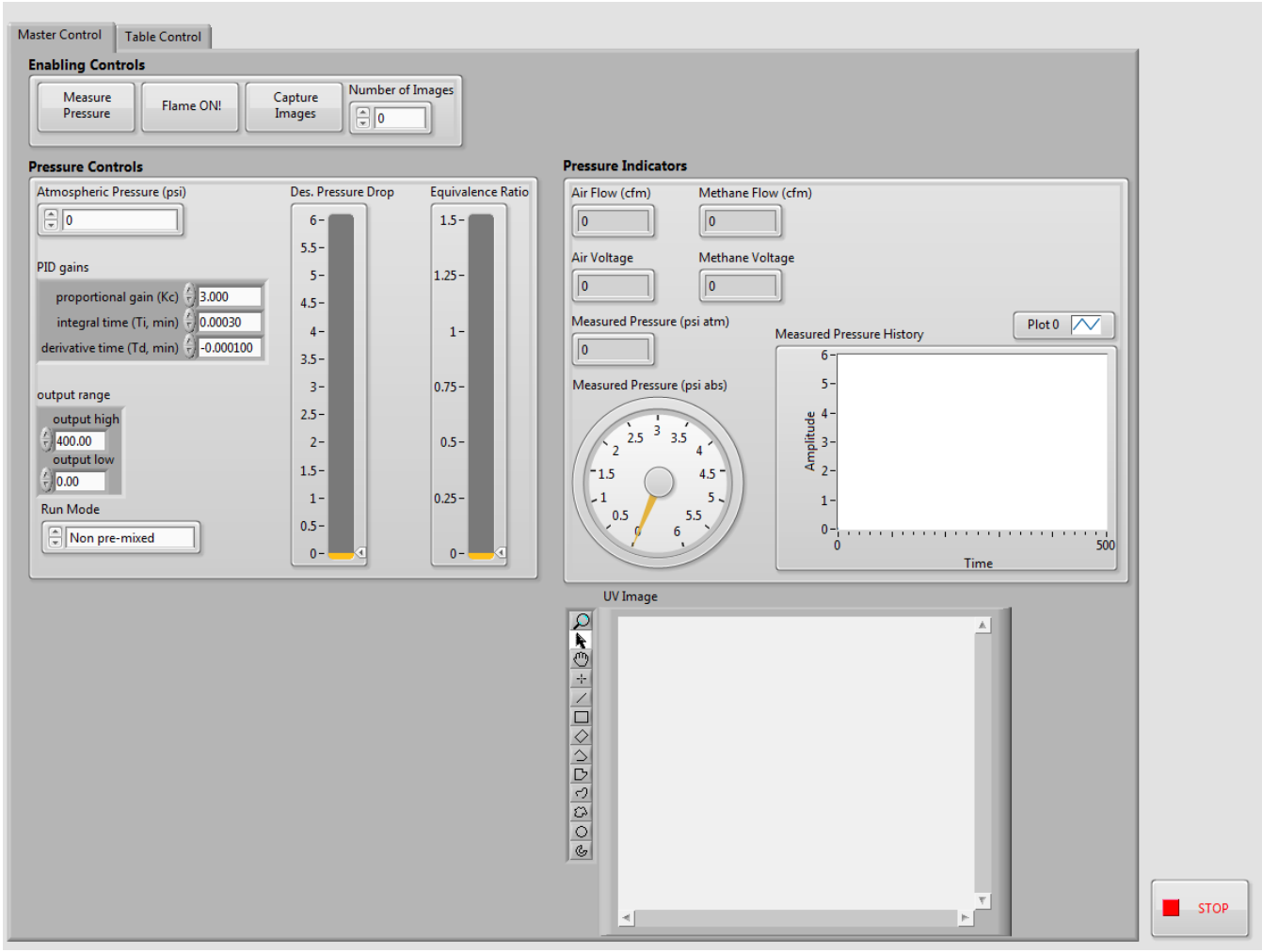

Figure 2-11: Main VI for lab automation. Main user inputs are flow controller enable button (“Flame ON”), desired equivalence ratio and pressure drop, and camera controls.

CHAPTER 3. LDI COMBUSTOR DESIGN

3.1 Introduction

In parallel to building the lab facilities was the design and construction of the first combustor available to the lab – a single element Lean Direct Injection (LDI) combustor. This combustor would be used by multiple groups of students: those within the research group, ME 597 Gas Turbine Combustion I (GTCI) for the Fall 2013 semester, ME 597 Gas Turbine Combustion II (GTCII) for the Spring 2014 semester, and undergraduate Senior Design students (ME 463), also for the Spring 2014 semester. During the semester, each class would focus on a single component of the LDI to study, modify, and test. Each class had their own needs of the LDI which were all incorporated during the design process. After the requirements were defined, the design was completed, and manufactured by an outside machine shop.

From the efforts of the students and course instructors, several accomplishments were achieved with the LDI combustor:

- Advanced Swirler Design and Testing – GTCI
- CFD and Chemiluminescence Imaging – GTCII

- Design and fabrication of fuel injector actuators, a variable impedance exit area, stereoscopic imagers, and improved confinements – ME 463, Spring 2014

The following sections will discuss the design of the LDI, hardware developed by the Purdue classes, and the experimental results of the classes and research students.

3.2 LDI Combustor Design

3.2.1 Need for Developmental Combustor

Mechanical Engineering Professor Galen King and Professor Hukam Mongia saw an opportunity to get non-research students access to combustor design and experimental testing, and also frame it in a way that benefitted the research group with the products of these classes. The experimental testing portion of the courses would require a baseline combustor, whose components were modular to make part revisions inexpensive and easy for the class students. The major components to be designed and manufactured for this baseline combustor were the swirler, venturi, fuel injector, burner housing, and confinement (Figure 3-1). The requirements used to design the LDI were:

- LDI with throat area = .195 in^2
- Inexpensive, replaceable, and quick to change swirlers
- Variable axial injector position: +/- .125”
- Independent coflow circuit for dome cooling
- Expandable to 4 single element LDIs for development progression

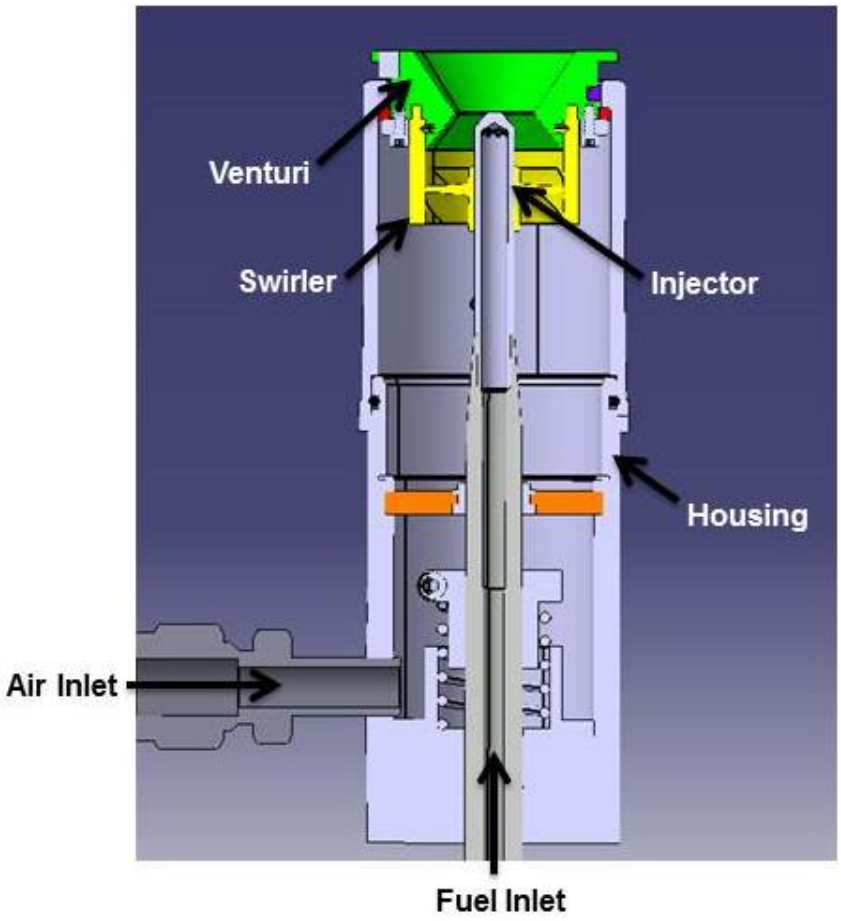

Figure 3-1: LDI cutaway view showing main components: fuel injector, venturi, swirler, and burner housing.

3.2.2 Existing Burner

To save time and expenses, a combustor from a previous project (Figure 3-2) was adapted for the LDI. This combustor could originally be set up in either a Rijke (open-open) or Schmidt (open-closed) configuration. From the original combustor, the base plate, coflow circuit, sintered dome, and 4” confinement chamber were adapted for the LDI, saving many hours and expense.

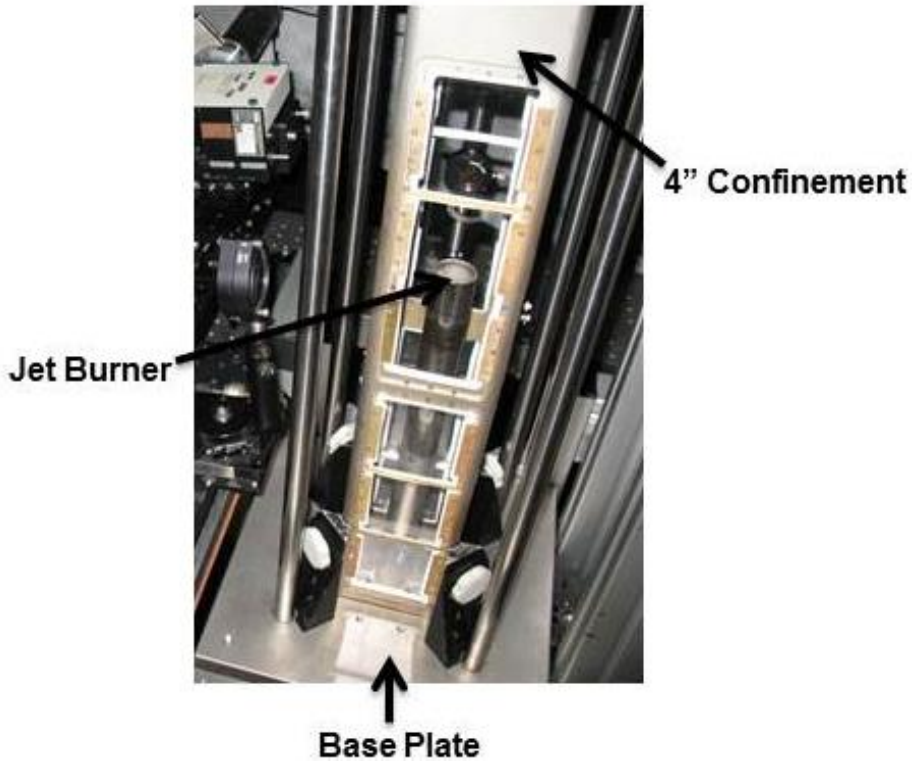

Figure 3-2: Original tube combustor that was reconfigured for LDI. Base plate, 4” confinement, coflow circuit, and sintered dome were reused. Photo courtesy of Andrew C. Nobel.

3.2.3 LDI Design Features

The mixer design is based around a pressure atomizer injector our research group previously possessed. This injector is similar to those used for a Swirl-Venturi LDI (SV-LDI) mixer configuration (Figure 3-3) [22]. This configuration and geometry was adopted for the LDI design because it had been validated for the injector we had, and it could be easily modified to include distinct swirler separate from the venturi, and an axial adjustable fuel injector.

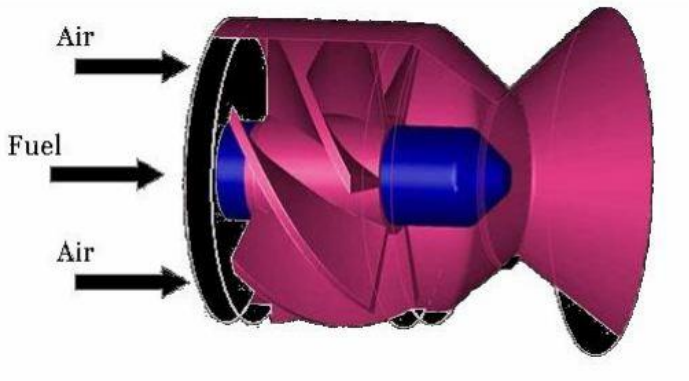

Figure 3-3: NASA-Woodward Swirl-Venturi Lean Direction Injection concept [22].

Since the NASA-Woodward mixer geometry was optimal for the liquid injector supplied to our group, we based the design of our first mixer off this geometry. Some modifications were made to make the swirler separate from the venturi (Figure 3-4), but for the most part it's identical. For the initial testing to be done, containment of liquid fuels was a concern, so a gas injector was designed. The geometry of the mixer was kept constant, except the diameter of the fuel injector was changed to nominal size of .25", for manufacturability.

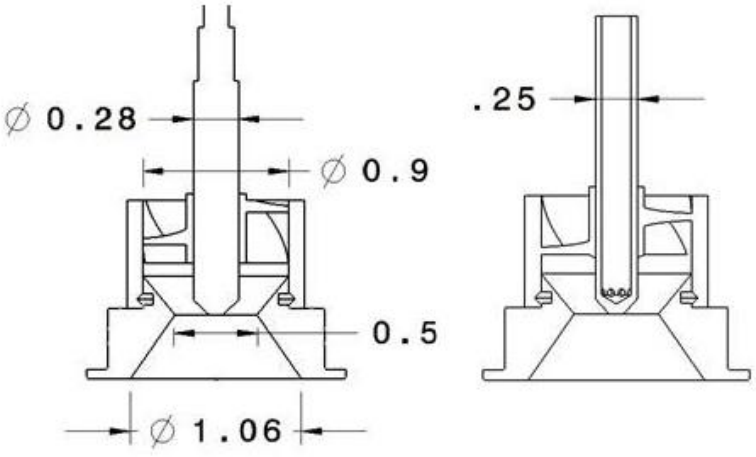

Figure 3-4: Liquid mixer vs. gaseous mixer dimensions. Diameter of gaseous injector reduced to nominal size for manufacturability.

One of the main areas of development for the GTC classes was advanced swirler design. The instructors wanted the students to be able to create many swirler prototypes, so the design goal for the baseline swirler was to make it inexpensive and quick to manufacture. Various research groups have successfully tested 3D rapid-prototype swirlers in atmospheric combustors, so this was selected as the manufacturing method of the baseline swirler. The plastic used by the 3D printer has a melting temperature around 200° F, and survives the combustion environment because the radiant heat from the flame is blocked by the venturi, and the conductive heat transfer through the venturi is offset by the cooling of the combustion air. In testing, for conditions where the flame is detached in the confinement, the swirler doesn't exceed its material limit temperature of 150° F. The failure mode of the swirlers has been heat induced hardening, leading to cracking at the band that engages the venturi. Typical life is a few hours of test time which is more than adequate for these parts that cost a few dollars each.

An additional benefit of the 3D printing is the additive nature of the process allows designs that are not possible by traditional removal-only processing. The students in the classes realized this possibility and took full advantage of it. An example is presented in Figure 3-5, where a fin was added to the swirler blade, for the purpose of creating turbulence to aid mixing.

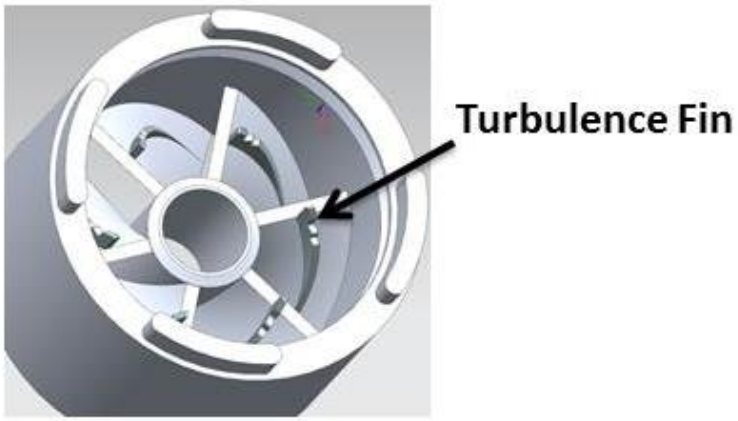

Figure 3-5: GTCI designed swirler with fin added to aid in mixing. This feature would not have been practical with traditional machining, but with 3D printing, it was no more difficult than a normal swirler.

Since students unfamiliar with the burner would be doing the testing, the swirler needed to be easy to install. The swirler is inside the burner housing and cannot be seen, so a mounting system not requiring tools or fasteners was needed. The solution, shown in Figure 3-6, was for the swirler to slip over a shoulder on the venturi. When pushed over the shoulder, the swirler goes over a wire ring installed on the venturi compressing it until the ring reaches a groove in the swirler, where it can expand. This engagement of the ring into the groove provides an axial force keeping the swirler from disengaging. When designing the swirler-venturi interface, it wasn't known if the friction at the interface would be greater than the torque applied from swirling the air. To mitigate this, anti-rotation tabs were added to the swirler that engage pockets in the venturi. After testing, it was determined the friction at the interface is enough and the tabs are not needed.

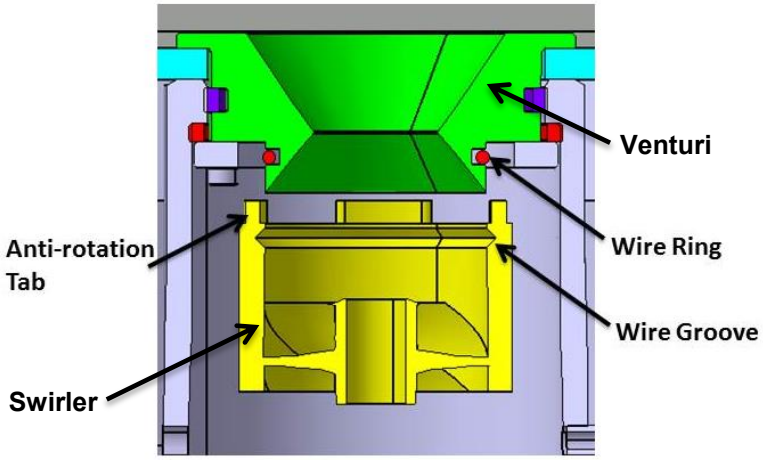

Figure 3-6: Interface between swirler and venturi. The wire ring installed on the venturi expands into a groove of the swirler providing an axial force to keep the swirler on the venturi. The anti-rotation tab engages a pocket on the venturi to keep the swirler form rotating.

To access the swirler to change it, the burner housing separates in two pieces, and the half containing the fuel injector is pulled away from the burner (Figure 3-7). Once the swirler is installed, the fuel injector is guided into the swirler until the burner housing halves engage. The clamp plate, which holds the burner housing in place, is then secured with over-center latches. With this method, the swirler can be changed in less than a minute.

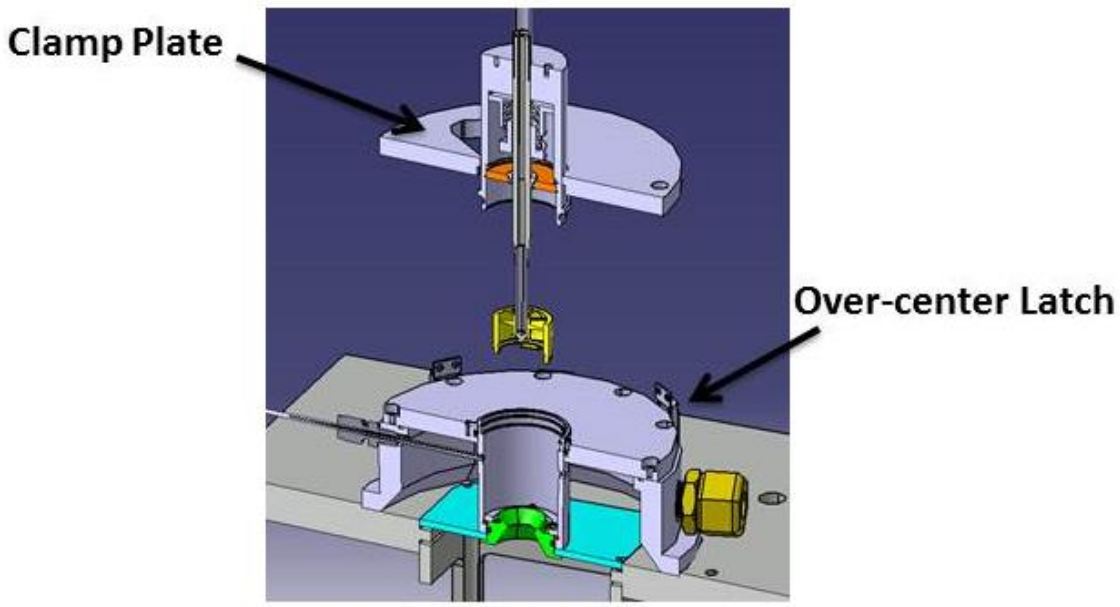

Figure 3-7: Split burner housing to allow installation of swirler. Once installed, the fuel injector is guided into the swirler until the burner housing halves engage. The clamp plate, which holds the burner housing in place, is then secured with over-center latches.

The axial location of the fuel injector was made adjustable by mounting the injector in two bushings (Figure 3-8). These bushings are a precision fit and polished to reduce friction and leakage. An internal compression spring pushing against an external micrometer locates the injector axially. The spring keeps the system always against one side of the micrometer backlash, improving repeatability of the position. The spring seat on the injector is a collar held by the clamping force of a tightened screw. This system allows for +/- .125” of travel from the nominal injector location, which is adjustable by where the collar is tightened on the injector.

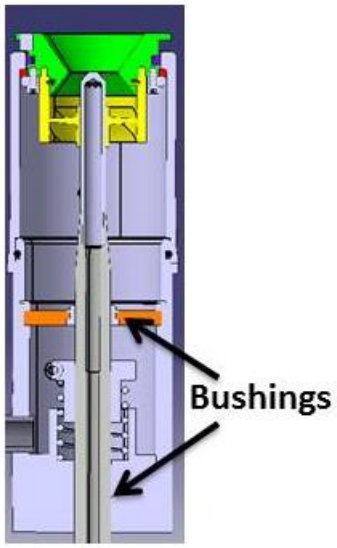

Figure 3-8: Bushing that fuel injector slides in. The top bushing is an aluminum insert into the sintered disc (orange). The bottom bushing is a precision bored hole polished to reduce friction and wear.

To automate the injector movement for control purposes, the micrometer was replaced by a Firgelli L12-50-100-12-I Servo actuator (Figure 3-9 and Figure 3-10). This actuator can travel up 0.5 inches per second, has a maximum force of 10 lbf, and has an accuracy of 0.004 inches. It also has position feedback processed by an onboard microcontroller, so the only inputs are +12 V power and an analog reference signal. For $30 each, this is a great solution for the injector actuator.

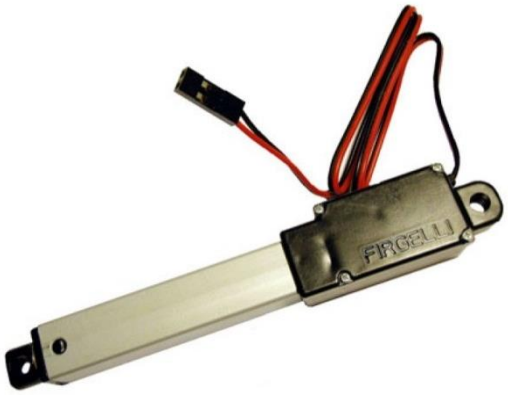

Figure 3-9: Firgelli L12-50-100-I linear actuator used for fuel injector movement.

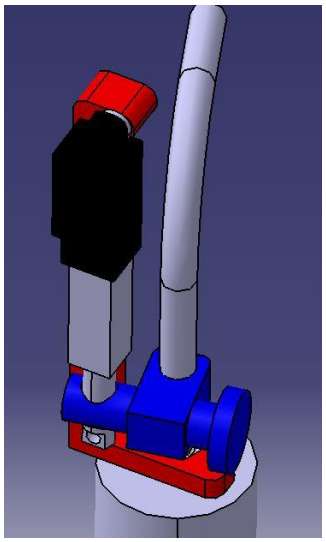

Figure 3-10: Firgelli linear actuator mounted to burner housing by bracket (red), and micrometer clamp (blue).

The base plate for the LDI combustor was reused from the Tube combustor mentioned previously, and had a coflow incorporated into the burner plate (Figure 3-11). This seemed potentially useful for future LDI testing, so the base plate was kept and a new manifold was designed for it. The air enters the manifold on the sides and axially flows through the dome plate to enter the combustion chamber. The dome plate is made of a stainless sintered metal that is fairly restrictive. This restriction creates a pressure gradient across the dome,

which results in a more uniform flow into the combustion chamber. The sintered metal also provides a flashback prevention method, in case premixes are used in the futuref.

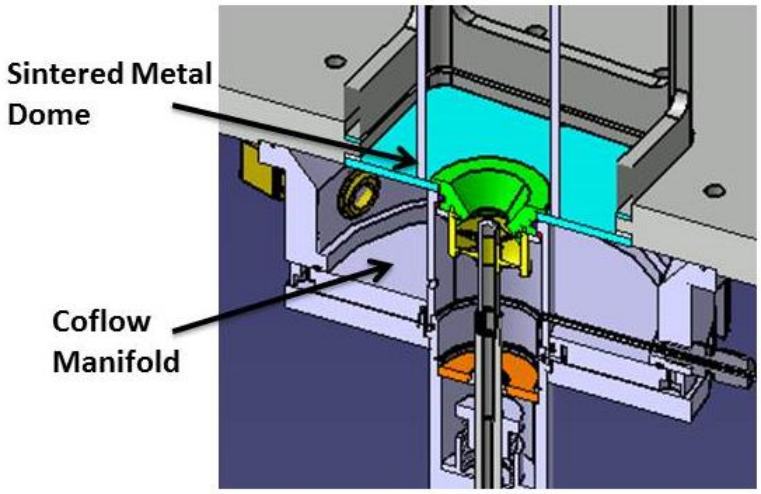

Figure 3-11: LDI Coflow manifold. Manifold air flows through sintered metal dome (blue) into combustion chamber.

After the single element configuration testing had been completed, the testing would move on to a multi-element LDI. To save cost and time, the single element LDI burner housing was designed narrow enough to allow four of them in the 4” x 4” dome (Figure 3-12 and Figure 3-13). This allows all of the original LDI features to be kept and used with the multi-element configuration.

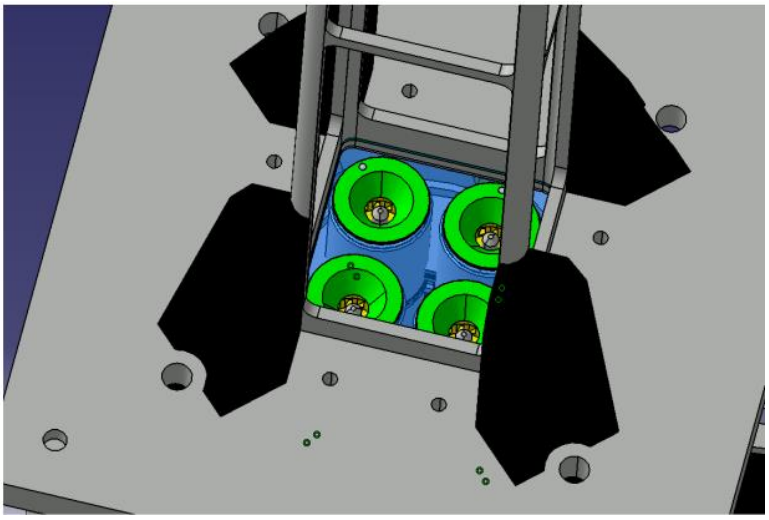

Figure 3-12: Top view of 4 element LDI. This configuration reuses the single element LDI housing 4 times, eliminating costs and design time. It would also allow the original features of the LDI to be kept: variable injector position, independent fuel and oxidizer flows, and independent swirler choice.

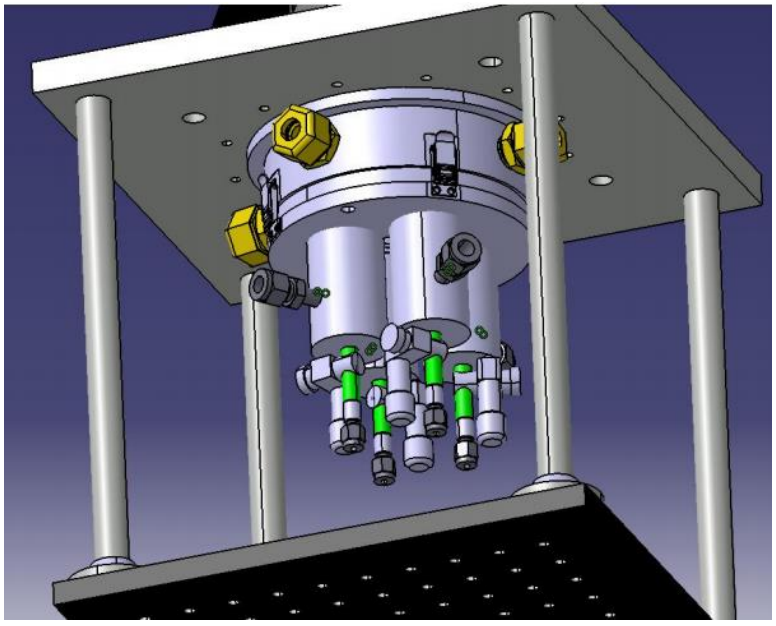

Figure 3-13: Bottom view of 4 element LDI. A new clamp plate and base plate would be needed in addition to three additional burner setups: venturi, fuel injector, swirler, burner housing.

3.2.4 Purdue Class Contributions

The senior design students of ME 463 showed that Graduate students aren't the only ones that can produce good combustion hardware. The projects for this class included stereo imaging devices, confinement chambers, mass flow meters, actuators for the variable injector position, and a variable acoustic impedance area for the exit of the confinement. Two that have already been tested with the LDI and show great potential are a 2" quartz confinement, and the variable impedance exit area. The details as provided by ME 463 will be discussed below.

The 2" quartz confinement group was given the challenge to research existing confinement designs, improve upon them, and reduce cost. The idea they came up with and built (Figure 3-14), has four panes of glass held together by corner pieces of metal angle. There is a ceramic gasket between the metal and glass to reduce vibrations. The design has no machined parts, just beveled glass and 1/2" metal angle, which were both bought to length.

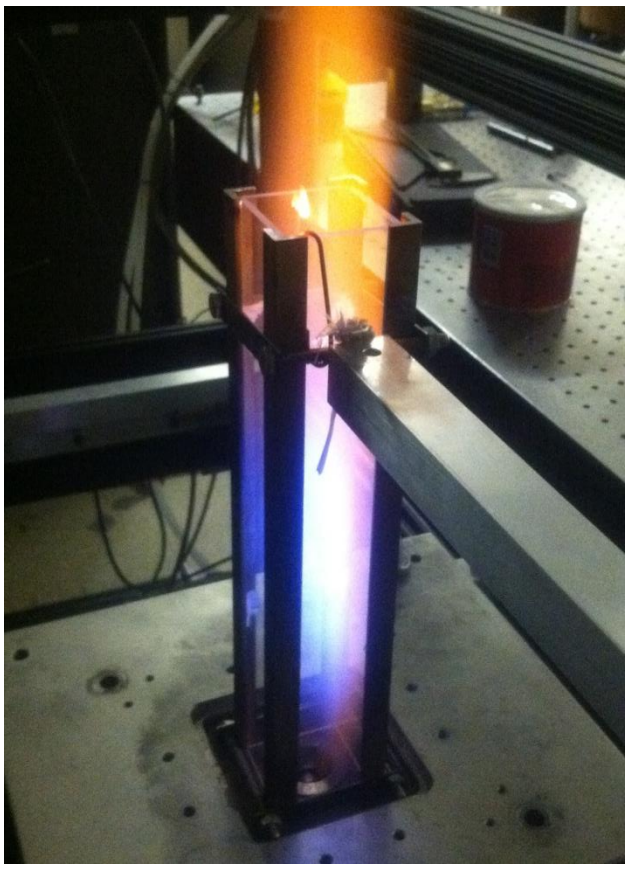

Figure 3-14: ME 463 2” confinement tube being tested with a 45° swirler.

The second device developed by 463 is the variable impedance exit area. The idea behind this device is that an acoustic instability can be tuned out by changing the boundary conditions at the exit of the combustor confinement. Practically, this was done by moving two plates relative to each other to vary the square orifice opening (Figure 3-15).

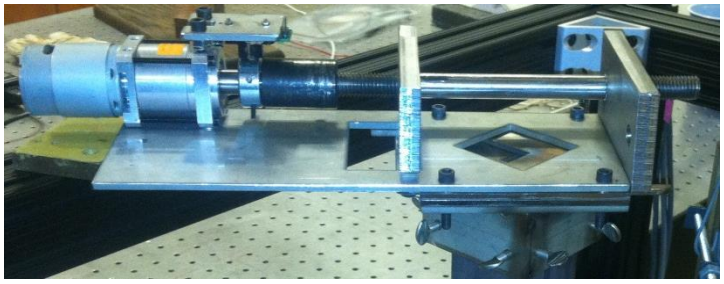

Figure 3-15: Variable impedance exit area developed by 463. The two plates form an exit opening that is varied by moving the plates relative to each other.

The two plates were moved by a common screw joining them. The screw had a right-hand and left-hand thread, so that the plates moved at equal rates but opposite directions (Figure 3-16). This kept the exit opening centered in the confinement. The screw was turned by DC motor being counted by an encoder. An electronics box with manual controls was made to operate this device.

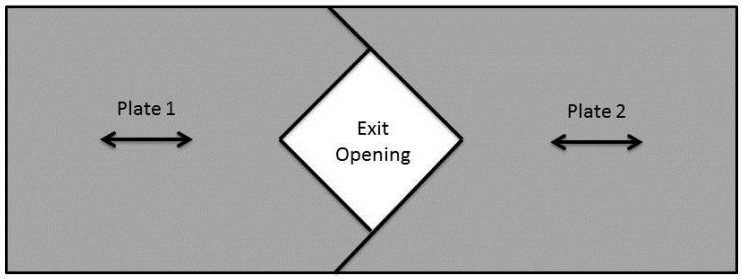

Figure 3-16: Concept of varying exit area by moving 2 plates in equal by opposite directions.

3.3 LDI Test Results

From the class experiments of GTCI and GTCII, and the research students' experiments, much has been learned about combustion testing and development. In the sections below, some of these initial results are discussed.

3.3.1 GTCI Swirler Development

The first course to use the LDI combustor was GTCI for the fall of 2013. Their main objective for the semester project was to design, make, and test their own swirlers. Testing was kept to unconfined flames for simplicity, and the fuel was methane. Over 30 unique swirlers were made by the class participants, all of which still exist, either in storage in the lab, or by a copy of the CAD model. A phenomenon not realized until the end of the semester was the difference adding a confinement makes to flame stability. While testing unconfined, the only flames that had lean blow offs (LBO) near an equivalence ratio of 1 were with high vane angle swirlers with vane angles greater than 60 degrees. Lower angle swirlers such as 45 degrees, had LBOs closer to equivalence ratios of 3 or higher. At the end of the semester, when a 4”x4” confinement was added, we observed that high angle swirlers could now operate closer to an LBO equivalence ratio of 0.6, while low angle swirlers had LBOs around 1.5 on average. Even though the unconfined testing data and images were not of much relevance to combustion development, the time spent testing was good practice at running experiments, and capturing images.

3.3.2 GTCII Injector Position Study

GTC II had fewer students, but more focused and in-depth projects. Rohit Kumar and Nitish Kumar, both graduate students in the School of Mechanical Engineering, did CFD non-reacting simulations of the confined single element LDI. Their work looked at three different injector positions, with 45° and 60° single zone swirlers. Relevant to this project, they found that the movement of

the injector had little impact on mixing improvement or flow field shape. The experimental work that looked at their same conditions found similar results. Figure 3-17 shows the operability curve for a 60° single element swirler, in a 2" confinement. The results show almost no change in LBO or RBO values due to moving the injector. Similar results were found with the 45° swirler.

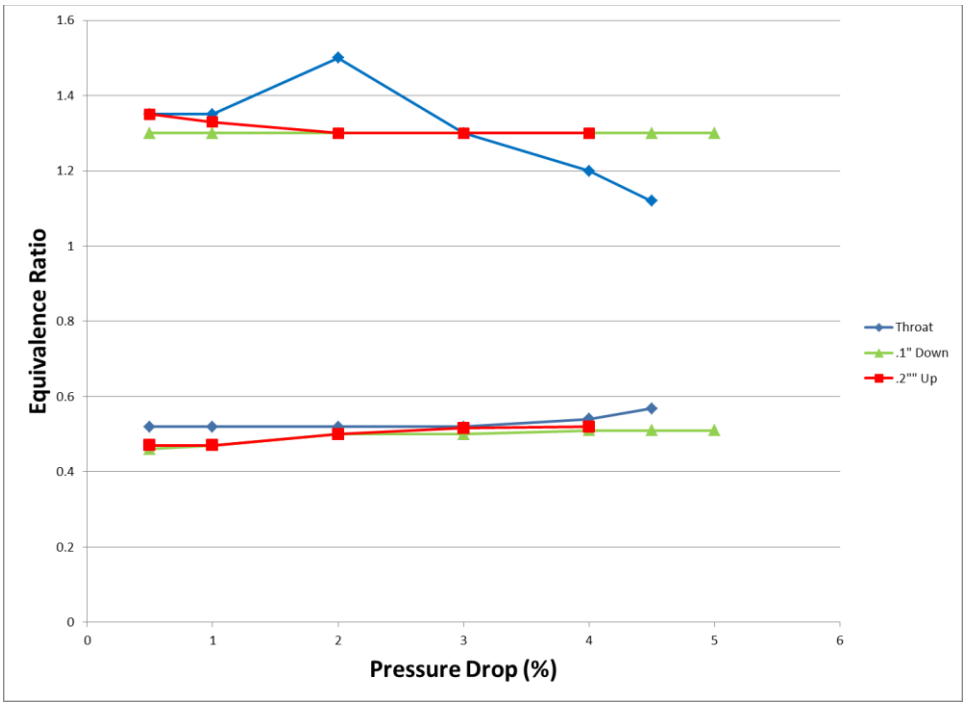

Figure 3-17: LBO and RBO for a 60° single element swirler, with multiple injector positions. Testing showed not significant change in these characteristics with injector movement.

These results are not unexpected. Originally, the mixer geometry was based around the liquid injector, and moving the injector axially would have moved where the fuel was introduced. As mentioned previously, for safety concerns the fuel type was switched to gaseous methane, but the mixer geometry was not changed. Varying the injector location with the gaseous fuel has very little impact, because of how easily the gaseous fuel mixes. Another

concept discussed earlier was the pintle injector, which works by varying the effective area of the mixer [18]. Figure 3-18 shows the measured effective area of the mixer for three different injector positions, for no swirler, a 45°, and a 60° swirler. The results show the 60° effective area is least affected by the injector change. Overall, the effective area of both of the swirlers doesn't vary enough to significantly impact the flow field, and will be a design change for the future.

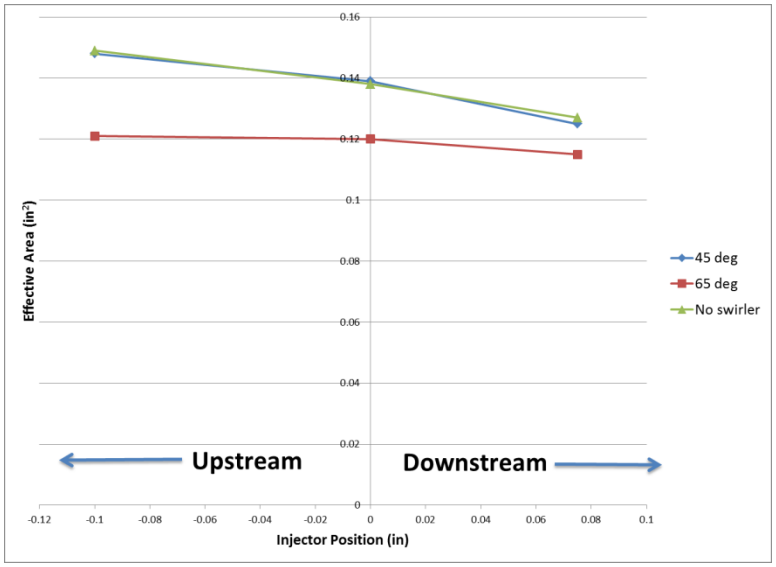

Figure 3-18: Effective area of mixer vs. injector position for no swirler, 45°, and 60°. 60° effective area is least effected by injector change. Effective area ratio of largest over smallest is 1.18 for 45°, 1.05 for 60°.

3.3.3 Chemiluminescence Imaging

An idea for characterizing the effect that the injector had on the flame was to perform chemiluminescence imaging of the flame, as equivalence ratios and injector position varied. Not only was this an interesting idea for studying the flame, but it provided an opportunity to develop our knowledge of chemiluminescence imaging. At the start of this work, although images could be collected and saved, no image processing had been developed. Over the course

of this work, our image processing toolbox was developed and many problems were solved. Some of challenges come from imaging OH, where the CCD camera only has a quantum efficiency of 8%, making signals very weak. The following work will discuss issues associated with generating time-averaged images, and challenges of imaging in the UV.

The experimental setup for this imaging was the LDI combustor with the 2" quartz confinement. Only enough time was available to image one swirler, so the 60° swirler was selected because it had a more defined flame structure than the 45°, and exhibited acoustic instabilities, which the group was very interested in studying. The pressure drop was held constant at 2% because this gave a strong, well-defined flame without burning through too much fuel. The equivalence ratios used were .55, 0.6, 0.7, 0.8, and 0.9. The fuel injector was put at 0.2" upstream, the throat position, and 0.1" downstream.

One issue with imaging the flame comes from a flaw in the geometry of the LDI shown in Figure 3-19. The dome lies in a pocket at ½" below the base plate. This limits the vertical view of any attached flames, like the 60° swirler flame tested here. Also, the width of the corner pieces of the quartz confinement limits the field of view as well; see Figure 3-14. Both of these issues will be addressed for future work.

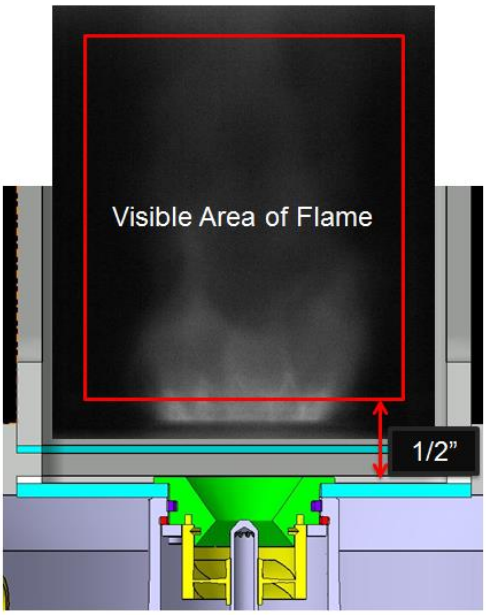

Figure 3-19: View of flame by camera is blocked by walls of confinement, and because the dome lies in a recession that is a ½” below the base plate.

The left hand image of Figure 3-20 shows a time-averaged image of the mean OH intensity. The OH is a very weak signal because of the low quantum efficiency of the camera at 310 nm. Typically, the camera is set with a high sensitivity to increase signal strength (Table 1), but this adds noise and introduces new problems. One of those is a background “ghost” image, as it’s sometime referred to in photography. This “ghosting” is from trapped electrons in the wells of the image sensor. With visual flame imaging, this would not be seen because the voltage added by these is low, but the OH signals are on the same voltage level so it becomes noticeable.

The background ghost image is fairly constant. If the lens cap is put on the camera to provide total darkness, the ghost image is clearly present for at least an hour after the last exposure. Since it was constant, it was found that it could

be subtracted from the time-average images. This was done by taking several images with the lens cap on, and calculating a mean image of the background. This was then subtracted from the time-averaged images. The right hand image of Figure 3-20 shows the image after the background is removed. The vertical fading in the boarder is gone and more contrast can be seen in the flame region.

Table 1: Camera settings during testing.

Camera Parameter/Filter Type	**Visible**	**CH**	**OH**
Exposure Time (ms)	7	28	28
Master Gain	2048		
Master Offset	1050		
Video Output (bits)	12		
LUT Mode	Linear		
Camera body distance to flame	50.5”		
Camera centerline height above dome	3.5”		

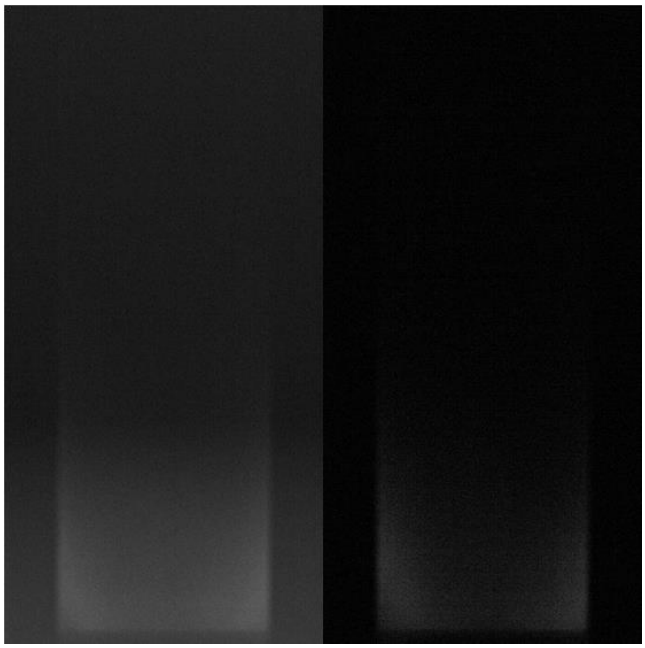

Figure 3-20: Initial image (left); image after background noise removal (right).

Once the ghosting was removed from the time-averaged images, it was possible to calculate the probability density functions (pdfs) of the flame at the various conditions. Figure 3-21 shows the mean, root mean square (RMS), and standard deviation calculated for a particular setting of the injector location and equivalence ratio. When comparing the mean and the RMS, it was noticed that the two were very similar despite expecting more variation due to the turbulent flame. This is due to the relative size of the mean compared to the amplitude of pixel fluctuation. In terms of signal power, the ratio of power from the mean component to the fluctuating is typically 30 to 1, thus making the RMS ineffective at showing pixel fluctuation. For this reason, standard deviation will be used, as opposed to RMS, to characterize pixel fluctuation.

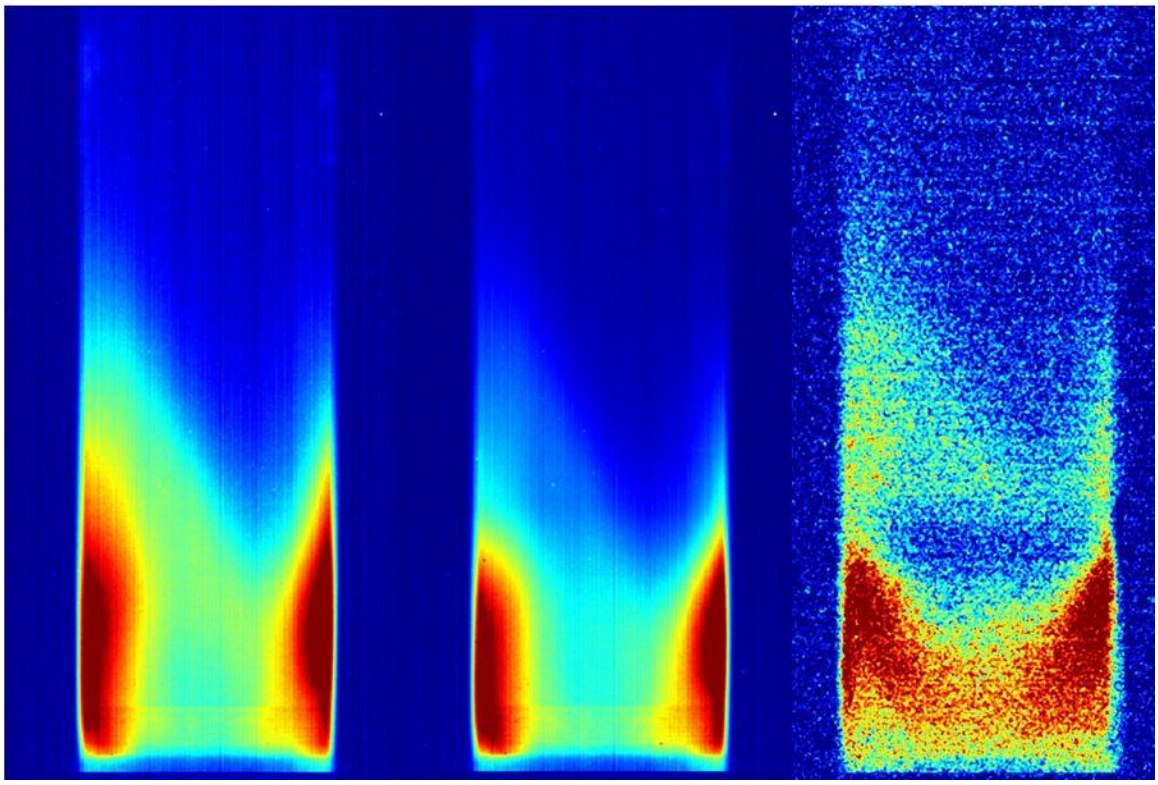

Figure 3-21: Three images showing the mean, RMS, and standard deviation.

The standard deviation being more sensitive to fluctuation also makes it more sensitive to noise on the image if the amplitudes are similar. This produces a “grainy” look, as seen in the left image of Figure 3-22. To reduce this, a digital spatial filter tool in MATLAB, “imfilter”, was applied to the standard deviation images. The kernel used was a correlation type with equal weights. No padding for the boundaries was used since the region of interest, the flame, was not near them. Future work will have to be done to validate that no information of interest is lost.

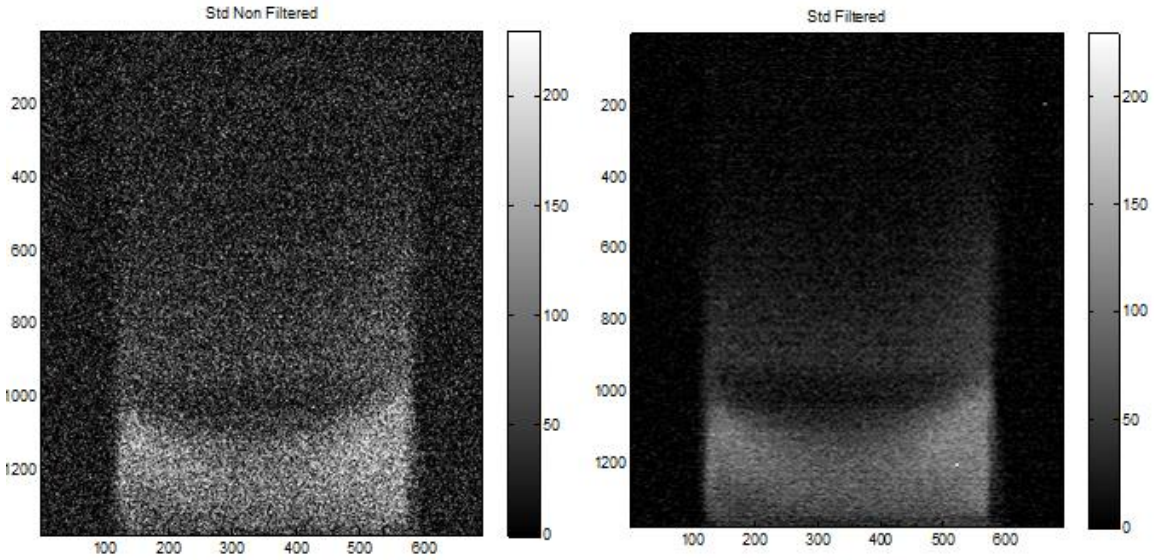

Figure 3-22: Image before and after spatial filtering.

After the imaging toolbox was developed to create time-averaged images from the instantaneous photos, as well as improve noise issues, false color pdfs were created to begin to characterize the flame. Figure 3-23 through Figure 3-26 show the mean and standard deviation of CH and OH intensity. The panels are arranged with increasing equivalence ratio in the x-direction and injection position changing in the y-direction.

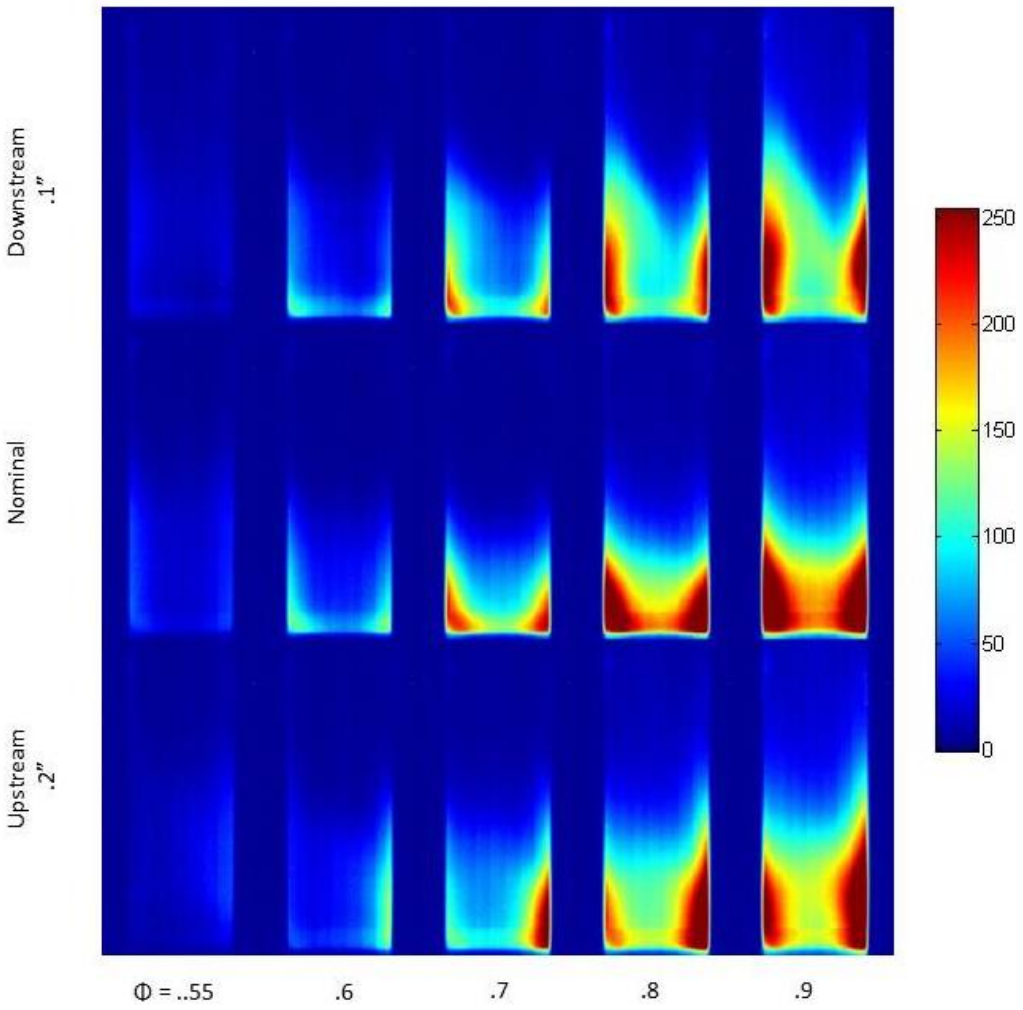

Figure 3-23: Panel showing mean CH images. Flame profile progression with equivalence ratio is as expected.

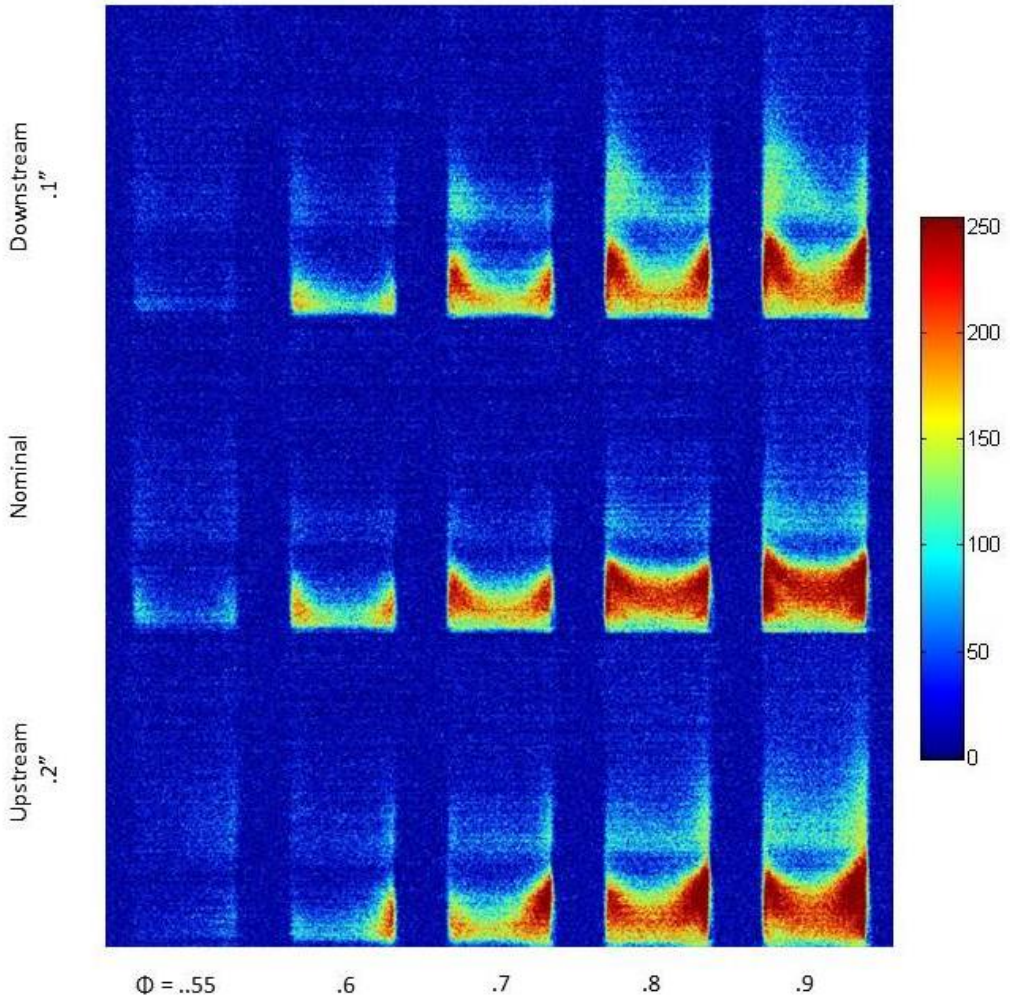

Figure 3-24: Panel showing standard deviation of CH images. The light colored area immediately above the flame is believed to be an artifact of the background noise removal process.

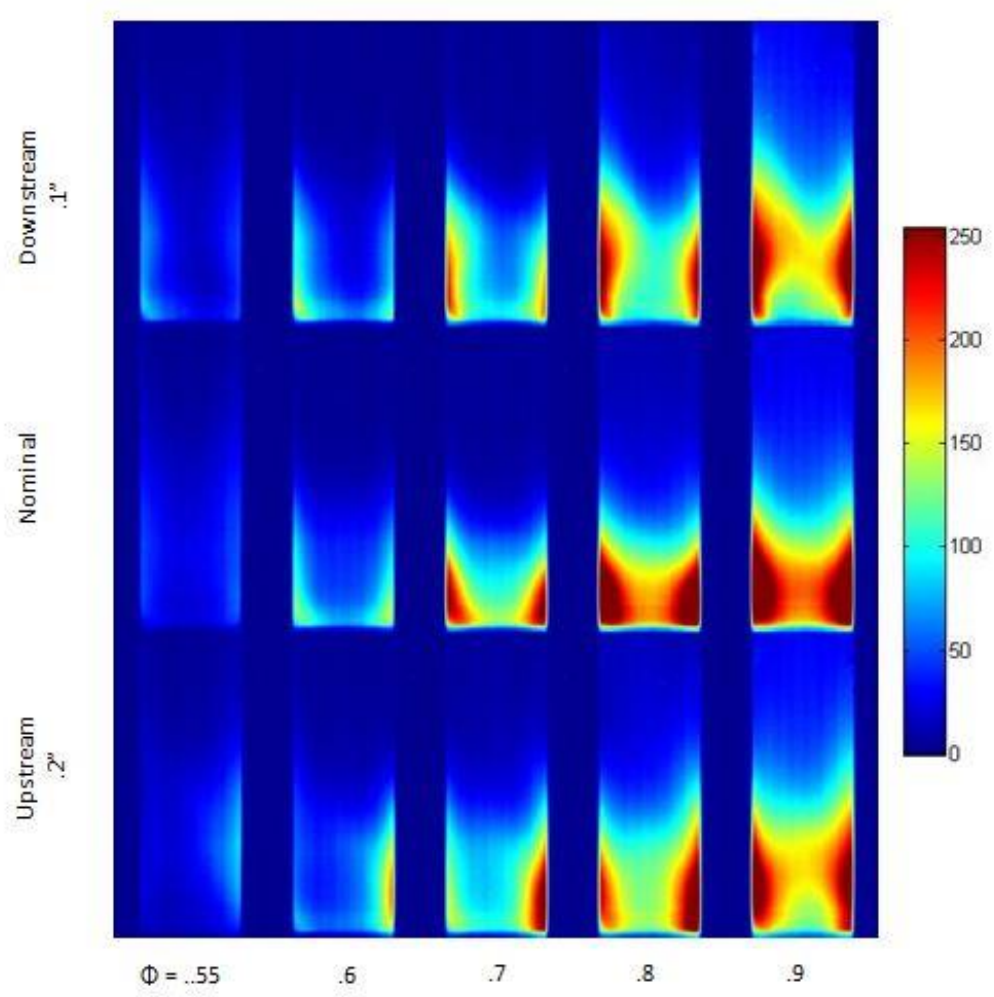

Figure 3-25: Panel showing mean of OH images. Concentrations were expected to be outside of the areas that CH occupied; however, we see that both CH and OH lie in the same region.

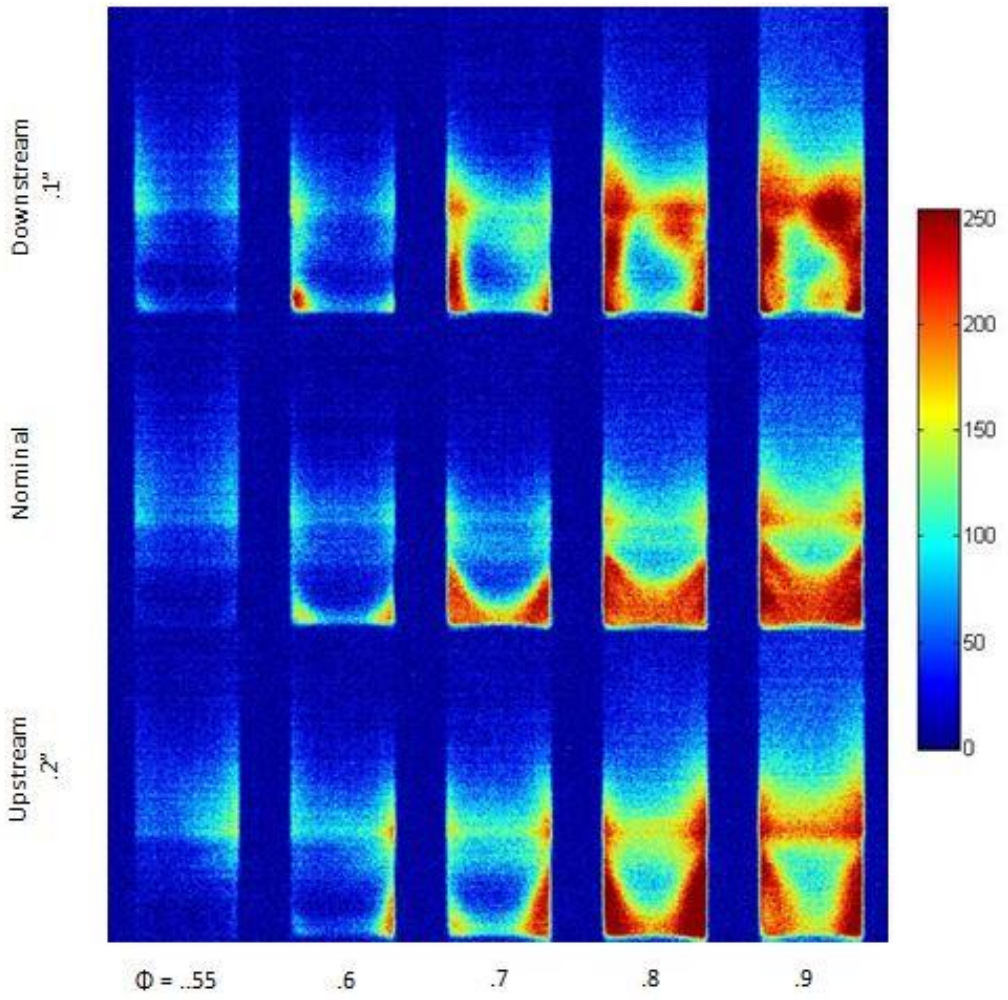

Figure 3-26: Panel showing standard deviation of OH images. The light colored area immediately above the flame is believed to be an artifact of the background noise removal process.

The OH and CH images did not show the results expected. With OH being a product on the lean side of the flame, and CH being a product on the rich side, it was expected the OH and CH concentrations would be located in different regions. This distinction is not present in the images. This is believed to be partially due to the limited optical visibility issue discussed above. The images are of the tail and plume of the flame where OH concentrations will be weaker,

and mixing of the products has occurred. The background noise removal will have to be corrected in another manner, as it's believed there are artifacts from it mentioned in Figure 3-24 and Figure 3-26.

During testing, it took approximately 90 seconds to acquire 100 images. This is a significant amount of time, so the images were checked for consistency from start to end. Figure 3-29 shows the statistics for a particular pixel from the flame area over the 100 samples taken. The three panels show pixel intensity, mean pixel value, and standard deviation of pixel value. A window of 20 samples was used to calculate the mean and standard deviation.

Figure 3-27 and Figure 3-28 show the mean and standard deviation CH image panels where each image is the time average of 20 images from the same combustor setting. The panels are binned by 1-20, then 21-40, up to 100. Visual observation shows little variation in either the mean or standard deviation, indicating the flame is consistent over the 90 seconds it took to acquire the images.

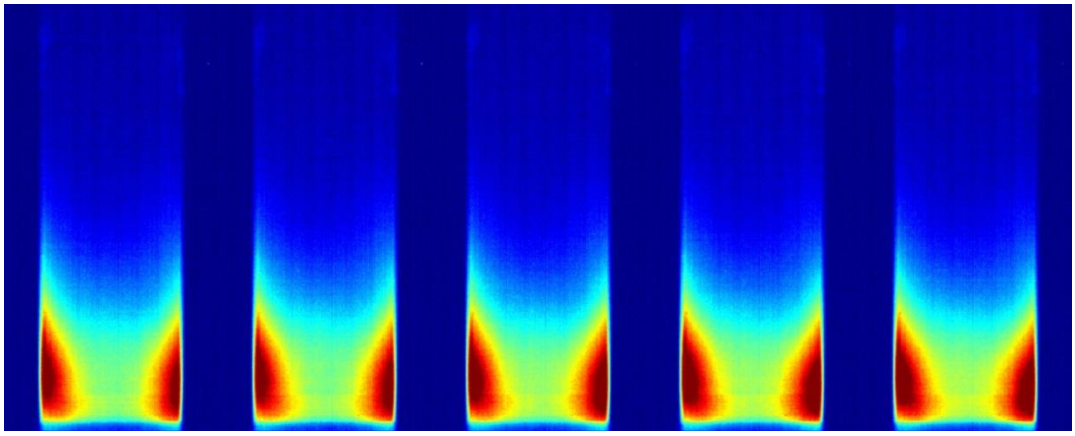

Figure 3-27: CH image mean variation over 100 samples; binned by 20 images.

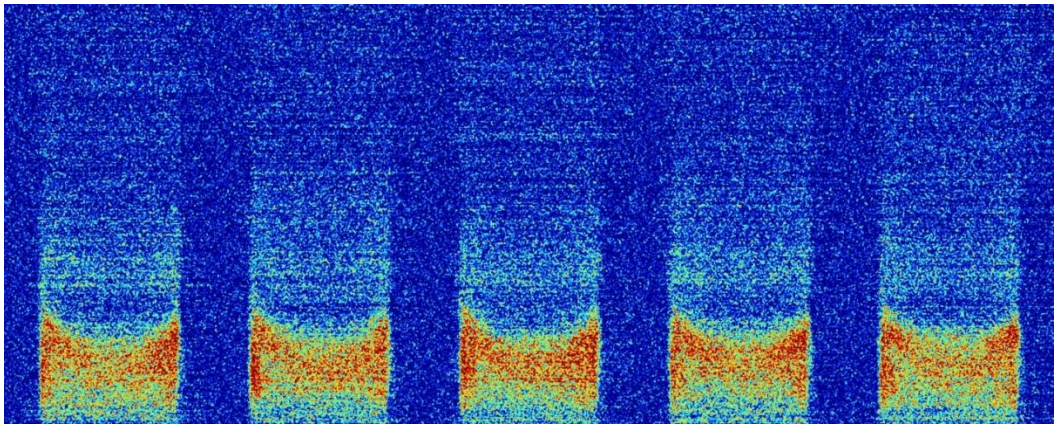

Figure 3-28: CH image STD variation over 100 samples; binned by 20 images.

Taking 90 seconds per combustor configuration to acquire 100 images is too long. Reducing this time would help minimize the change in the time-dependent conditions of the combustor giving better diagnostics. Combine this time with having to do it at every test point of interest and doing a full mapping of a combustor becomes impractical for the operator's time, fuel cost, and time on hardware. Although the capture rate for the images can and will be improved in the future, reducing the number of images needed is one of the easier solutions to reduce the total time of the experiment. Figure 3-30 shows the convergence of the mean and standard deviation with sample size and indicates a much smaller sample size could be used. This convergence is somewhat based on the exposure time of the camera and turbulence of the flame. A longer exposure would lead to less variation in the pixel intensity due to the integration effect of exposure time. A more turbulent flame would need more samples to converge. A method to choose sample size for future test would be to take a large sample size at the exposure setting of interest of the flame at a test point of interest and look at the convergence rate to select the sample size for the rest of the test.

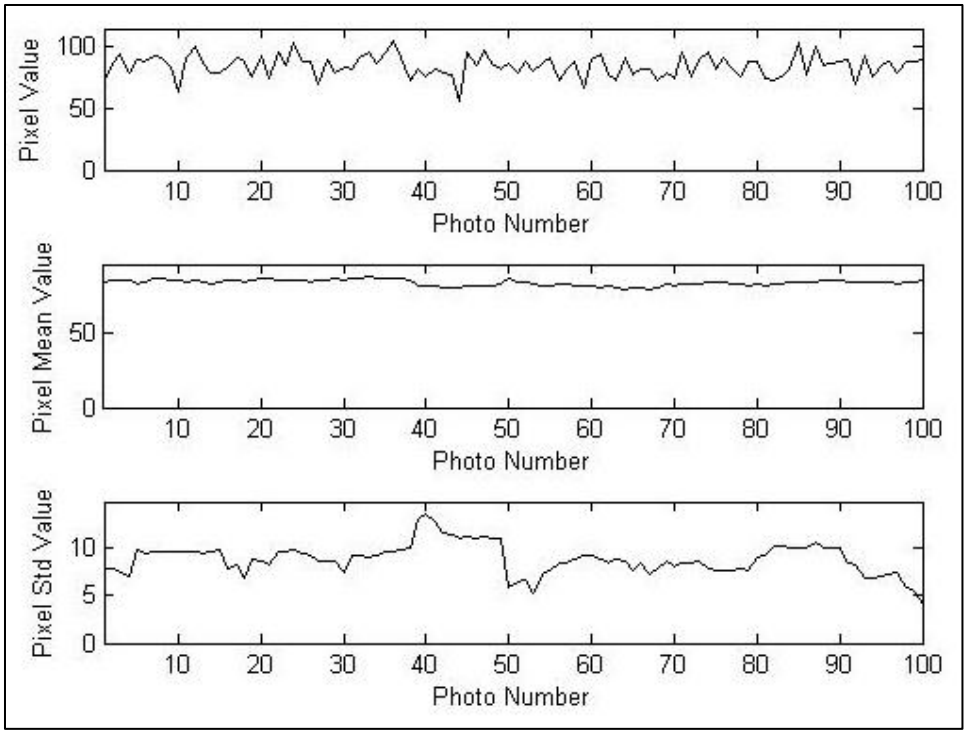

Figure 3-29: Variation of statistics as over samples taken.

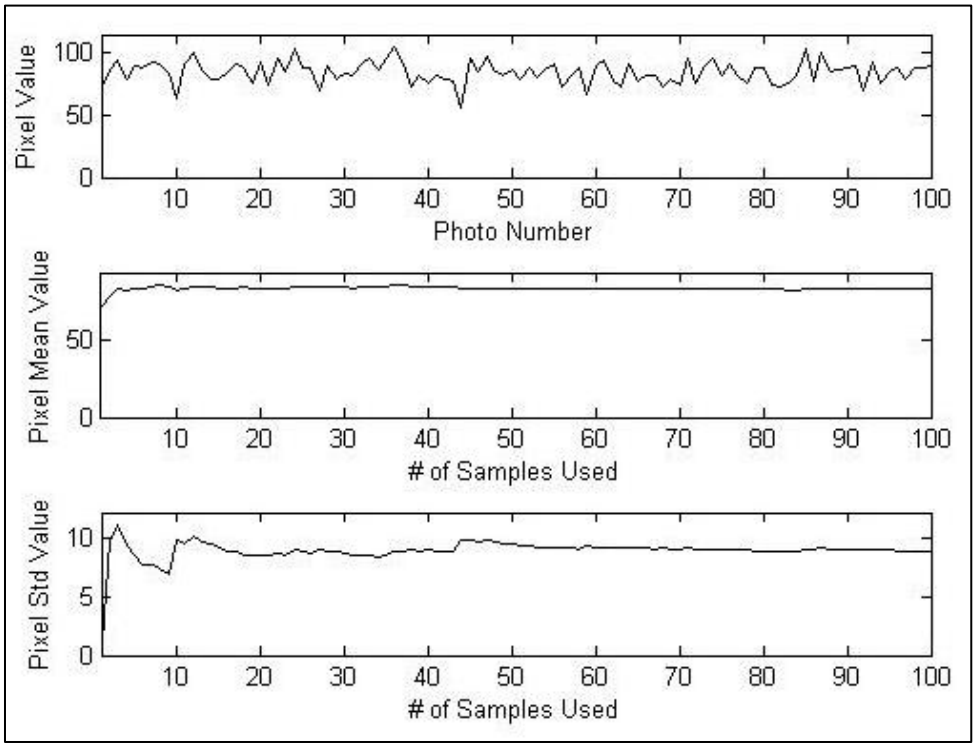

Figure 3-30: Convergence of statistics with number of samples taken.

3.3.4 Combustion Instabilities

A key element that future combustion control must deal with is combustion instabilities. While instabilities are a problem for the combustor designer, in our case, it was a positive result to find that our setup could produce them, since they will be necessary to test future control methods.

The instability was found to be dependent on the vane angle, only occurring with a 60° swirler, and not the 45° swirler used previously in the chemiluminescence imaging. The instability was also found to be strongest when the injector was at 0.2” upstream. Injector positions at the throat and 0.075” downstream were also tested. The throat exhibited some instability signature while the downstream case had none detectable.

The instability was strongly dependent on equivalence ratio, and occurred in a range of 0.6 to 1.1. Figure 3-31 shows a test where equivalence ratio was swept as the pressure was measured. Of interest was the instability frequency, so the data from the equivalence ratio sweep was selected at a few points for a Fast Fourier Transform (FFT) to be performed.

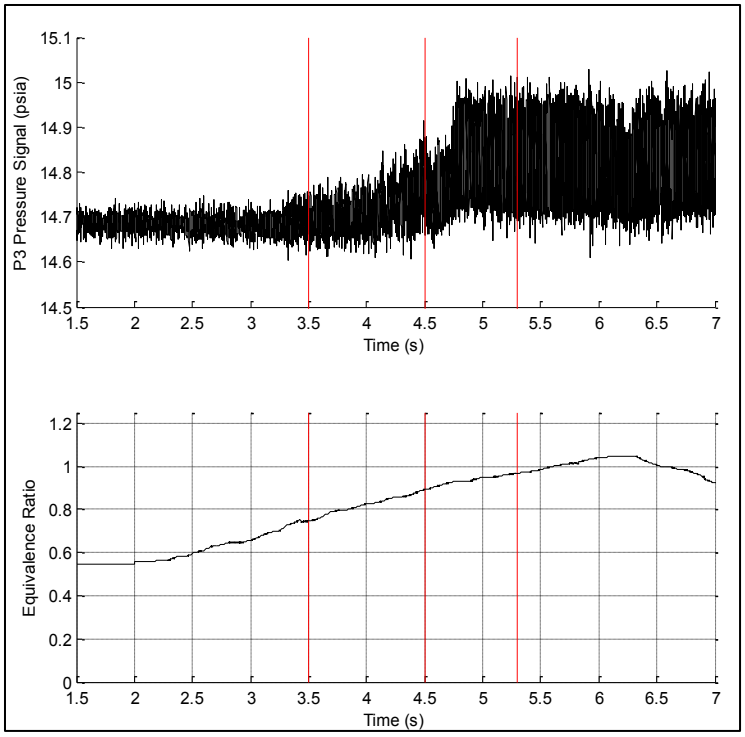

Figure 3-31: Measured instability as equivalence ratio was swept. Instability was found to exist in between .6 to 1.1 with maximum strength at .9. Red lines indicate center point of window for FFT.

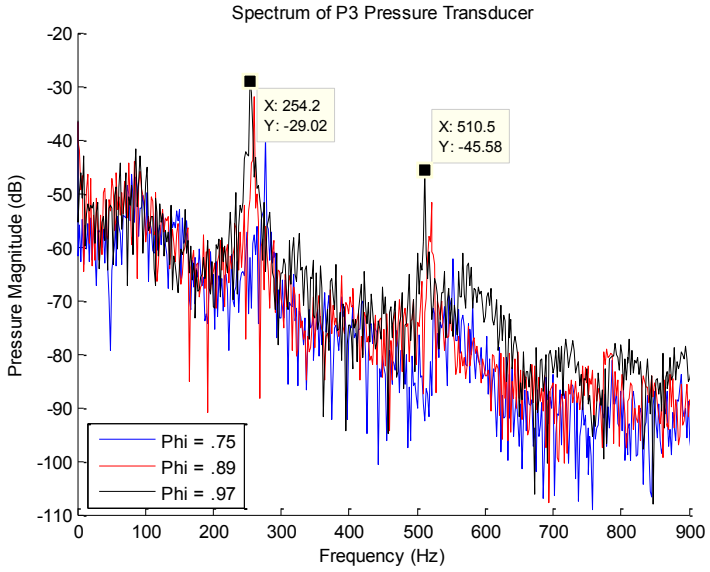

Figure 3-32: Instability spectra at three different equivalence ratios. The primary modes as seen in this figure are at 255 and 510 Hz. The data also indicates the instabilities decrease in amplitude as equivalence ratio increases.

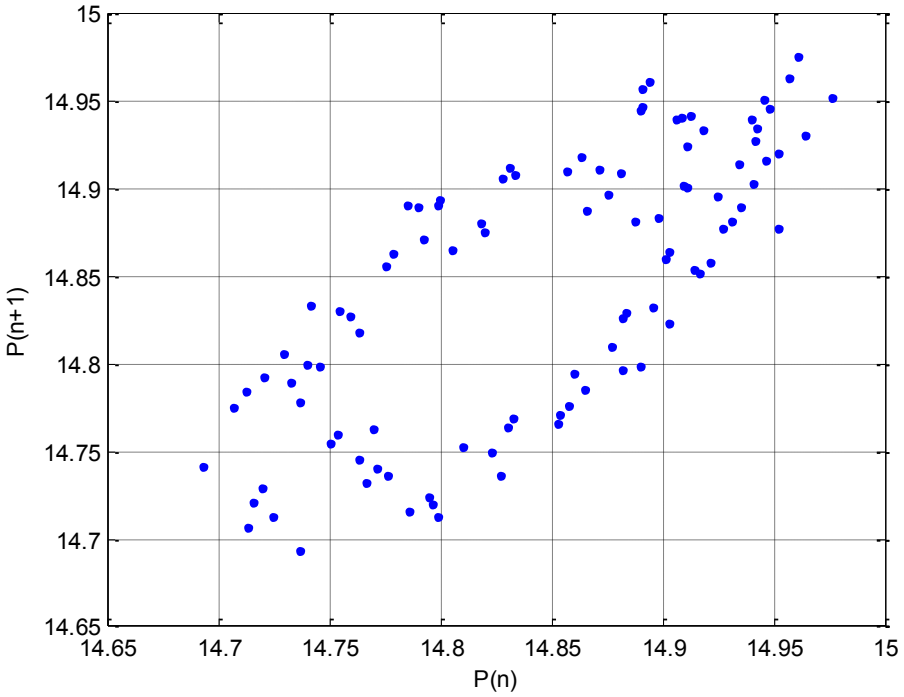

Figure 3-33: Phase plane of time lagged pressure measurement.

The frequency spectrum is shown in Figure 3-32. The main amplitudes are approximately 255 and 510 Hz. As shown in the figure, the peak frequencies decrease as equivalence ratio increases. The reason for this is unknown at this time.

The second test was performed in order to see the ability of the ME 463 Variable Impedance Orifice to dampen the instability. To do this, the device was set at a measured opening, the flame was lit, and the pressure was recorded. During all these tests, the pressure drop and equivalence ratio were constant at 2% and .9 respectively.

Figure 3-34 shows the pressure trace from the 2nd test condition which had an orifice area of 1.83 in^2. The first obvious feature of the series is its growth

with time. This growth was heard and very noticeable. To try and minimize the error due to the transient nature of the instability, the FFT's for the four time series were calculated as close to the end of the series as possible. Figure 3-35 shows the frequency spectra for the four exit areas tested. The responses show the instability decreases as the exit area is closed.

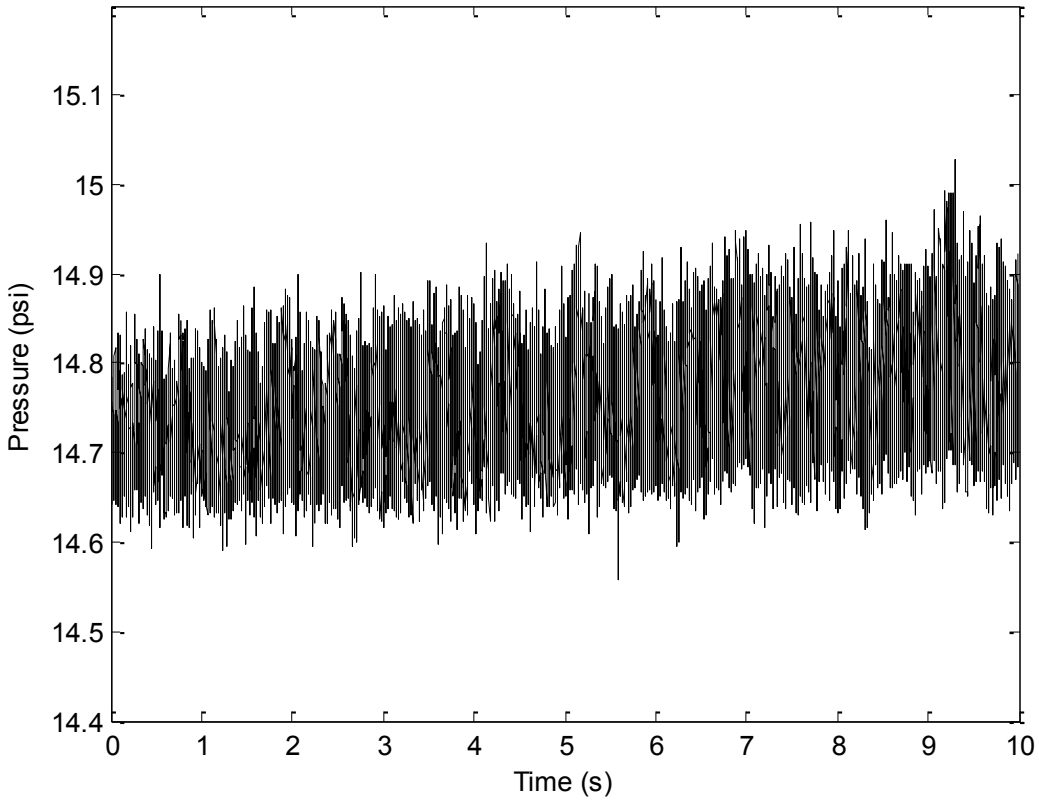

Figure 3-34: The pressure trace from the second test condition.

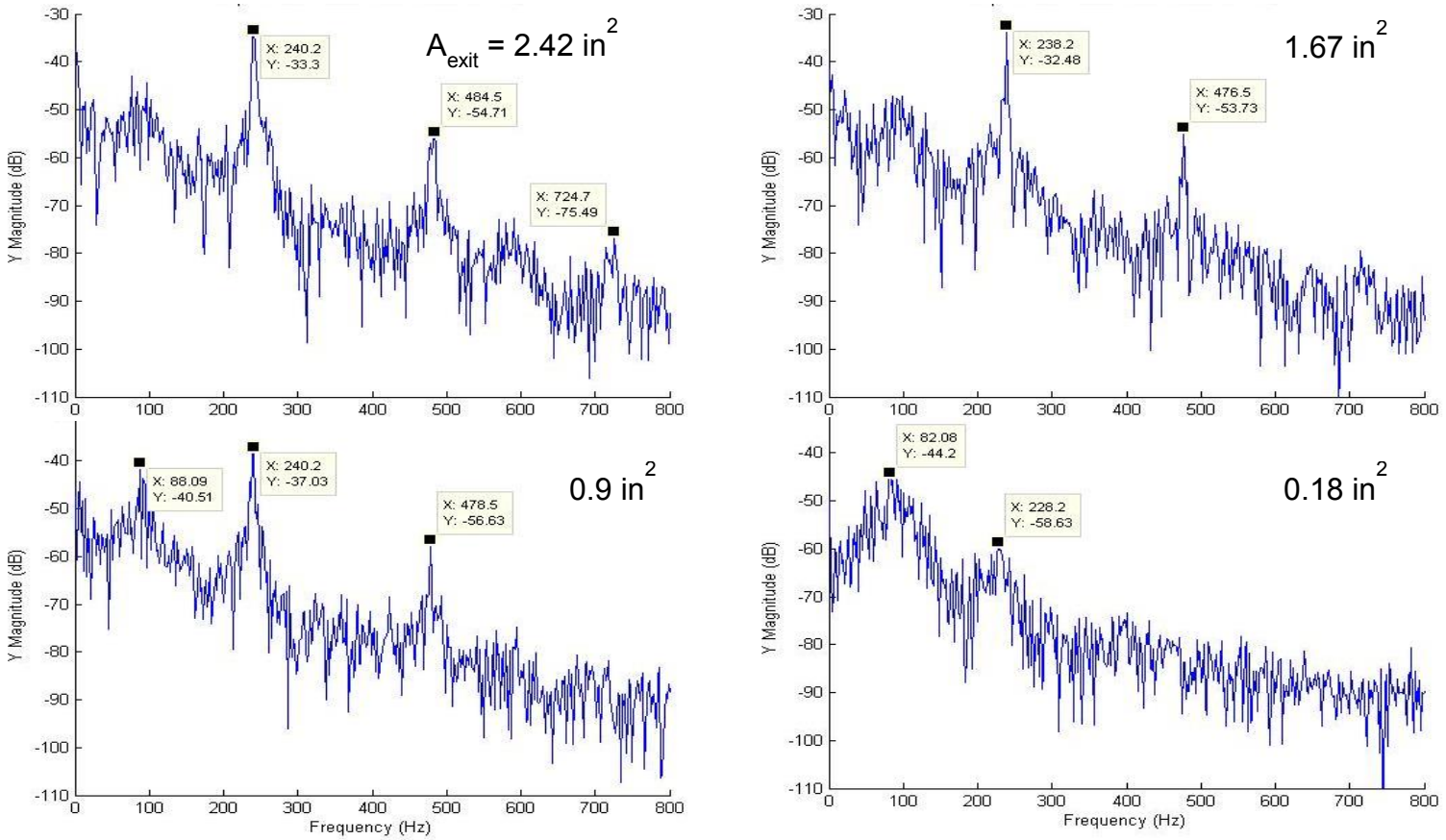

Figure 3-35: Frequency responses for the four exit areas tested.

3.4 Conclusions and Future Work

A LDI single element combustor has been designed, built, and tested. Initial results regarding operability range, flame shape, and acoustical characteristics are promising for future controls and combustion development. From inviting classes to interact with the research group and participate in combustor development, new hardware was made, and analyses were done that helped everyone involved gain a better understanding of the field. The classes also served as good practice for the research students in running experiments and using the equipment such as the CCD camera.

The near future work will see better instrumentation of the combustor to build a combustor database. Now that the CCD camera basics have been learned, some methods available in publication can researched for application to the experiment. There is also a lot of hardware available now, such as the injector actuator or variable impedance area, which await integration and testing to see what impact these devices combined into one system could have.

CHAPTER 4. OPTICAL TRANSLATION TABLE

4.1 Introduction

One of the diagnostic tools available in the lab is the picosecond laser system that can be set up for two different diagnostic mehthods: Laser-induced Fluorescence Triple-integration Method (LIFTIME) or Picosecond Time-resolved Laser-induced Fluorescence (PITLIF) [23], [24]. These are quantitative methods for the spatial and time resolved measurements, at the flame front, of species such as OH and NO. With this system, a method was needed to move the combustor relative to the optics. The optics could be moved, but the picosecond system is one of several diagnostics tools planned, so moving the combustor, or target, requires less independent stages. With this philosophy, at least a three axis stage was needed to move the combustor. In addition to having multiple diagnostic methods planned, the lab also planned to do rapid testing of multiple burners with quick turnaround time between them. A set of three translation stages per burner was impractical and costly, and there would not be enough time to switch burners on one set of stages; therefore the best option was to make a three axis table that could hold multiple burners.

Figure 4-1 shows the custom translation table. The table consists of four main sections: ground rails, main frame, Z table, and Y table (Figure 4-2). The

main frame slides along the linear rails that form the ground rails. The Z table is supported from lead screws inside the main frame and traverses in the vertical direction. The Y table slides along linear rails mounted to the Z table. The table was constructed as a space frame to give as much access to the burners as possible. With this concept, there is plenty of room to get the plumbing and instrumentation lines to the burner.

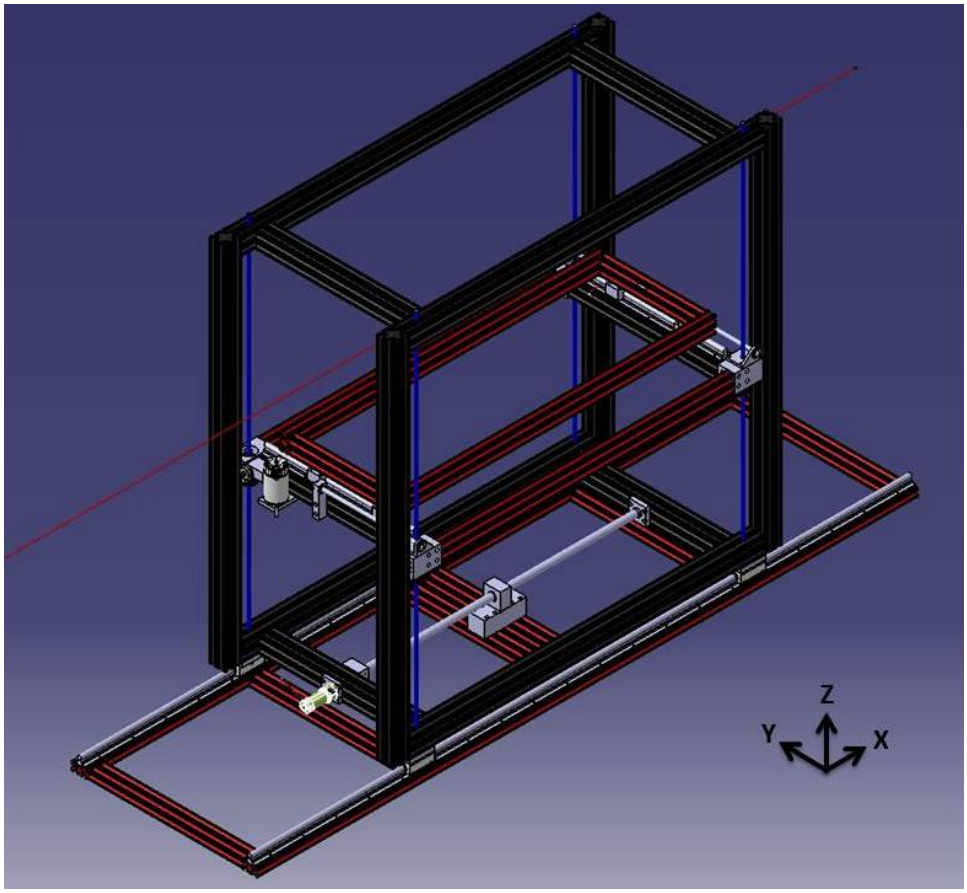

Figure 4-1: Translation table and axis definition.

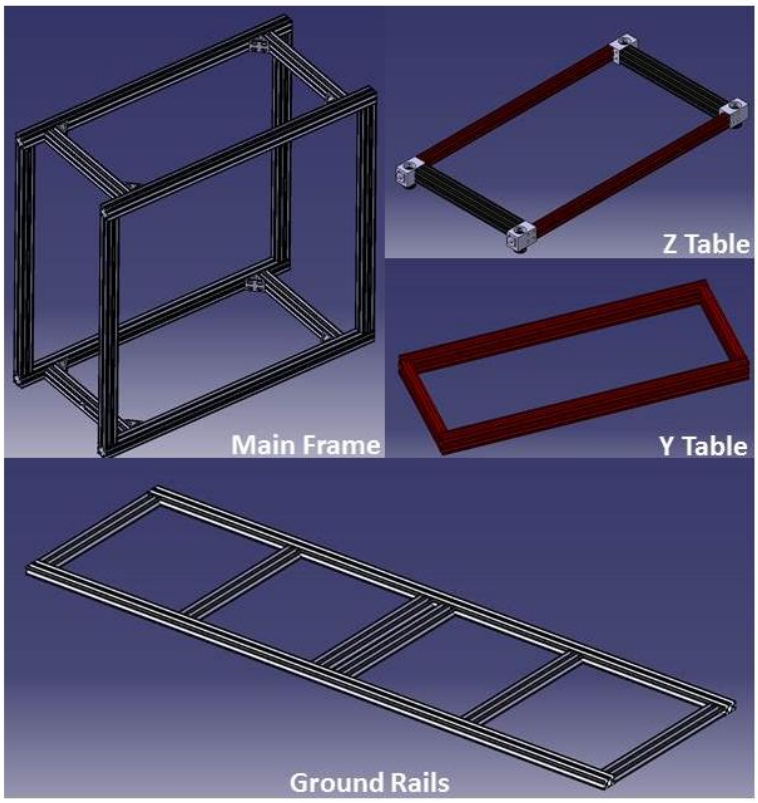

Figure 4-2: Translation table main sections.

Since this table was a custom design and would be a key component in our diagnostic system, careful consideration was given to the requirements of the device. To be determined prior to the start of the design, these requirements were needed to define travel range and speed, weight capability, and outer dimensions.

The travel range is dictated by the flame dimensions to be scanned by the picosecond system. Flames from full scale combustors don't typically exceed 6" in maximum width, so this became the minimum range needed in the X and Y axes. The range for the Z axis is determined by the length of the flame, which is typically less than 12", so the initial design had these travel targets in mind. Once

some initial concepts were formed and vetted, the current layout with the burners along the X axis was chosen. With this arrangement, the X range was extended to not only scan a flame, but travel between the farthest mounted burners. Using dimensions from common burners, this distance was set at 24”. Initial pricing for the components revealed it wouldn’t add much cost to the assembly to make the Z axis have the maximum travels of the components available for purchase, 36”. This additional travel would allow taller burners to be used; the table would have to be lowered to keep the flame at the laser centerline. The final requirements for travel were: X axis – 30”, Y axis – 8”, and Z axis – 36”.

The picosecond system scans point by point with a typical distance of 1 mm between points. This became the maximum resolution requirement of the table. The overall time required to scan a flame is based largely on the travel time between points. A target of 1 mm per second was proposed as the minimum speed required, but a general goal to maximize speed between points was kept during the design process.

The weight capacity requirement of the table was based on the weight of some high pressure burners which can be up to 300 lbs each. With this in mind, and a minimum safety factor of two desired, the minimum weight requirement was 600 lbs, and components were sized for this or greater.

The lab space where the translation table sits is limited by the distance between the optics tables, and the width of the collection optics table. In between the optics table, an aisle was needed to access the hardware on the table. The table could also not be wider than the collection optics table, so as not to extend

into the aisles. In order to achieve the required travel in the Y direction without adding width to the frame, it was necessary for the Y table to travel to the edge of the frame. This change added complexity to the table and component designs but was determined necessary.

4.2 Mechanical Design

The design for each of the three axes has the common components of a linear stage: rails to constrain five of six degrees of freedom, a lead screw on the moving degree, and a servo motor to power the lead screw. With the X axis, the stationary component is the ground rail while the moving part is the rest of the table. The main frame is mounted to open linear bearings that slide on linear rails mounted to the ground rails (Figure 4-3). Open bearings were selected over closed bearings for the fully supported nature of the open bearing. A lead screw constrains the ground rail to the main frame, and is turned by a geared DC motor. An acme screw thread was selected over a ball screw thread for its high friction angle making it non-backdriveable, and relative low cost. Position measurement is achieved by an optical linear encoder with a resolution of 500 lines per inch (US Digital EM1-500-I). All encoders used are this resolution and also have an index mark and the center of travel serving as a reference to start counting from.

Figure 4-3: Assembled table ground rails.

The Y axis design is similar to X axis, except the Y table could not be driven from the center for practical reasons, so it's driven from the sides with two lead screws. This was required to avoid the binding that driving from the side with one lead screw would cause. The motor couples to the back of one lead screw, then a timing belt (WM Berg Min-E-Pitch) connects that screw to another screw. Static belt tensioners were made and applied to all belts to ensure adequate belt wrap, and reduce backlash from belt flex. The Y axis system is shown in Figure 4-4.

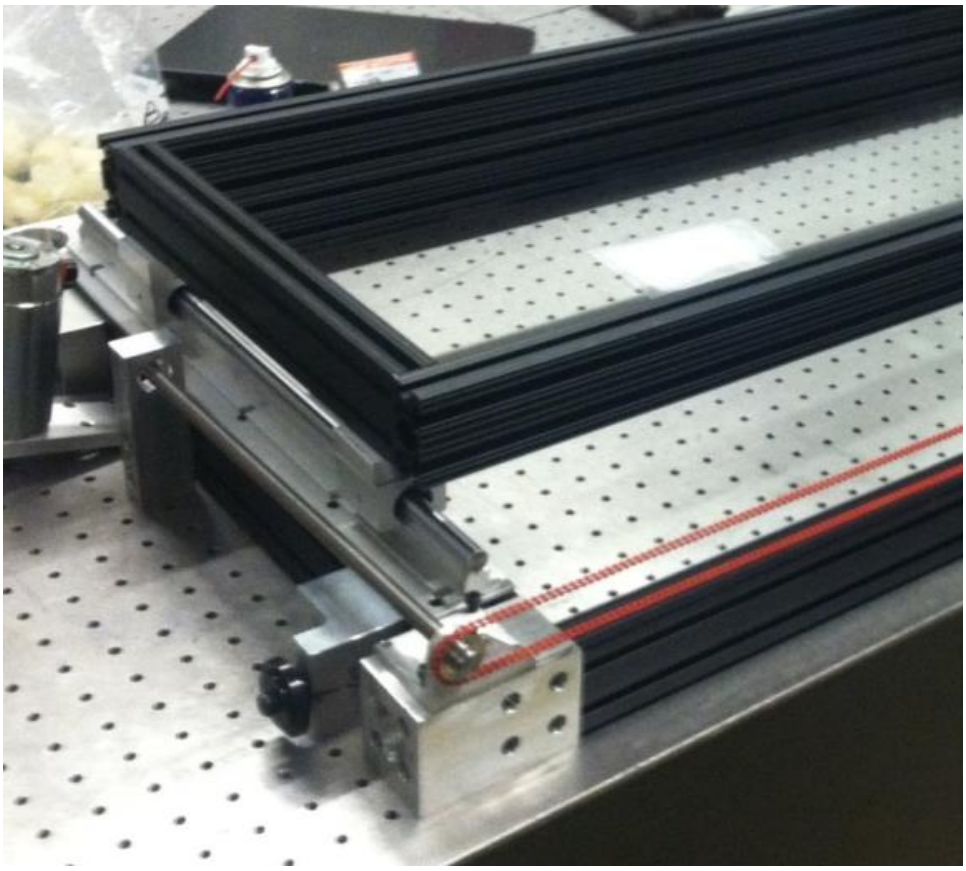

Figure 4-4: Y Axis drive system and linear rails.

The Z-axis is a different configuration than the X or Y. With this axis, the main constraints are rollers that ride in the grooves of the 80/20 on one face, and ball rollers that roll against the 80/20 surface on the other. These constrain the table in the X-Y direction and also the twist motion about the vertical axis. The 4 vertical lead screws constrain the table in twist about the X and Y axis, and the translation in the vertical direction. An Acme lead screw was used here over a ball screw explicitly for the non-backdriveability of the Acme profile. This keeps the Z table from backdriving down the lead screws due to its weight (Figure 4-5).

Figure 4-5: Assembled table showing suspended Z Axis.

In this design, the lead screw is stationary while the lead nut spins about the screw. Both options, spinning the lead screw or spinning the nut, were considered. Spinning the nut required less hardware and was a more compact design. Spinning the nuts in the four corners is done with a large DC brush motor powering one nut, which is then coupled to the others by timing belts (Figure 4-6). Figure 4-7 shows a cross section of a corner bearing block. The lead nut is threaded into a spindle. The spindle has the timing gear attached to it, and rotates in two bearings. The lower bearing is a tapered roller bearing that transmits the vertical load of the table to the lead screw. The upper spindle bearing is a radial bearing that supports moment created by the belt tension.

Figure 4-6: Z Table belt path (bottom view).

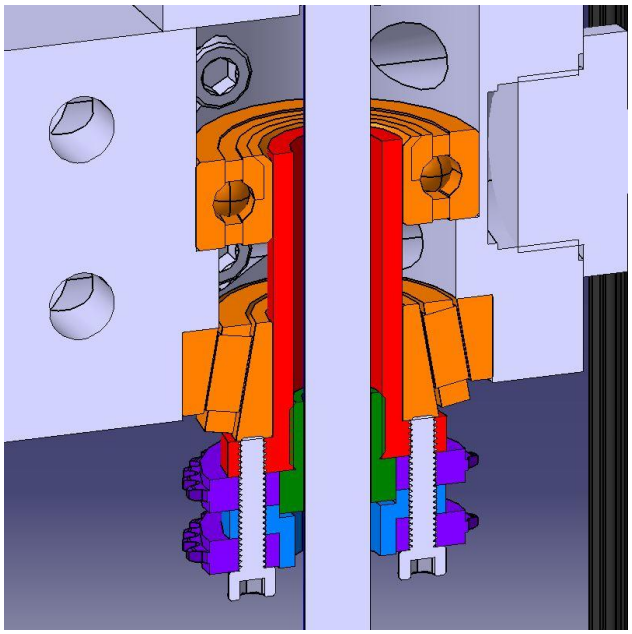

Figure 4-7: Z Table bearing block showing spindle (red), bearings (orange), Acme nut (green), WM Berg sprockets (purple), and bearing block (gray).

Belt stretching was a concern for the Z axis with the combination of high loads needed to lift the table, and the long belt length from the motor to the last driven corner. Since on all axes the table positions are measured with only one encoder, any backlash or misalignment due to belt stretch would go unmeasured and add error in position certainty. If the backlash is great enough, it could cause

binding as well. A solution was found in the WM Berg product line of Min-E-Pitch cables. The cables, which is a deceiving name because they act the same as a timing belt running over a toothed sprocket, are constructed from two stainless cables that are 1/32” in diameter, joined by polyurethane rungs. The stainless cables give the belts a higher stiffness and strength than a typical timing belt made with rubber and high-tensile fibers. The higher strength allows for a smaller belt cross section, good for compact cases. Belt wraps of almost 180 degrees are on every sprocket so tooth load is minimized. Static belt tensioners were also designed and added to reduce the slack in the belt and ensure adequate tooth wrap.

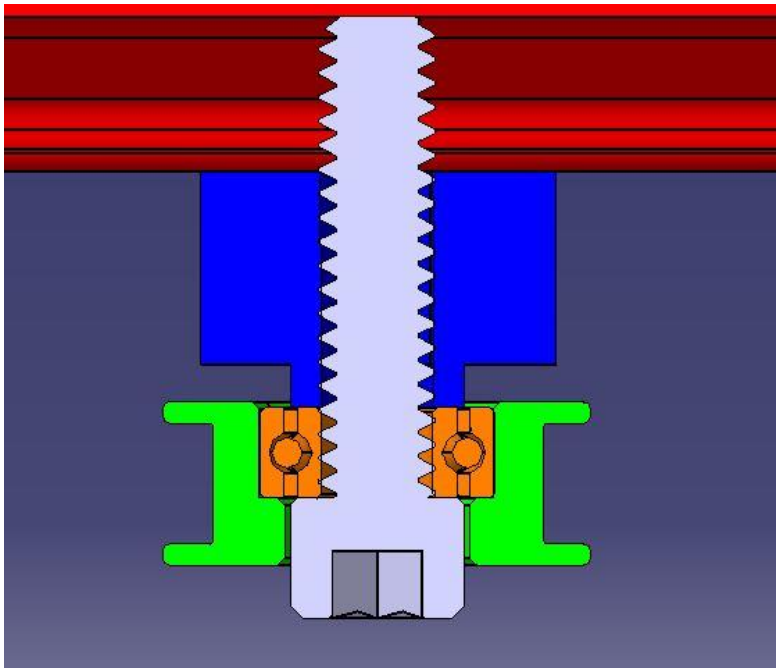

Figure 4-8: Cross section of idler pulley design showing pulley (green), bearing (orange), and spacer (blue).

The encoders used need to be precisely aligned to avoid wearing the ink on the encoder strip, and to maximize the reading ability. The first step of the alignment process is to get the strip aligned to the linear rail axis. All pieces were precision machined, so variation was typically less than 0.020”. Shim stock pieces (Figure 4-9) were made for the strip mounts and encoder mount. The shims were first installed to get the strip parallel, and then shims were installed behind the encoder mount to set the nominal 0.02” clearance to one side of the reader head. To adjust for the variation in the other direction, the mounts were made with play when installed in the 80/20 so they could be loosened and adjusted.

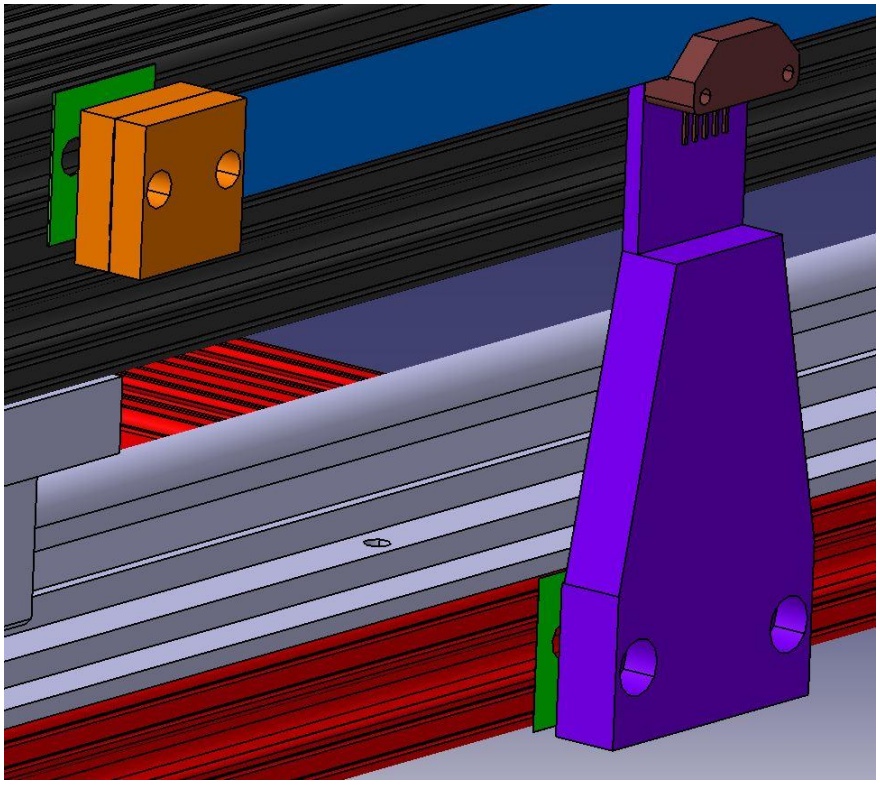

Figure 4-9: Encoder alignment with shim stock: X encoder mount (purple), encoder strip mount (orange), encoder (brown), shims (green), and encoder strip (blue).

4.3 Electrical Design

The electrical system for the translation table has four tasks: read the linear encoders, output a Pulse Width Modulation (PWM) signal to each motor, read inputs from the user control box, and calculate the control signal to move the table point to point.

The motor for each axis is a 24 V DC brush motor driven by a PWM H-bridge motor driver. The X and Y motors are geared DC brush motors (Pittman GM8224S010), necessary to get the torque and speed required at the lead screws. The Z axis has a 2.7:1 gear reduction through the motor pinion and main sprockets, so a direct drive motor was used (Pittman 14203S009).

To assist in selecting the motors, power supply, and gear ratios, a simulation of each axis was done using SIMULINK. The simulations followed a standard dc brush motor model that included the rotor resistance, inductance, inertia, damping, Motor Torque constant, and Back EMF constant. The apparent inertia at the motor shaft was calculated, taking into account table mass, inertia of rotating components, gear ratios, and estimated lead screw friction. The simulation for each axis focused on a step response and maximum speed. As mentioned earlier, the scan time for a flame will mostly be dependent on the travel time between points, so this was minimized. A trade study was done simulating different combinations of motor parameters and gear ratios to find an optimal combination. Figure 4-10 shows the measured step response to a 1 mm step, the smallest the table would be commanded. The response speed is acceptable, reaching the final value in 0.6 seconds. The oscillations about the

steady state points are believed to be from the cyclic friction of the lead screw. The accuracy of the system is acceptable (+/- .003”), but could be improved by aligning the lead screw better to reduce binding and friction. Figure 4-11 shows the maximum speed of the table. The response of the motors’ maximum speed is quick, traveling 1” in under 0.5 seconds with an average speed of 2.3” in/s. Test data for Y and Z axes wasn’t available due to some repairs. However, one can assume the Y axis will perform as well or better since it has as much power, less weight, and less friction. Observations of the Z axis during initial testing put the average speed at 2 in/s.

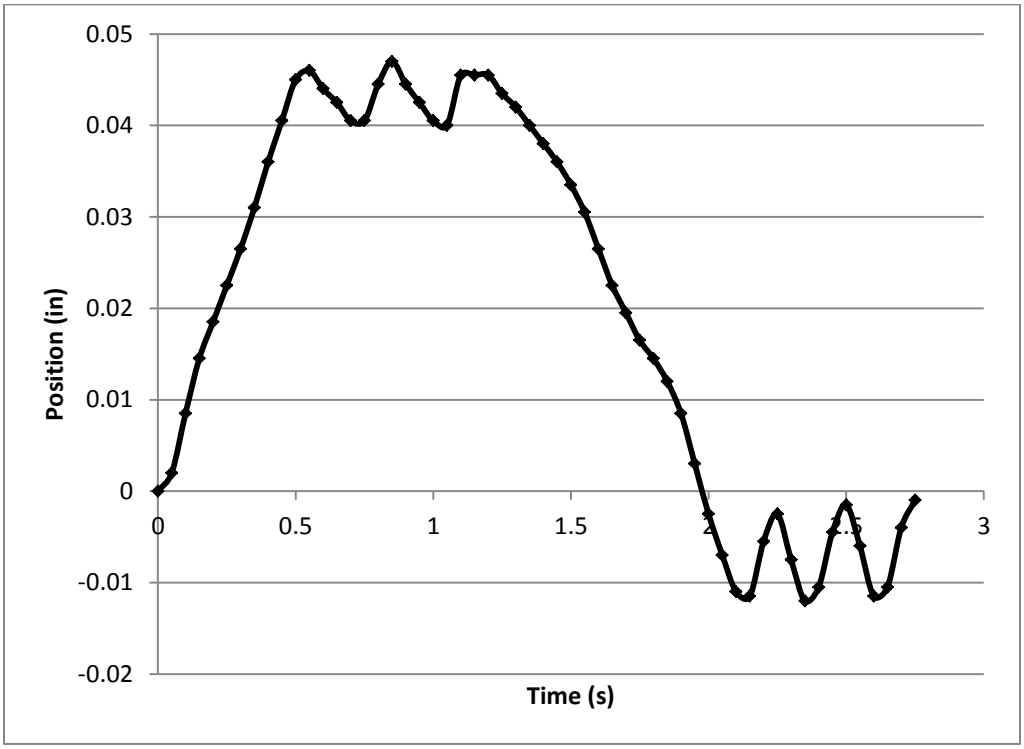

Figure 4-10: 1 mm (.040 inch) step response test. Oscillations are due to undersampling the position measurement.

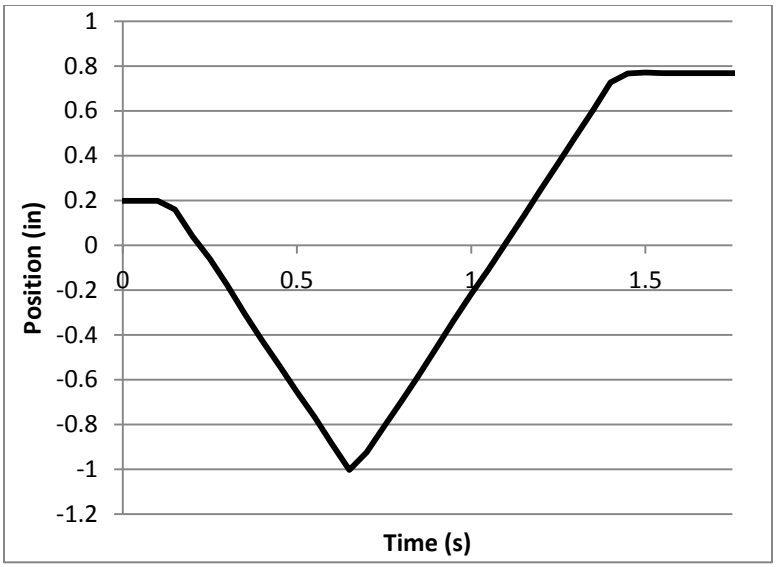

Figure 4-11: X Axis motor maximum speed – 2.3 in/s.

The concern for having an axis overshoot its position from a software glitch or bad user input was mitigated by installing limit switches and emergency stop buttons. These are wired into a standard start-stop circuit configuration using a relay. In this configuration, the user presses the *Start* button to close the relay (Figure 4-12). The coil is then self-energizing and will stay closed when the *Start* button is released. If a limit switch is contacted, it opens and the power to the relay coil is temporarily opened. Once open, even for a few milliseconds, the relay contacts open, breaking power to the motors and to the coil. The power then stays off until the limit switches are closed, and the *Start* button is closed again. The e-stop buttons are in series with the limit switches and function in a similar manner.

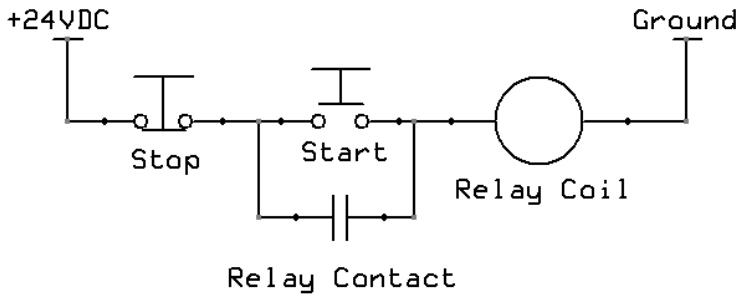

Figure 4-12: Relay start-stop circuit.

Motor command signals to the motor drivers come from the PXI-1033 chassis that runs a VI for the table control. The motor drivers (Pololu 1213, 755) are essentially H-bridges used to amplify the PWM input signal, with the voltage to the motor being proportional to the PWM duty cycle. Motion direction is controlled by the set polarity to the DIR pin on the driver.

As described earlier, position measurement is done with optical linear encoders. Each encoder is a quadrature design and has two outputs that must be read to get position and direction. Interrupts must be used to read the encoder output to ensure no counts are missed, but the PXI-1033 chassis didn't have enough for the three of the table. A solution was developed by Nathan Toner, another student in the lab, using an Arduino DUE acting to count the pulses and then report the position via a data bus to the PXI-1033. The DUE was an excellent board for its many interrupt channels and processing speed, but uses 3.3 volt digital logic versus the more common 5 volt. This proved to be a challenge as both the optical encoders, and PXI-1033 chassis could only operate at 5 volts. To overcome this, Nathan developed a circuit board that incorporated logic level converters on all lines needed, converting between 3.3 and 5 volts.

Table position can either be directly set through the VI, or adjusted by a manual control box (Figure 4-13). This control box contains a two direction switch for each axis, the relay start button, and a speed selection switch. The direction switch for each axis is a three position switch used to specify the direction to move. The speed selection switch is either for low speed or high speed, and the speed for each is programmed in software. Low speed is used for fine adjustments in position when near the burner, whereas high speed is to move between burners.

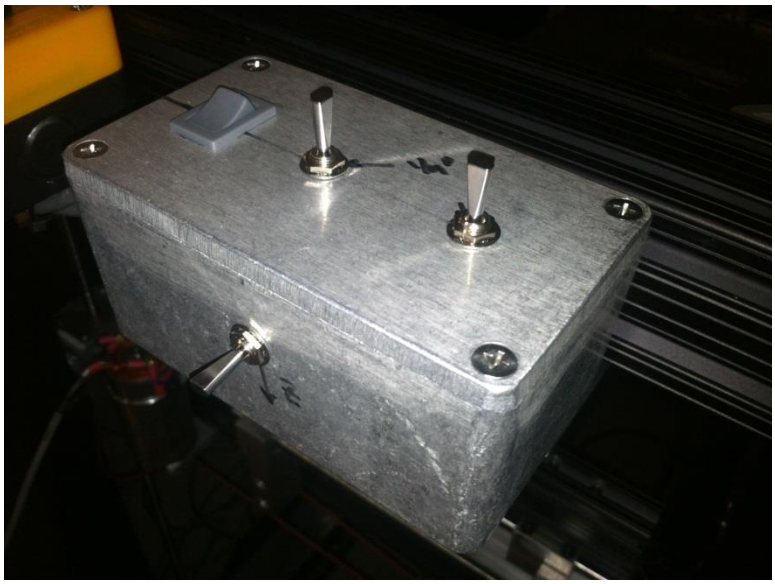

Figure 4-13: Manual user control box.

The same VI that operates the flow metering equipment was modified to operate the translation table (Figure 4-14). The table portion of this VI communicates with the DUE to get the updated table position, outputs PWM motor control signals to the drivers, reads the direction switches from the user control box. This VI outputs control signals and updates position at 20 Hz. This is currently limited by the data bus rate and will be updated in the future. The

control structure currently being used is a PID. Although the system could eventually benefit from a more advanced controller, the current limitation as seen by the oscillations in the step response is the update rate of the position (Figure 4-10).

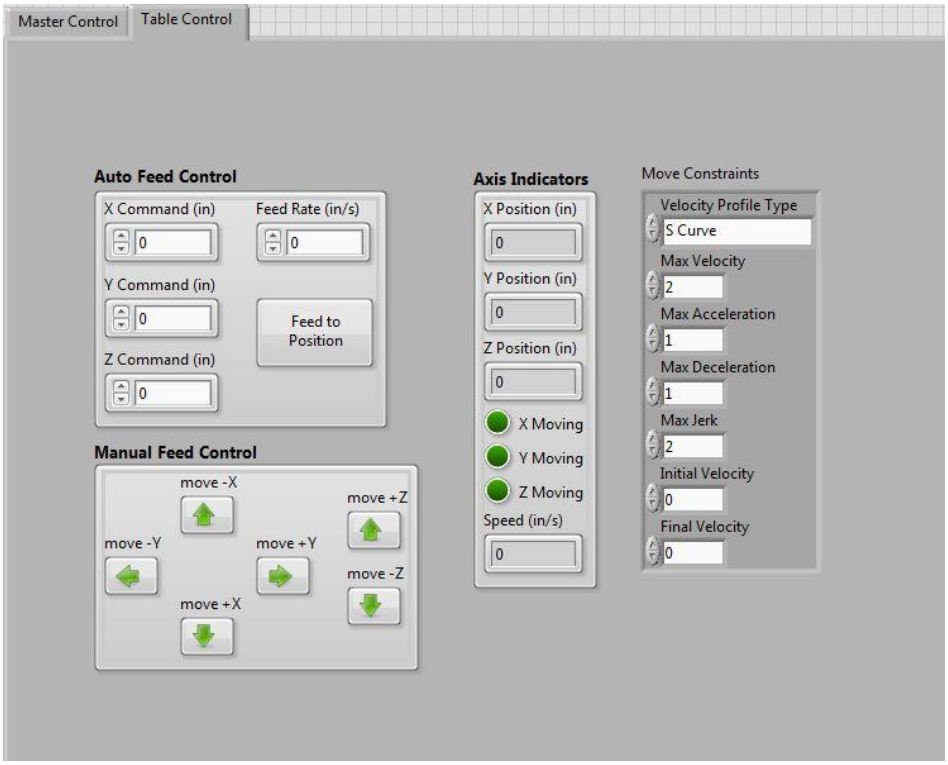

Figure 4-14: Translation table panel of Main VI.

An electronics box was built to house the Arduino, motor drivers, relay, and input/output plugs (Figure 4-15). This box was mounted on the table to reduce the number of wires that had to flex due to the movement of the table relative to the PXI-1033, which was stationary on the ground. A cooling fan was added to the electronics box for the motor drivers. This is a 24 V fan that runs off the 24 V power supply to the motors. The 24 V power supply is capable of 16 A continuous output and is mounted next to the PXI, off the table.

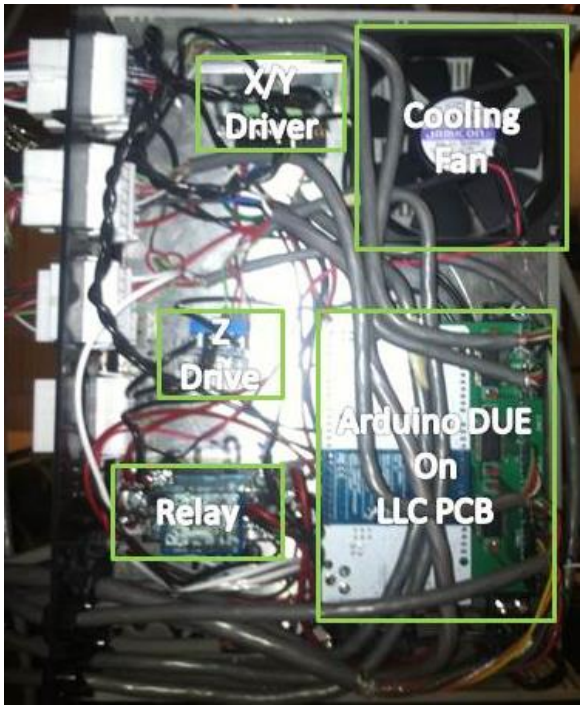

Figure 4-15: Translation table electronics box.

4.4 Conclusions and Future Work

A three axis translation table has been developed to support future combustor development and diagnostic efforts. Initial performance measurements indicate the table speed and precision surpass the original requirements, and will enable fast scanning of flames compared to other translation options. In addition to good performance, the size of the table relative to its travel was minimized through compact design, leaving extra space around the table to access the burners, and allowing more burners to be mounted on the table.

The horizontal plane stiffness of the table was a concern from the beginning, due to the open box structure of the frame. It is planned that after a few months of using the table to get familiar with it, shear stiffening panels can be

designed to stiffen the structure but not limit access to the burners. A trial has already been done where a shear panel was clamped on to the frame work, and deflection at the top of the table was decreased by an order of magnitude.

In addition to stiffening the structure, a redesign of the table is planned that will eliminate the framework above the Z table. This will give unobstructed access to the combustor for both maintenance and optical work. This again was a change that could only happen after the table was built, and used for a while, in order to visualize possible solutions.

The table position control portion of the VI will be updated to allow path generation of a point vector file supplied from another measurement device. This will enable automatic scanning of a flame to significantly increase our data collection and accuracy.

CHAPTER 5. CONCLUSION

This chapter reviews the main accomplishments of this research. In addition to this review, ideas of things to be studied in the future will also be discussed.

5.1 Lab Infrastructure

The lab facilities and infrastructure have successfully been developed which will support future combustor development and diagnostic efforts of our research group. The completed development included lab layout and organization, facilities, measurement and instrumentation, automation of the majority of the processes associated with testing, and an imaging tool for diagnostics.

5.2 LDI Combustor Design

A LDI single element combustor has been designed, built, and tested. Initial results include operability range, flame shape, and acoustical characteristics. These results are promising for future controls and combustion development that our lab group hopes to achieve. From inviting classes to interact with the research group and participate in combustor development, new hardware was made, and analyses were done that helped everyone involved gain a better understanding of the field. The classes also gave the research

students good practice in running experiments and using the lab equipment, such as the CCD camera.

5.3 Optical Translation Table

A three axis translation table has been developed to support future combustor development and diagnostic efforts. Initial performance measurements indicate the table speed and precision surpass the original requirements, and will enable fast scanning of flames compared to other translation options. In addition to achieving our desired performance, the size of the table relative to its travel was minimized through compact design, leaving extra space around the table to access the burners, and allowing more burners to be mounted onto the table.

5.4 Future Work

With the equipment now available to the lab, more in-depth combustion research can begin. One of the first projects will be the application of the LIFTIME to the LDI to assist in combustor design. With the experience gained on the CCD camera, there exists the potential to use the image processing capabilities of the LabVIEW software to perform real-time flame geometry analysis.

Although the initial requirements of our translation table were achieved, a redesign is planned that will eliminate the framework above the Z table. This will give unobstructed access to the combustor for both maintenance and optical work. This was a change that could only happen after the table was built, and used for a while, in order to visualize possible solutions.

It is believed that with some minor revisions to our chemiluminescence method, it will be a very useful tool for our lab. Its first application could be to assist in developing an effective variable position injector for the LDI. While waiting to design this new injector, the variable impedance exit area designed by the ME 463 can be used as an alternative control input to our system. This will give us the ability to begin exploring the field of control of combustion instabilities.

Since beginning the development of our lab, we have seen the lab research group triple in size. The work of this thesis did not directly result in any novel combustion development; however, due to this work a fully-functional combustion lab is now available for all of the current and future students to use. In addition to providing resources for the students of our research group, this lab will continue to support Senior Design students as well as those in graduate level combustion courses.

LIST OF REFERENCES

LIST OF REFERENCES

[1] C. Jardine, “Calculating the Environmental Impact of Aviation Emissions.” .

[2] C.-M. Lee, “NASA project develops next generation low-emissions combustor technologies,” in 51st AIAA Aerospace Sciences Meeting including the New Horizons Forum and Aerospace Exposition, American Institute of Aeronautics and Astronautics.

[3] J. DeLaat, “NASA Overview: Combustion Dynamics and Control for Ultra Low Emissions in Aircraft Gas-Turbine Engines,” presented at the 36th Joint Propulsion Conference and Exhibition, Huntsville, Alabama, 17-Jul-2000.

[4] K. Suder, J. Delaat, C. Hughes, D. Arend, and M. Celestina, “NASA Environmentally Responsible Aviation Project's Propulsion Technology Phase I Overview and Highlights of Accomplishments,” in 51st AIAA Aerospace Sciences Meeting including the New Horizons Forum and Aerospace Exposition, American Institute of Aeronautics and Astronautics.

[5] H. C. Mongia, “N+3 and N+4 Generation Aeropropulsion Engine Combustors: Part 6: Operating Conditions, Target Goals and Lifted Jets,” in 49th AIAA/ASME/SAE/ASEE Joint Propulsion Conference, American Institute of Aeronautics and Astronautics.

[6] H. C. Mongia, “N+3 and N+4 Generation Aeropropulsion Engine Combustors Part 5: NOx, CO, HC and Smoke Emissions,” in 49th AIAA/ASME/SAE/ASEE Joint Propulsion Conference, American Institute of Aeronautics and Astronautics.

[7] S. Garg, “Sensor and Actuator Needs for more Intelligent GTC,” presented at the Turbo Expo, Glasgow, Scotland, United Kingdom, 2010.

[8] B. Haller, “Overview of Subsonic Fixed Wing Project: Technical Challenges for Energy Efficient, Environmentally Compatible Subsonic Transport Aircraft,” presented at the 3rd NASA Glenn Propulsion Control & Diagnostics Workshop, Cleveland, OH, 28-Feb-2012.

[9] H. Mongia, “Engineering Aspects of Complex Gas Turbine Combustion Mixers Part V: 40 OPR,” in 9th Annual International Energy Conversion Engineering Conference, American Institute of Aeronautics and Astronautics.

[10] A. Prociw, J. Ryon, and J. Goeke, “Low NOx Combustion Concepts in Support of the NASA Environmentally Responsible Aircraft Program,” pp. 297–307, Jun. 2012.

[11] M. Konarski, “Variable geometry exhaust nozzle,” US4375276 A, 01-Mar-1983.

[12] J. SANBORN, H. MONGIA, and J. KIDWELL, “Design of a low emission combustor for an automotive gas turbine,” in 21st Aerospace Sciences Meeting, American Institute of Aeronautics and Astronautics.

[13] Y. G. Li and R. L. Hales, “Steady and Dynamic Performance and Emissions of a Variable Geometry Combustor in a Gas Turbine Engine,” pp. 527–535, Jan. 2002.

[14] G. Li and E. J. Gutmark, “Effects of Swirler Configurations on Flow Structures and Combustion Characteristics,” pp. 423–433, Jan. 2004.

[15] A. K. GUPTA, J. CHOMIAK, N. MARCHIONNA, and M. S. RAMAVAJJALA, “Burner geometry effects on combustion and NO(x) emission characteristics using a variable geometry swirl combustor,” J. Propuls. Power, vol. 7, no. 4, pp. 473–480, 1991.

[16] W. J. Dodd, “A Variable Geometry Combustor for Broadened Fuel Properties.”

[17] Donald Schultz, GROUND IDLE PERFORMANCE IMPROVEMENT OF A DOUBLE-ANNULAR COMBUSTOR BY USING SIMULATED VARIABLE COMBUSTOR GEOMETRY. .

[18] F. Giuliani, J. Woisetschläger, and T. Leitgeb, “Design and Validation of a Burner With Variable Geometry for Extended Combustion Range,” pp. 155–165, Jun. 2012.

[19] “UV CoastalOpt® SLR Lens.” .

[20] “RM-4200CL User Manual.” .

[21] “Kodak Image Sensor KAI-4021.” .

[22] K. M. Tacina, “Swirl-Venturi Lean Direct Injection Combustion Technology,” presented at the Cental States Section of the Combustion Institute, 2012.

[23] S. D. Pack, M. W. Renfro, G. B. King, and N. M. Laurendeau, “Photon-counting technique for rapid fluorescence-decay measurement,” Opt. Lett., vol. 23, no. 15, p. 1215, Aug. 1998.

[24] S. D. PACK, M. W. RENFRO, G. B. KING, and N. M. LAURENDEAU, “Laser-induced Fluorescence Triple-integration Method Applied to Hydroxyl Concentration and Fluorescence Lifetime Measurements,” Combust. Sci. Technol., vol. 140, no. 1–6, pp. 405–425, 1998.

APPENDICES

Appendix A. LDI Combustor Design Drawings

In the pages that follow are the drawings for the single element LDI combustor.

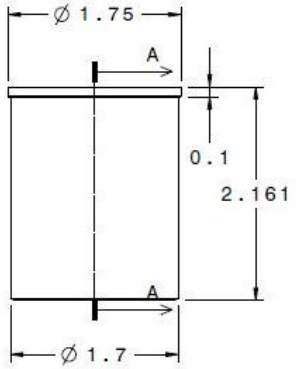

Front view
Scale: 1:1

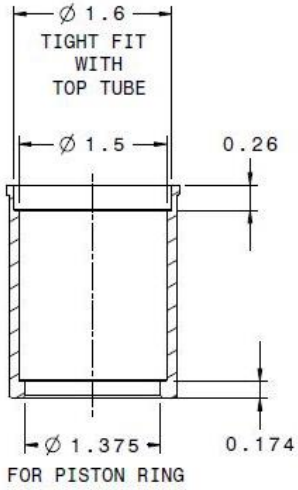

Section view A-A
Scale: 1:1

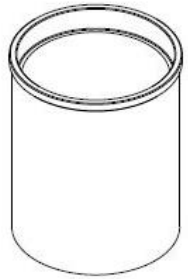

Isometric view
Scale: 1:1

	BOTTOM TUBE			
MATERIAL: STAINLESS TUBING	DUSTIN CRUISE			
	SIZE	FSCM NO	DWG NO XXXXXXX	REV
	SCALE X:X	12/10/12	SHEET X of X	

Isometric view
Scale: 3:1

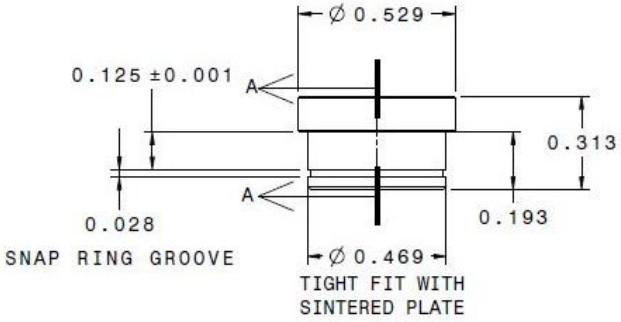

Front view
Scale: 3:1

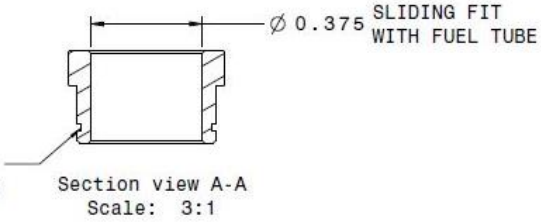

Section view A-A
Scale: 3:1

	BUSHING, FUEL TUBE			
MATERIAL: 6061-T6	DUSTIN CRUISE			
	SIZE	FSCM NO	DWG NO XXXXXXX	REV 0
	SCALE X:X	12/10/12	SHEET X of X	

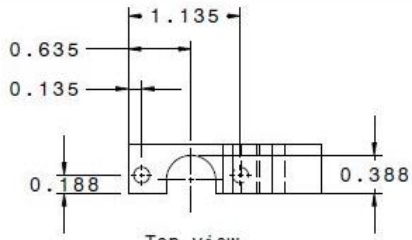

Top view
Scale: 1:1

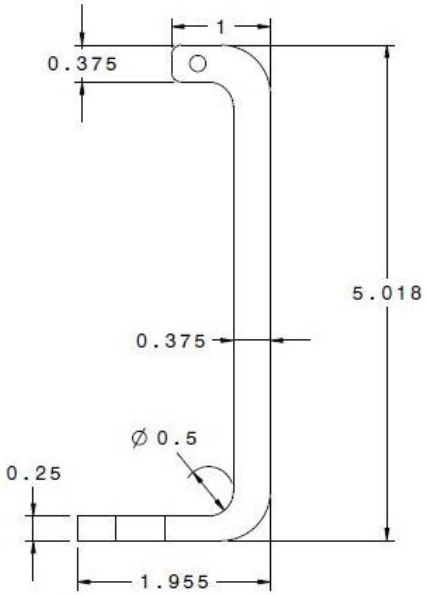

Front view
Scale: 1:1

STEPS:
1. CUT OUTSIDE SHAPE
2. DRILL HOLES, END MILL
3. CUT PROFILE
4. MILL EDGES
5. ROUND CORNERS
6. TEST FIT AND MARK HOLE LOCATION

	FUEL INJECTOR BRACKET			
	DUSTIN CRUISE			
	SIZE	FSCM NO	DWG NO XXXXXXX	REV
	SCALE X:X	XX-XX-XX	SHEET X of X	

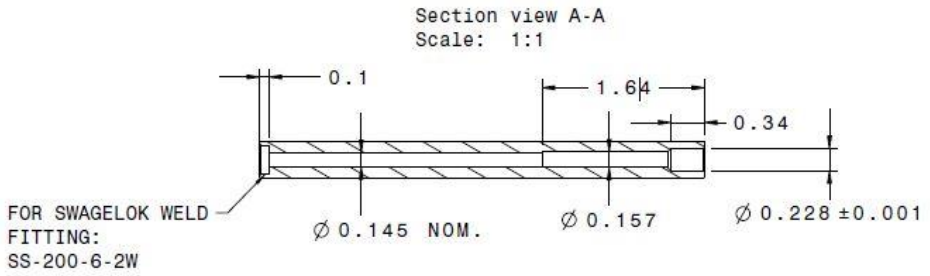

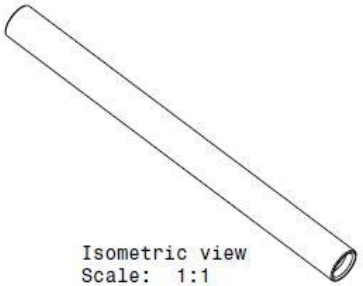

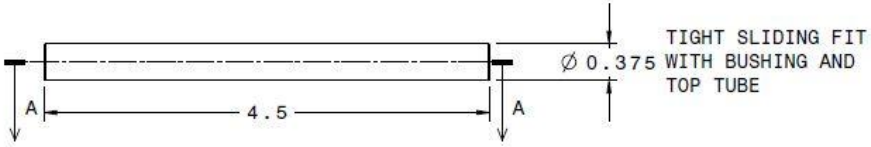

	Injector Tube			
MATERIAL: SS TUBING	DUSTIN CRUISE			
	SIZE	FSCM NO	DWG NO XXXXXXX	REV 0
	SCALE X:X	12/10/12	SHEET X of X	

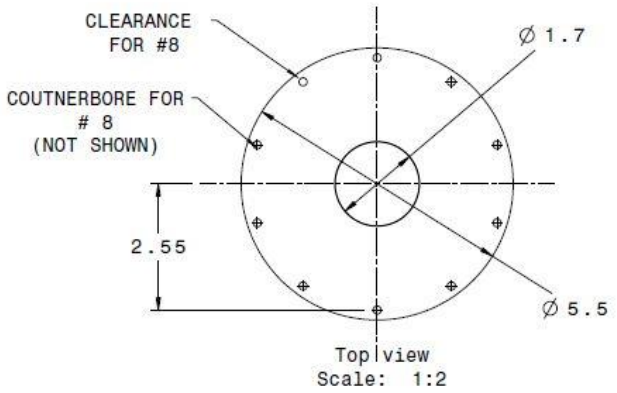

Top view
Scale: 1:2

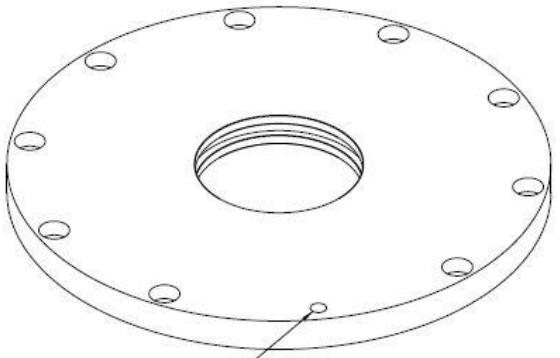

Isometric view
Scale: 1:1

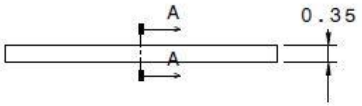

Front view
Scale: 1:2

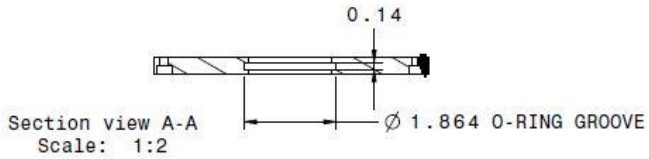

Section view A-A
Scale: 1:2

	PLATE, MANIFOLD			
MATERIAL: 3/8" PLATE 6061-T6	DUSTIN CRUISE			
	SIZE	FSCM NO	DWG NO XXXXXXX	REV
	SCALE X:X	12/10/12	SHEET X of X	

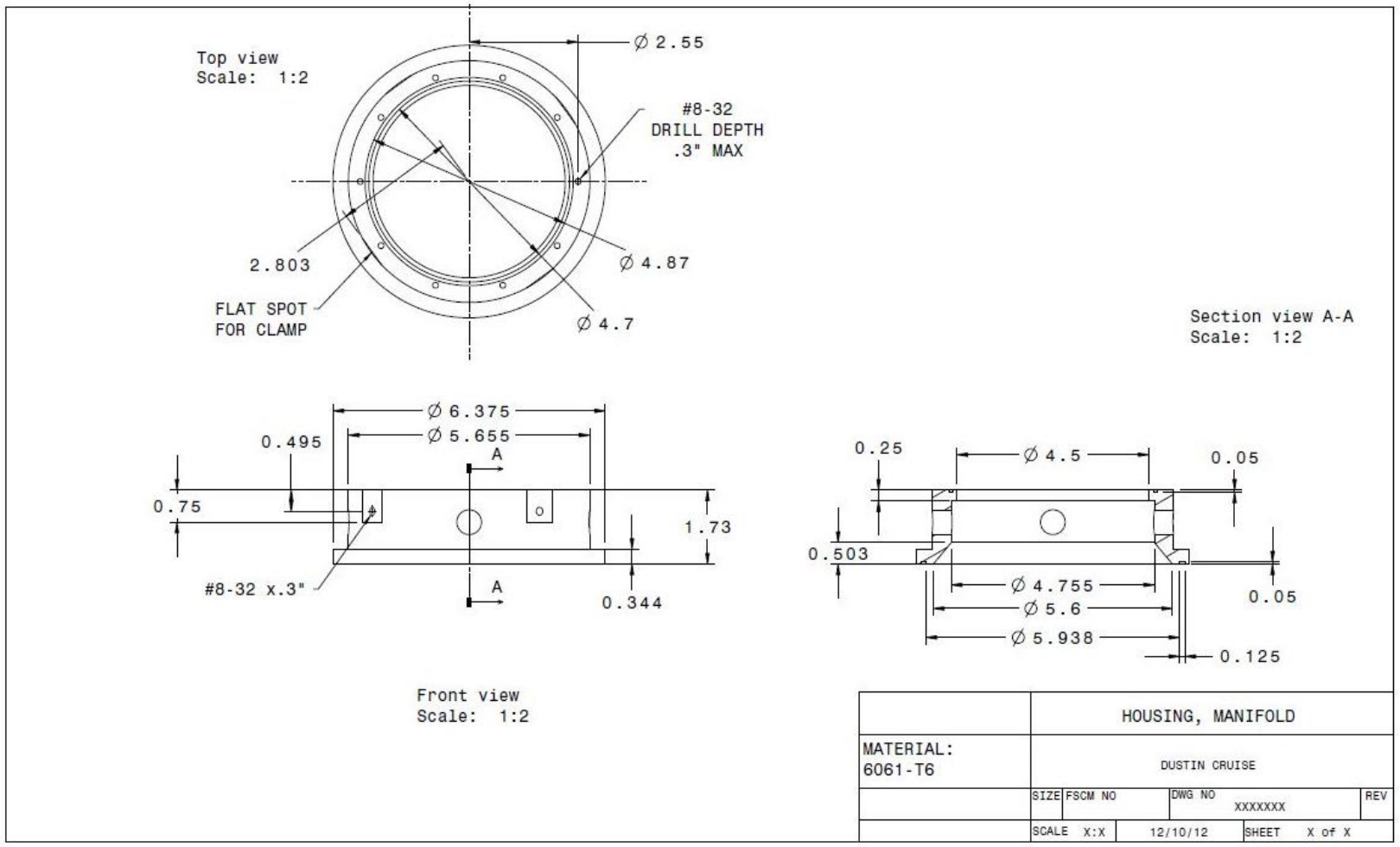
Top view
Scale: 1:2
Ø 2.55
#8-32
DRILL DEPTH
.3" MAX
2.803
Ø 4.87
FLAT SPOT
FOR CLAMP
Ø 4.7
Section view A-A
Scale: 1:2
Ø 6.375
Ø 5.655
0.495
A
0.75
1.73
#8-32 x.3"
A
0.344
0.25
Ø 4.5
0.05
0.503
Ø 4.755
Ø 5.6
Ø 5.938
0.05
0.125
Front view
Scale: 1:2
HOUSING, MANIFOLD
MATERIAL:
6061-T6
DUSTIN CRUISE
SIZE
FSCM NO
DWG NO
XXXXXXX
REV
SCALE X:X
12/10/12
SHEET X of X

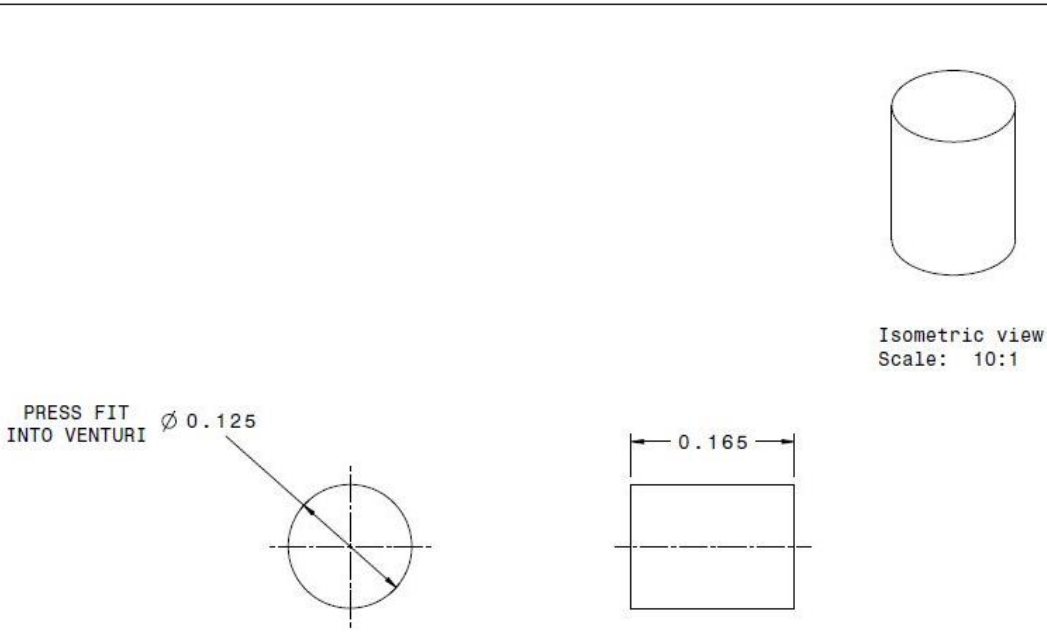

	ALIGNMENT PIN			
MATERIAL: SAME AS VENTURI	DUSTIN CRUISE			
	SIZE	FSCM NO	DWG NO XXXXXXX	REV 0
	SCALE X:X	12/10/12	SHEET X of X	

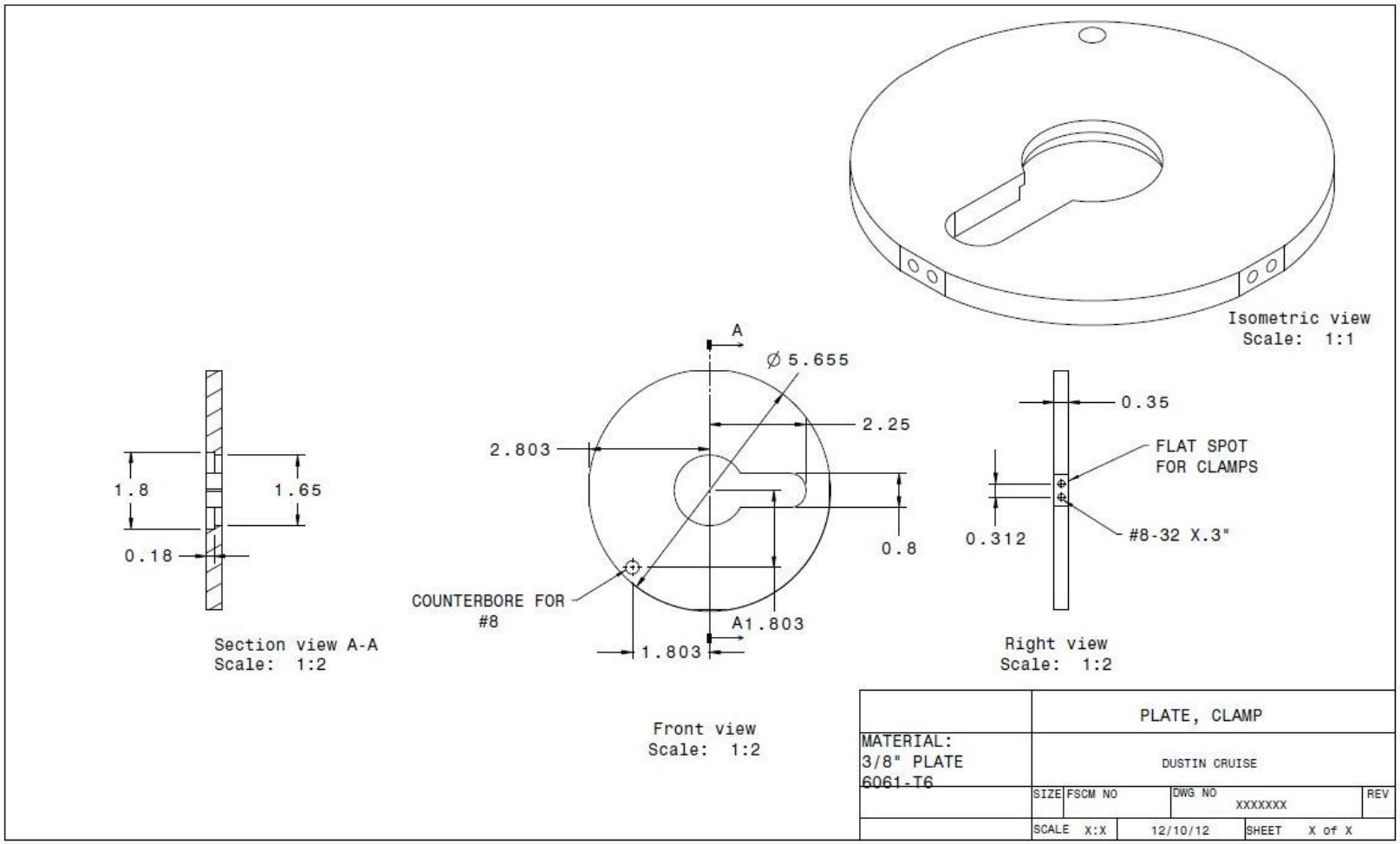
Isometric view
Scale: 1:1
A
Ø 5.655
2.25
2.803
0.8
COUNTERBORE FOR
#8
A1.803
1.803
Front view
Scale: 1:2
1.8
1.65
0.18
Section view A-A
Scale: 1:2
0.35
FLAT SPOT
FOR CLAMPS
0.312
#8-32 X.3"
Right view
Scale: 1:2
PLATE, CLAMP
MATERIAL:
3/8" PLATE
6061-T6
DUSTIN CRUISE
SIZE
FSCM NO
DWG NO
XXXXXXX
REV
SCALE X:X
12/10/12
SHEET X of X

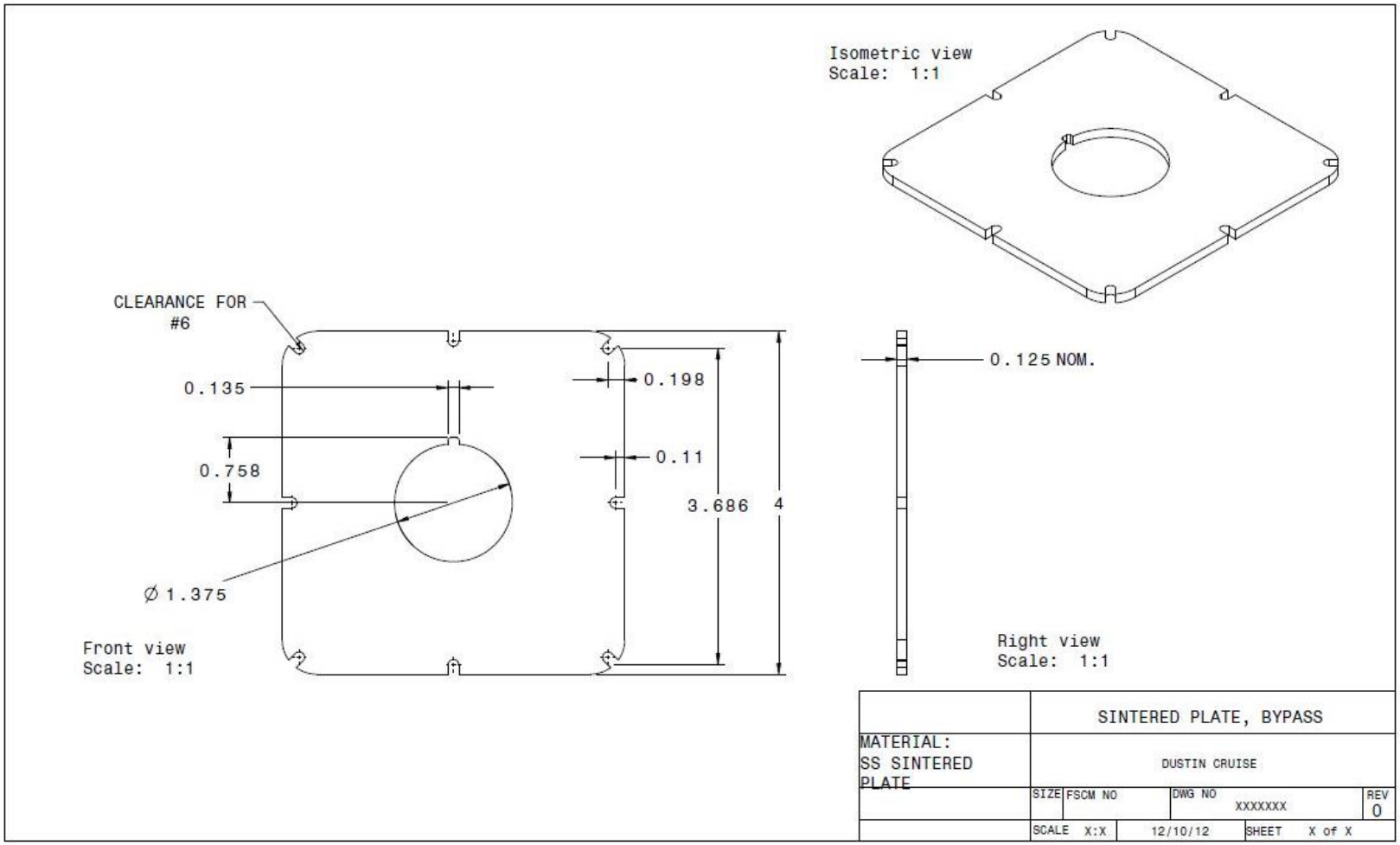
Isometric view
Scale: 1:1
CLEARANCE FOR
#6
0.135
0.758
Ø 1.375
0.198
0.11
3.686
4
Front view
Scale: 1:1
0.125 NOM.
Right view
Scale: 1:1
SINTERED PLATE, BYPASS
MATERIAL:
SS SINTERED
PLATE
DUSTIN CRUISE
SIZE
FSCM NO
DWG NO
XXXXXXX
REV
0
SCALE X:X
12/10/12
SHEET X of X

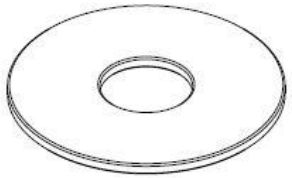

Isometric view
Scale: 2:1

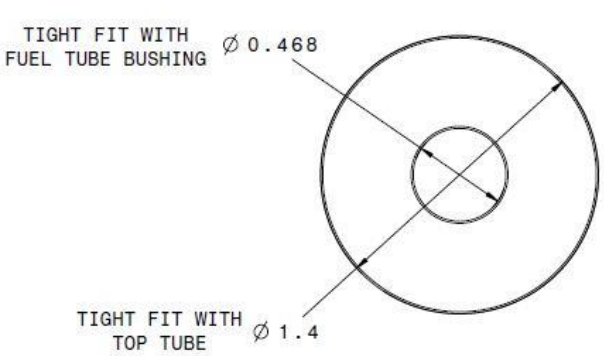

Front view
Scale: 2:1

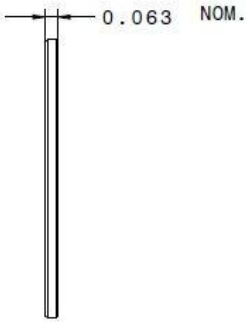

Right view
Scale: 2:1

	SINTERED PLATE, TUBE			
MATERIAL: 1/16" SINTERED S.S.	DUSTIN CRUISE			
	SIZE	FSCM NO	DWG NO XXXXXXX	REV
	SCALE X:X	12/10/12	SHEET X of X	

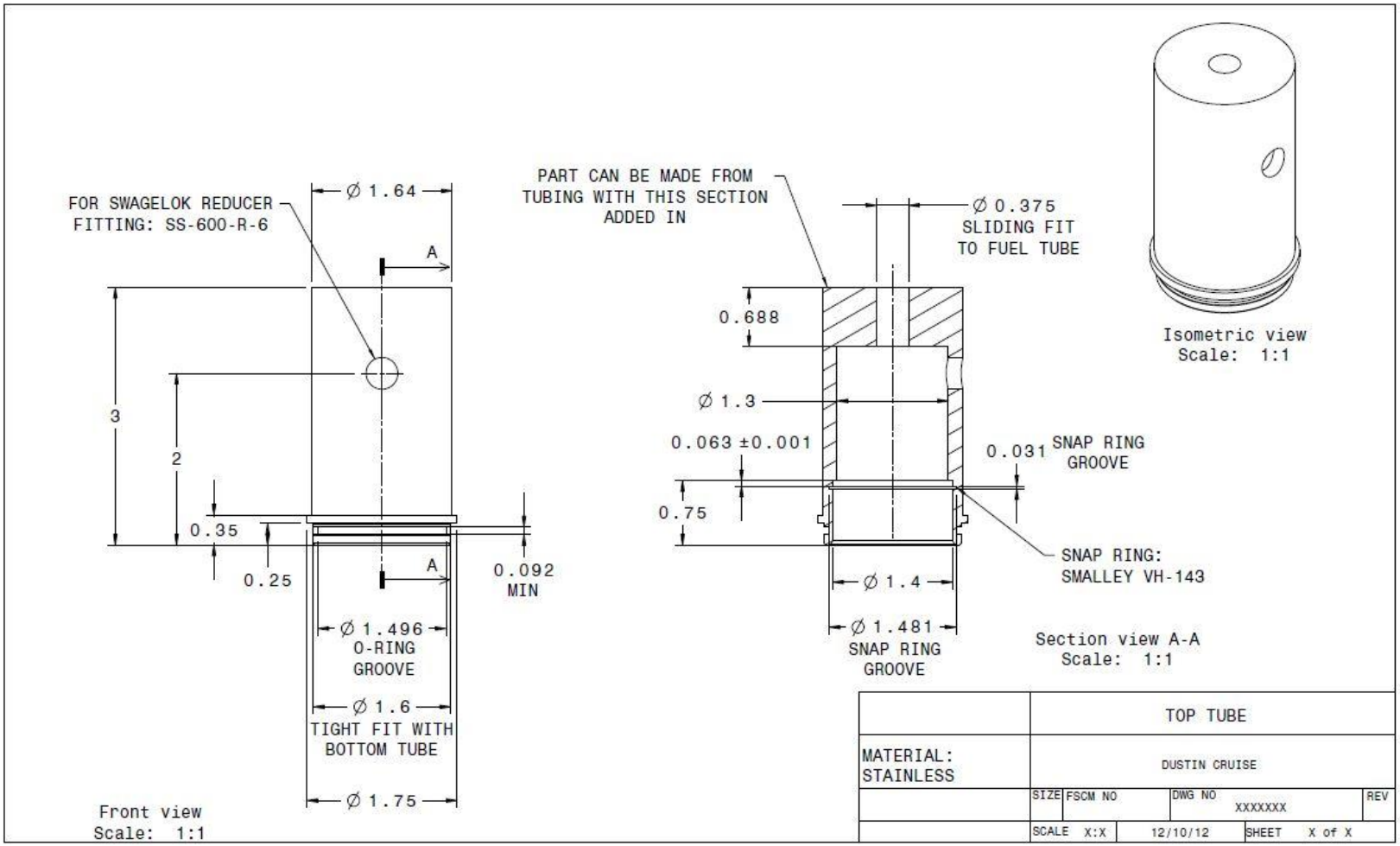
FOR SWAGELOK REDUCER FITTING: SS-600-R-6
Ø 1.64
A
3
2
0.35
0.25
A
0.092 MIN
Ø 1.496 O-RING GROOVE
Ø 1.6 TIGHT FIT WITH BOTTOM TUBE
Ø 1.75
Front view Scale: 1:1
PART CAN BE MADE FROM TUBING WITH THIS SECTION ADDED IN
Ø 0.375 SLIDING FIT TO FUEL TUBE
0.688
Ø 1.3
0.063 ±0.001
0.031 SNAP RING GROOVE
0.75
SNAP RING: SMALLEY VH-143
Ø 1.4
Ø 1.481 SNAP RING GROOVE
Section view A-A Scale: 1:1
Isometric view Scale: 1:1
TOP TUBE
MATERIAL: STAINLESS
DUSTIN CRUISE
SIZE
FSCM NO
DWG NO XXXXXXX
REV
SCALE X:X
12/10/12
SHEET X of X

Isometric view
Scale: 1:1

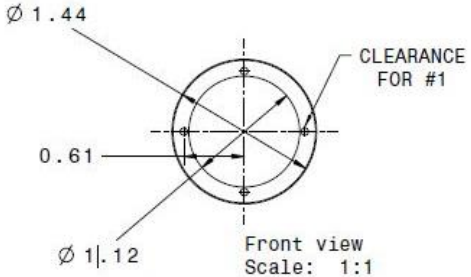

Front view
Scale: 1:1

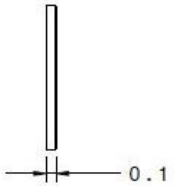

Right view
Scale: 1:1

	VENTURI CAP			
MATERIAL: 6061-T6	DUSTIN CRUISE			
	SIZE	FSCM NO	DWG NO XXXXXXX	REV
	SCALE X:X	12/12/12	SHEET X of X	

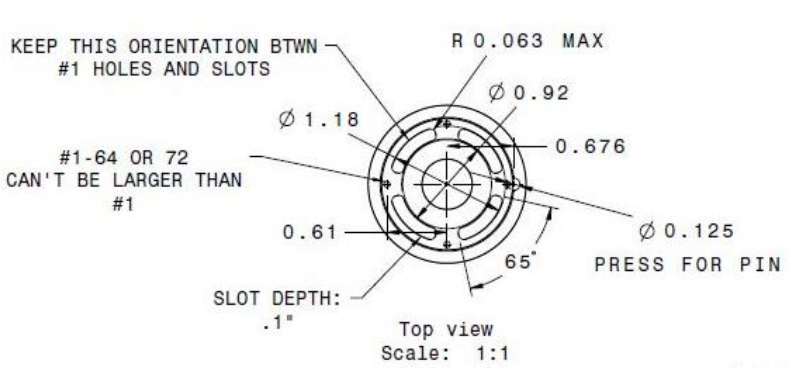

Top view
Scale: 1:1

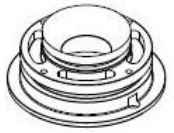

Isometric view
Scale: 1:1

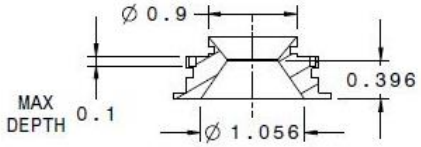

Section view A-A
Scale: 1:1

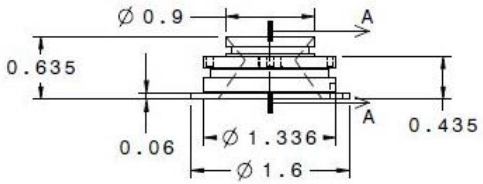

Front view
Scale: 1:1

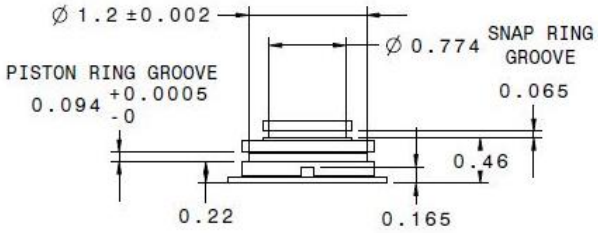

Right view
Scale: 1:1

	Venturi			
MATERIAL: STAINLESS	DUSTIN CRUISE			
	SIZE	FSCM NO	DWG NO XXXXXXX	REV
	SCALE X:X	12/10/12	SHEET X of X	

Appendix B. LabVIEW Wiring Diagrams

In the pages that follow are the wiring diagrams from the LabVIEW program used to automate the components of the lab.

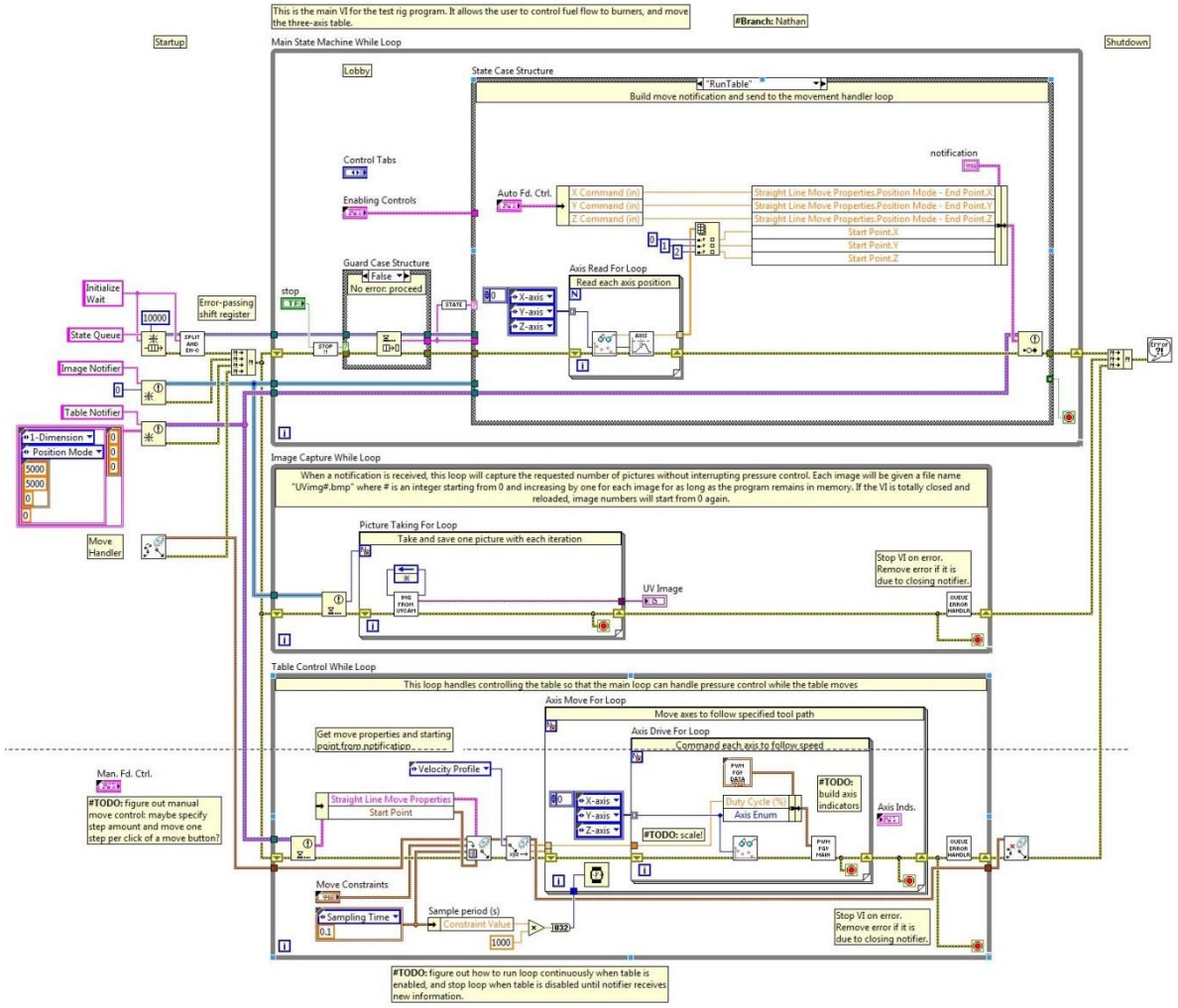
This is the main VI for the test rig program. It allows the user to control fuel flow to burners, and move the three-axis table.
#Branch: Nathan
Startup
Main State Machine While Loop
Shutdown
Lobby
State Case Structure
"RunTable"
Build move notification and send to the movement handler loop
Control Tabs
Enabling Controls
Auto Fd. Ctrl.
X Command (in)
Y Command (in)
Z Command (in)
notification
Straight Line Move Properties.Position Mode - End Point.X
Straight Line Move Properties.Position Mode - End Point.Y
Straight Line Move Properties.Position Mode - End Point.Z
Start Point.X
Start Point.Y
Start Point.Z
Guard Case Structure
False
No error: proceed
stop
Axis Read For Loop
Read each axis position
X-axis
Y-axis
Z-axis
Initialize Wait
10000
State Queue
Error-passing shift register
Image Notifier
Table Notifier
1-Dimension
Position Mode
5000
5000
0
0
Move Handler
Image Capture While Loop
When a notification is received, this loop will capture the requested number of pictures without interrupting pressure control. Each image will be given a file name "UVimg#.bmp" where # is an integer starting from 0 and increasing by one for each image for as long as the program remains in memory. If the VI is totally closed and reloaded, image numbers will start from 0 again.
Picture Taking For Loop
Take and save one picture with each iteration
UV Image
Stop VI on error. Remove error if it is due to closing notifier.
Table Control While Loop
This loop handles controlling the table so that the main loop can handle pressure control while the table moves
Axis Move For Loop
Move axes to follow specified tool path
Get move properties and starting point from notification
Axis Drive For Loop
Command each axis to follow speed
Velocity Profile
Straight Line Move Properties
Start Point
Duty Cycle (%)
Axis Enum
#TODO: build axis indicators
Axis Inds.
#TODO: scale!
Man. Fd. Ctrl.
#TODO: figure out manual move control: maybe specify step amount and move one step per click of a move button?
Move Constraints
Sampling Time
0.1
Sample period (s)
Constraint Value
1000
I32
Stop VI on error. Remove error if it is due to closing notifier.
#TODO: figure out how to run loop continuously when table is enabled, and stop loop when table is disabled until notifier receives new information.

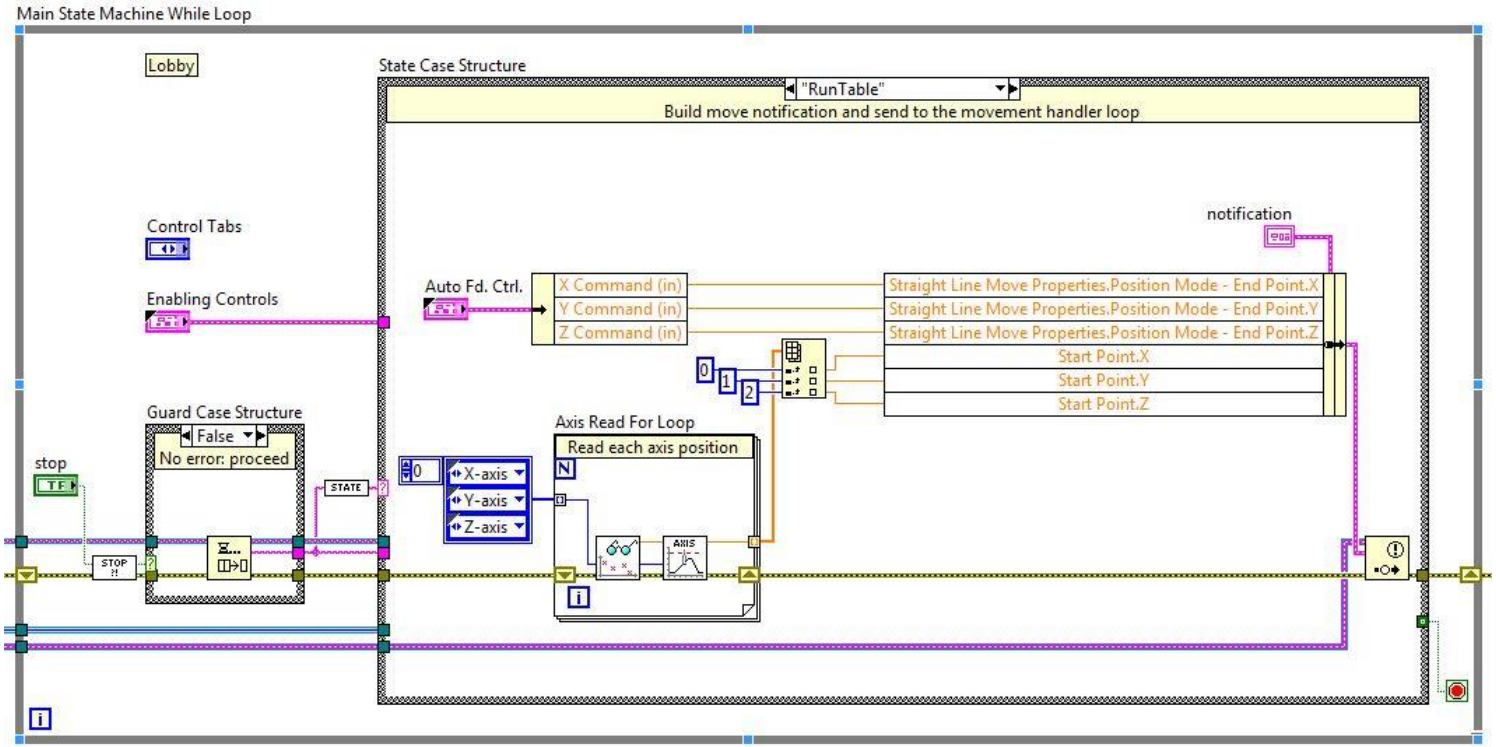
Main State Machine While Loop
Lobby
State Case Structure
"RunTable"
Build move notification and send to the movement handler loop
Control Tabs
Enabling Controls
Auto Fd. Ctrl.
X Command (in)
Y Command (in)
Z Command (in)
notification
Straight Line Move Properties.Position Mode - End Point.X
Straight Line Move Properties.Position Mode - End Point.Y
Straight Line Move Properties.Position Mode - End Point.Z
Start Point.X
Start Point.Y
Start Point.Z
Guard Case Structure
False
No error: proceed
stop
STATE
Axis Read For Loop
Read each axis position
X-axis
Y-axis
Z-axis
AXIS

Table Control While Loop

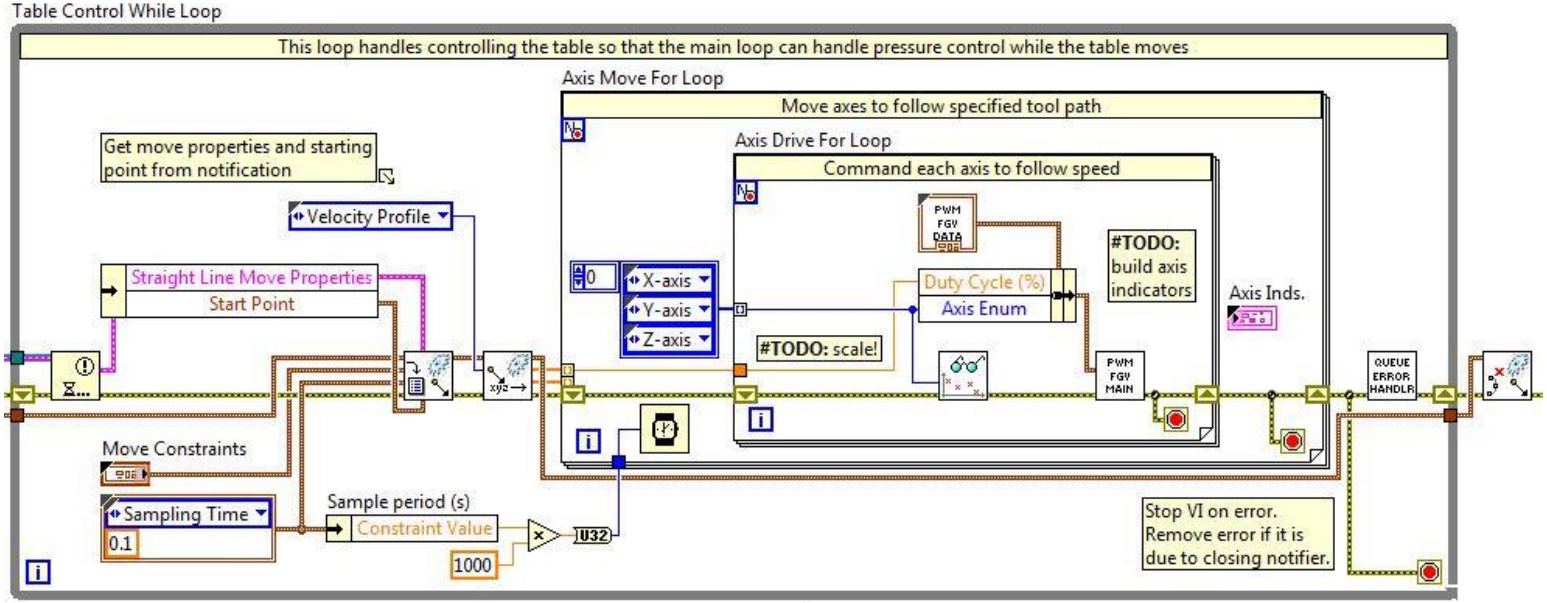

#TODO: figure out how to run loop continuously when table is enabled, and stop loop when table is disabled until notifier receives new information.

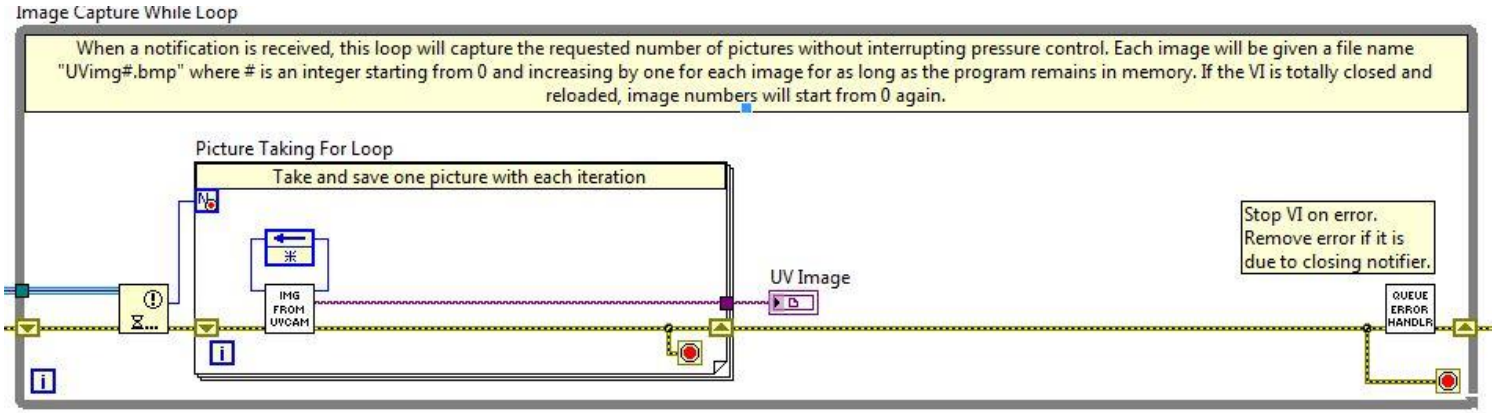
Image Capture While Loop
When a notification is received, this loop will capture the requested number of pictures without interrupting pressure control. Each image will be given a file name "UVimg#.bmp" where # is an integer starting from 0 and increasing by one for each image for as long as the program remains in memory. If the VI is totally closed and reloaded, image numbers will start from 0 again.
Picture Taking For Loop
Take and save one picture with each iteration
IMG FROM UVCAM
UV Image
Stop VI on error.
Remove error if it is due to closing notifier.
QUEUE ERROR HANDLR

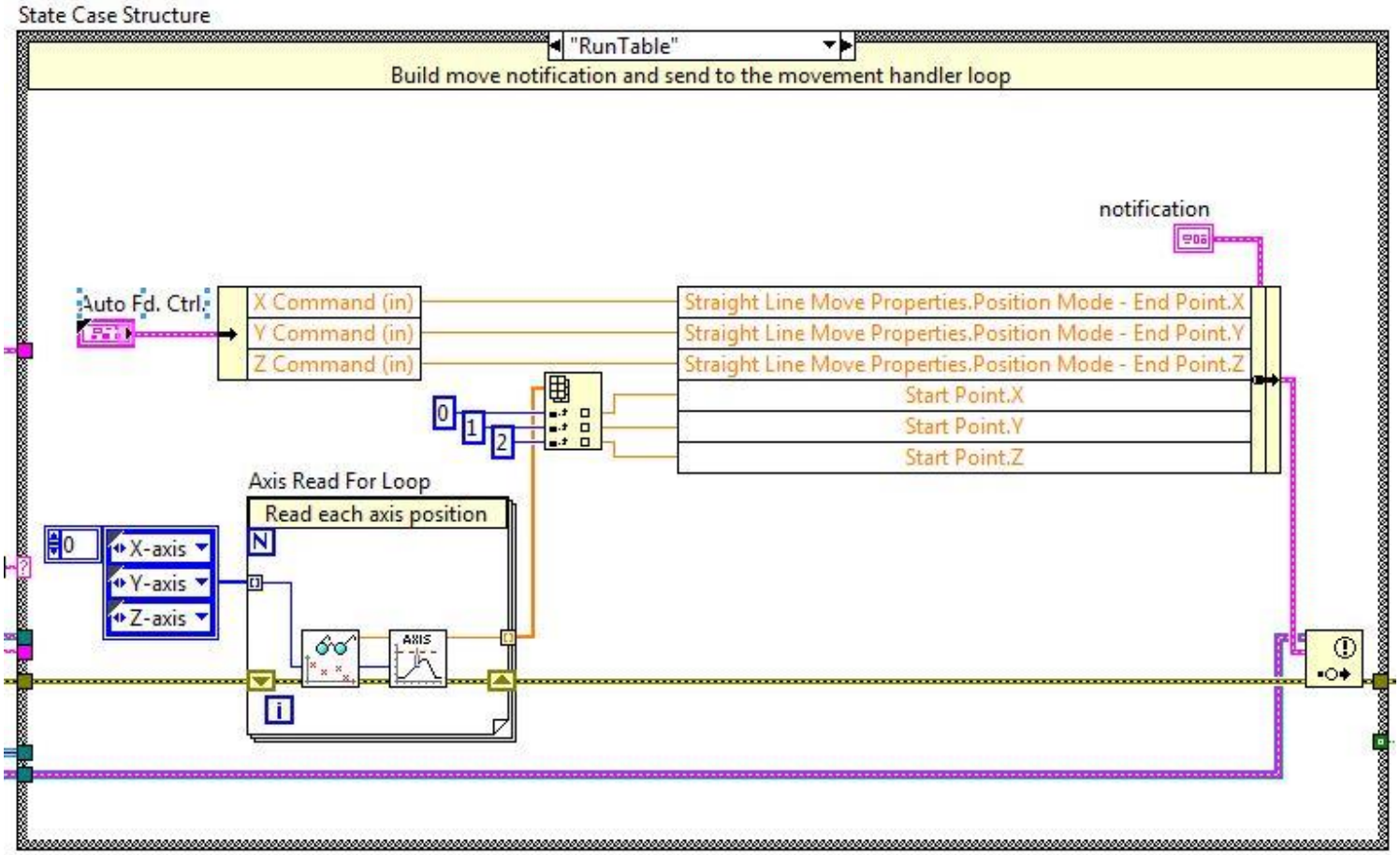
State Case Structure
"RunTable"
Build move notification and send to the movement handler loop
notification
Auto Fd. Ctrl
X Command (in)
Y Command (in)
Z Command (in)
Straight Line Move Properties.Position Mode - End Point.X
Straight Line Move Properties.Position Mode - End Point.Y
Straight Line Move Properties.Position Mode - End Point.Z
Start Point.X
Start Point.Y
Start Point.Z
0
1
2
Axis Read For Loop
Read each axis position
0
X-axis
Y-axis
Z-axis
N
AXIS
i

VITA

VITA

Dustin Cruise
Graduate School, Purdue University

Education
B.S., Mechanical Engineering, 2011, Purdue University, West Lafayette, Indiana
M.S., Mechanical Engineering, 2014, Purdue University, West Lafayette, Indiana

Research Interests
Combustion Controls
Intelligent Control